Development of A Low-Cost Adsorption Technique for Multiple Critical Mineral Recovery from Acid Mine Drainage

Final Report

U.S. Department of the Interior
Office of Surface Mining
Grant/Contract No.: S23AC00053
Technical Officer: Cecil Slaughter
Project Grant Period: 01/01/2023– 07/30/2025
Quarterly Reporting Period: Through 07/30/2025

SUBMITTED BY

West Virginia University
Department of Mining Engineering
1374 Evansdale Drive | PO Box 6070
Morgantown, WV 26506-6070

PRINCIPAL INVESTIGATOR

Dr. Qingqing Huang
Phone Number: +304-293-3456
E-Mail: qingqing.huang@mail.wvu.edu

Submission Date: May 14, 2026

Project Goals

The overarching goal of this project was to develop a low-cost adsorption-based process to selectively recover critical minerals (CMs) from acid mine drainage (AMD) raw water and produce multiple CM concentrates with a minimum purity of 50 wt.%. Successful development of this AMD treatment strategy will not only address water-quality issues associated with AMD but also generate economic value through the recovery of strategic critical metals. In addition, the process has the potential to incentivize the mining industry to adopt more sustainable AMD treatment approaches.

As a step toward this goal, the specific objectives of the proposed study include:

- Identify a promising AMD feedstock by characterizing multiple AMD samples to determine the full range of critical minerals present.
- Develop a low-cost adsorption recovery technique capable of producing CM concentrates with purities exceeding 50 wt.% from AMD.
- Propose an integrated processing flowsheet for CM recovery and value creation.
- Evaluate the technical and economic feasibility of the proposed process circuitry for future scale-up.

Building upon our past and ongoing research, we aimed to produce CM concentrates with purities greater than 50 wt.% while also generating remediated AMD water. Targeted CM concentrates include rare earth elements (REEs), manganese, cobalt, nickel, and zinc.

Project Accomplishments

In this project, the West Virginia University (WVU) Department of Mining Engineering research team focused on AMD sample collection, sample characterization, and laboratory-scale development of processing routes to selectively recover multiple critical minerals—including REEs, nickel, manganese, zinc, and cobalt. The team also conducted a techno-economic analysis (TEA) of the developed AMD treatment circuitry. A summary of accomplishments is provided below, and the finalized integrated process flowsheet is shown in Figure 1.

Key Accomplishments:

- Collected 14 AMD raw water samples from 14 different AMD ponds across the Central and Northern Appalachian regions.
- Conducted ICP-MS characterization on all samples to evaluate concentrations of REEs, critical minerals/elements, and major impurities, enabling identification of the most promising feedstock.

- Performed stage-wise precipitation tests on the selected AMD sample to determine precipitation behavior of metals and impurities across varying pH ranges.

- Conducted systematic recovery testing for nickel, cobalt, zinc, manganese, and REEs, using both ion exchange and selective precipitation methods.

- Verified the purity of recovered products—including nickel hydroxide, zinc sulfide, cobalt hydroxide, manganese oxide, and rare earth oxide—using ICP-MS analyses.

- The following products were obtained throughout the project: mixed rare earth oxide with a purity greater 95 wt%, nickel hydroxide (65 wt% purity), zinc sulfide (56 wt%), cobalt hydroxide (48 wt%), and manganese oxide (54 wt%).

Overall, this report covers AMD sampling and selection, extraction of critical elements, and product characterization. It compiles the successful laboratory tests, analyses, and corresponding results that form the foundation for the proposed AMD treatment and resource-recovery strategy.

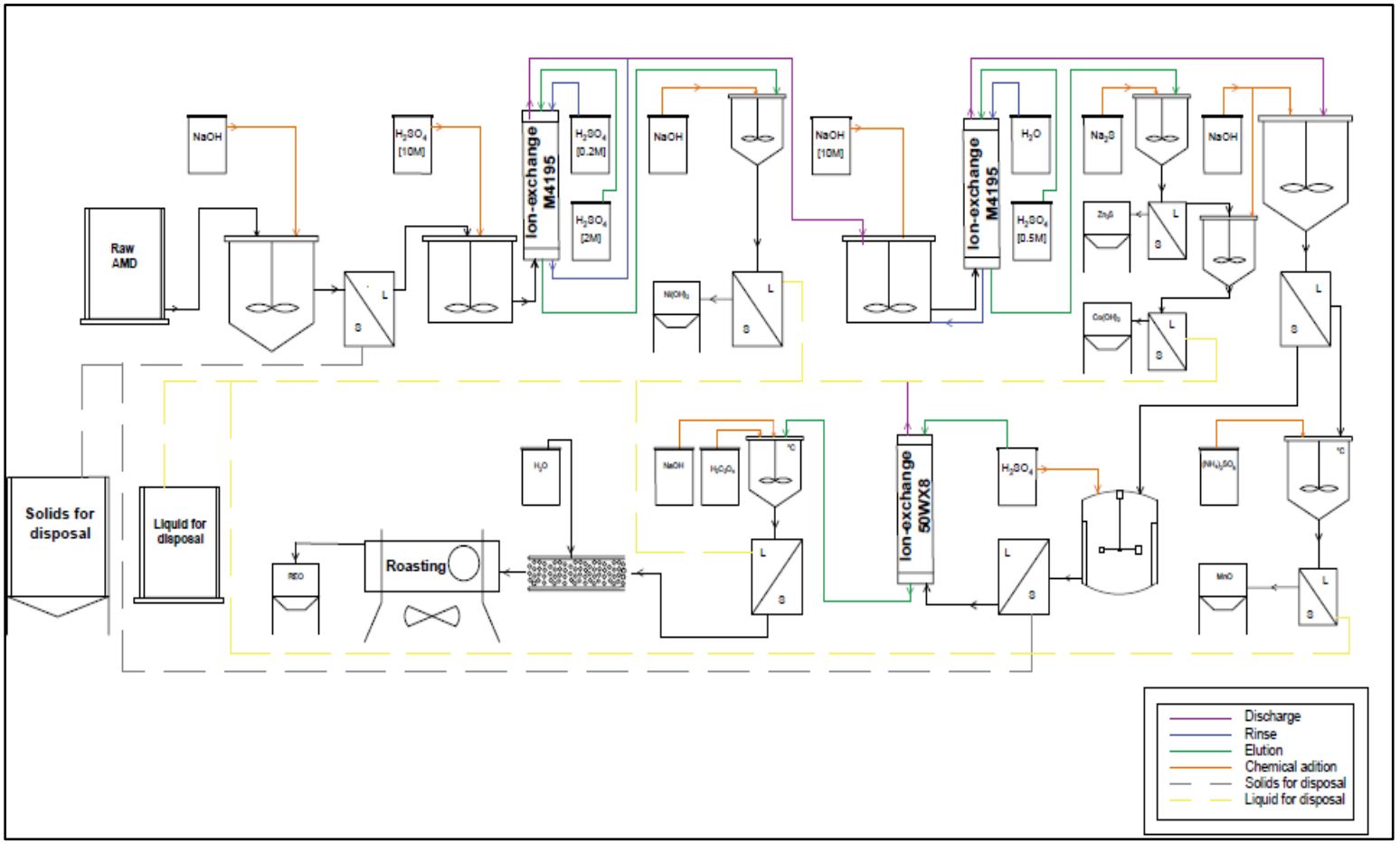

Figure 1. Flowsheet of process development for multi-element recovery from acid mine drainage.

1. Sampling

1.1 AMD Site Sampling

The research team at WVU contacted multiple coal mines and AMD treatment facilities for site selection and AMD sampling, including the Pennsylvania Department of Environmental Protection (PA DEP), American Consolidated Natural Resources (ACNR), Blackhawk Mining LLC, and CONSOL Energy. ACNR collected AMD raw water samples from their treatment sites in Monongalia, Harrison, and Marion Counties. These sites treat AMD originating from the Pittsburgh #8 coal seam.

Additional AMD raw water samples—Brubaker Run, MX7, Porcupine Run, and Reitz Run—were obtained from locations associated with the Lower Kittanning coal seam. AMD 074 represents a site associated with the Brookville coal seam, which is overlain by the Lower and Upper Kittanning seams. Both the Lower and Upper Kittanning coal seams include sandstone, claystone, and shale units; the Lower Kittanning in particular is known for its high silicon, aluminum, and iron content. The Brookville coal bed, located beneath the Lower Kittanning seam, is typically thin, discontinuous, and situated on or just above the Homewood Sandstone Member of the Pottsville Formation (Patterson, 1963). The base of this coal or its underclay marks the base of the Allegheny Formation and also contains sandstone and shale sequences (Patterson, 1963).

The remaining three AMD samples were collected from Blackhawk Mining LLC. Sampling sites were selected based on prior studies indicating the potential for higher concentrations of rare earth elements (REEs) and critical minerals (CMs), as well as their low pH values and historically high metal concentrations.

A summary of sampling locations and sample names is provided in Table 1, and representative sampling site photographs are shown in Figure 2.

Table 1. AMD raw water samples collected, name and location.

ID	Sample	Location
1	Harrison#1	WV
2	Harrison#2	WV
3	Harrison#3	WV
4	Marion	WV
5	Bench	WV
6	Low Gap	WV
7	Porcup. Rd	PA
8	Reitz Run	PA
9	Brubak.Run	PA
10	AMD MX7	PA
11	AMD 074	PA
12	47 Inflow	WV
13	VFII No 1	WV
14	VFII No 2	WV

Figure 2. Acid mine drainage sampling ponds.

1.2 Sample characterization

Once the samples arrived at the WVU mineral processing labs, the raw water samples were thoroughly mixed to ensure homogeneity. The samples were then filtered to remove suspended particles. The resulting filtrate was acidified with 5 vol% trace-metal-grade nitric acid before being sent to an external analytical laboratory for elemental composition analysis using Inductively Coupled Plasma-Mass Spectrometry (ICP-MS).

Table 2 presents the concentrations of 16 REEs identified through ICP-MS analysis. The table shows that cerium, yttrium, lanthanum, and neodymium are the most abundant rare earth elements in the tested water samples.

Table 2. Rare earth elements concentration.

ID	Rare earth elements, mg/L															
	Sc	**Y**	**La**	**Ce**	**Pr**	**Nd**	**Sm**	**Eu**	**Gd**	**Tb**	**Dy**	**Ho**	**Er**	**Tm**	**Yb**	**Lu**
1	0.05	0.40	0.13	0.20	0.03	0.19	0.07	0.02	0.10	0.02	0.08	0.02	0.04	0.00	0.02	0.00
2	0.03	0.16	0.10	0.12	0.02	0.09	0.03	0.01	0.04	0.01	0.03	0.01	0.02	ND	0.01	ND
3	0.03	0.16	0.15	0.17	0.02	0.11	0.04	0.01	0.04	0.01	0.04	0.01	0.02	0.00	0.01	ND
4	0.00	0.05	0.34	0.10	0.01	0.04	0.01	0.00	0.01	0.00	0.01	0.00	0.01	0.00	0.00	0.00
5	0.06	0.21	1.17	0.37	0.05	0.26	0.06	0.01	0.08	0.03	0.05	0.01	0.02	0.00	0.02	0.00
6	0.03	0.08	0.13	0.20	0.03	0.12	0.03	0.01	0.03	0.00	0.02	0.00	0.01	ND	0.01	ND
7	0.02	0.11	0.16	0.26	0.03	0.10	0.02	0.00	0.03	0.00	0.02	0.00	0.01	ND	0.01	ND
8	0.01	0.04	0.43	0.57	0.05	0.15	0.01	0.00	0.01	ND	0.01	ND	ND	ND	0.00	ND
9	0.01	0.08	0.45	0.61	0.06	0.17	0.02	0.00	0.02	0.00	0.01	0.00	0.01	ND	0.01	ND
10	0.01	0.16	0.50	0.71	0.07	0.23	0.03	0.01	0.04	0.01	0.03	0.01	0.01	ND	0.01	ND
11	0.02	0.13	0.46	0.65	0.06	0.21	0.03	0.01	0.03	0.00	0.02	0.01	0.01	ND	0.01	ND
12	0.02	1.23	0.63	1.40	0.18	0.79	0.19	0.05	0.23	0.03	0.20	0.04	0.10	0.01	0.08	0.01
13	0.00	0.19	0.08	0.14	0.02	0.10	0.03	0.01	0.04	0.01	0.03	0.01	0.02	0.00	0.01	ND
14	0.00	0.37	0.17	0.29	0.05	0.21	0.05	0.01	0.07	0.01	0.06	0.01	0.03	0.00	0.02	ND

Table 3 summarizes the concentrations of other critical minerals, including cobalt (Co), manganese (Mn), zinc (Zn), nickel (Ni), aluminum (Al), and magnesium (Mg), as defined in the U.S. Geological Survey's most recent critical minerals list (U.S. Geological Survey, 2022). Also, other elements such as iron (Fe), silicon (Si), calcium (Ca), thorium (Th), and uranium (U) were analyzed across all samples, as these are considered impurities.

Table 3. Other elements concentration.

	Critical elements, mg/L						Other elements, mg/L				
ID	**Co**	**Mn**	**Zn**	**Ni**	**Al**	**Mg**	**Fe**	**Si**	**Ca**	**Th**	**U**
1	0.37	8.48	3.86	0.86	100.29	119.8	372.11	350.01	87.57	0.02	0.02
2	ND	2.53	2.71	0.41	74.84	91.87	71.68	339.32	103.44	0.02	0.01
3	ND	2.69	2.98	0.44	78.03	79.85	62.6	334.14	69.5	0.02	0.02
4	0.00	2.93	2.01	0.00	41.16	62.39	3.55	327.05	61.85	0.01	0.00
5	0.33	3.33	3.38	0.93	105.46	52.54	371.73	343.35	66.96	0.04	0.02
6	ND	1.71	2.11	0.36	64.39	28.82	176.61	332.17	47.28	0.03	0.01
7	ND	14.4	3.35	0.45	57.75	232.88	67.24	72.43	87.76	0.00	0.00
8	ND	6.66	1.86	0.44	55.97	93.43	20.63	628.37	66.21	0.02	ND
9	0.82	44.92	2.85	1.20	59.13	195.58	39.64	641.7	54.28	0.02	ND
10	ND	18.52	2.00	0.48	56.2	131.79	24.7	621.88	43.48	0.02	0.00
11	0.93	66.81	3.55	1.53	111.62	364.88	113.14	647.7	63.75	0.03	0.01
12	4.09	161.24	6.87	3.94	147.02	497.24	7.34	43.09	49.26	0.00	0.01
13	0.56	45.42	1.25	0.90	20.08	436	0.59	21.64	69.89	0.00	0.00
14	0.56	45.42	1.25	0.90	39.66	451.47	0.88	31.57	64.00	0.00	0.00

Table 4 provides a detailed distribution of REEs for all collected samples, categorized as follows: Total Rare Earth Elements (TREE), representing the sum of all 16 REEs in parts per million (ppm); Light Rare Earth Elements (LREEs), which include La, Ce, Pr, Nd, Pm, Sm, and Eu; and Heavy Rare Earth Elements (HREEs), comprising Gd, Tb, Dy, Ho, Er, Tm, Yb, Lu, and Y. Also, the Critical Rare Earth Elements (CREEs) are highlighted based on the U.S. Department of Energy's (DOE) critical minerals list, which includes Dy, Nd, Pr, and Tb (Department of Energy, 2023). As seen, all the water samples had a total rare earth concentration varying from 0.59 ppm to 5.22 ppm, much higher than the average content of 282 µg/L based on a survey study of the Northern and Central Appalachian Coal Basins for the aqueous AMD influence (Vass et al.,2019a; 2019b). Additionally, pH and Eh were included in all the samples.

Table 4. Rare earth elements categories, pH, and Eh.

ID	Properties		Rare earth elements, mg/L				
	Ph	Eh (mV)	TREE	HREE	LREE	CREE	HREE/LREE
1	2.21	601	1.37	0.63	0.74	0.31	0.85
2	2.54	576	0.67	0.26	0.41	0.14	0.63
3	2.45	568	0.82	0.27	0.54	0.17	0.50
4	3.65	603	0.59	0.07	0.52	0.05	0.13
5	2.17	606	2.40	0.40	2.00	0.35	0.20
6	2.21	614	0.71	0.16	0.55	0.15	0.29
7	2.78	620	0.78	0.18	0.60	0.12	0.30
8	2.99	598	1.30	0.07	1.24	0.16	0.06
9	2.98	595	1.46	0.13	1.33	0.18	0.10
10	2.95	598	1.82	0.24	1.59	0.28	0.15
11	2.65	604	1.66	0.21	1.45	0.24	0.14
12	3.29	552	5.22	1.74	3.47	1.07	0.50
13	4.52	495	0.69	0.26	0.42	0.15	0.62
14	3.72	533	1.37	0.52	0.85	0.29	0.61

Based on the concentrations of TREE and CREE in each sample, sample 12 was selected as the feedstock for the study presented in this thesis. This sample is located in Kanawha County, WV, known for extensive coal mining (Rice, 1965). A more detailed breakdown of rare earth elements present in this sample is shown in figure 3.

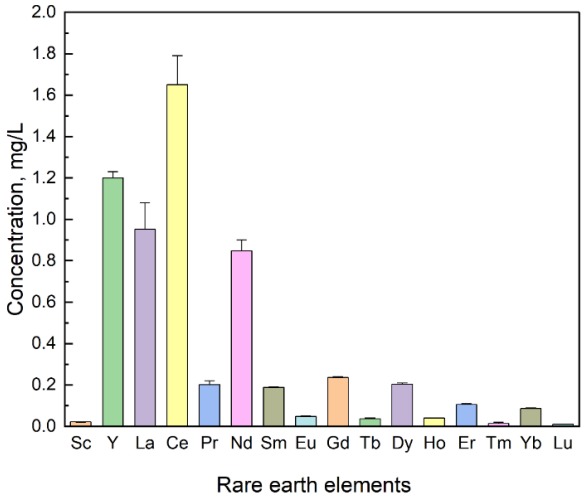

Figure 3. Rare earth elements concentration in the selected sample.

1.3 Sample Selection

Moreover, the elemental compositions of all the AMD water samples were further evaluated regarding various rare earth groups, including heavy rare earth elements (REEs), light rare earth elements (LREEs), critical (CREEs), and uncritical rare earth elements (UCREEs). In this report, HREEs refer to the REEs with an atomic number greater than 64, including Tb, Dy, Ho, Er, Tm, Yb, and Lu, as well as Sc and Y, due to their similar properties as other HREEs. On the other hand, LREEs include La, Ce, Pr, Nd, Sm, Eu, and Gd. Five of the REE elements, including Y, Nd, Eu, Tb, and Dy, have been identified as CREEs by the US Department of Energy, while the rest are classified as UCREEs.

Besides, the outlook coefficient ($C_{Outlook}$) was calculated for each sample to further evaluate the potential of using these water samples for rare earth recovery. The higher the outlook coefficient is, the more promising the ore is regarding the potential industrial value of the rare elements, and the equation below was used for the coefficient determination (Seredin and Dai, 2012).

$$C\_Outlook = \frac{\left(\frac{Nd + Eu + Tb + Dy + Er + Y}{\sum REE}\right)}{\left(\frac{Ce + Ho + Tm + Yb + Lu}{\sum REE}\right)} \quad (1)$$

The outlook coefficients, as shown in Table 5. Although, according to the laboratory results and the $C_{Outlook}$ analysis, the 47 Inflow stream has a lower coefficient, it is also important to consider that the 47 Inflow stream has the highest TREE as well as the highest CREE concentration values when compared to the other AMD samples. Based on the statement above, the research team decided that the AMD from the stream 47 Inflow is promising in terms of critical mineral concentration. Therefore, our future process will focus on the 47 Inflow sample and use it as our new feedstock for selective critical mineral recovery.

Table 5. Distribution of rare earth elements and critical minerals/elements in procured Blackhawk AMD water sample.

Sample ID	Elements, mg/L									HREEs/ LREEs	$C_{Outlook}$
	Total REE	HREE	LREE	CREE	UCREEs	Co	Mn	Zn	Ni		
Harrison#1	1.37	0.63	0.74	0.71	0.66	0.37	8.48	3.86	0.86	0.85	3.07
Harrison#2	0.67	0.26	0.41	0.29	0.37	ND	2.53	2.71	0.41	0.63	2.23
Harrison#3	0.82	0.27	0.54	0.32	0.5	ND	2.69	2.98	0.44	0.5	1.76
Marion	0.59	0.07	0.52	0.11	0.48	0	2.93	2.01	0	0.14	1.05
Bench	2.4	0.4	2	0.56	1.84	0.33	3.33	3.38	0.93	0.2	1.46
Low Gap	0.71	0.16	0.55	0.24	0.47	ND	1.71	2.11	0.36	0.29	1.15
Porcupine Road	0.78	0.18	0.6	0.25	0.53	ND	14.4	3.35	0.45	0.29	0.93
Reitz Run	1.3	0.07	1.24	0.21	1.1	ND	6.66	1.86	0.44	0.05	0.36
Brubaker Run	1.46	0.13	1.33	0.28	1.18	0.82	44.92	2.85	1.2	0.1	0.46
AMD MX7	1.82	0.24	1.59	0.44	1.39	ND	18.52	2	0.48	0.15	0.62
AMD 074	1.66	0.21	1.45	0.38	1.28	0.93	66.81	3.55	1.53	0.29	0.58
47 Inflow	5.21	1.74	3.47	2.3	2.91	4.09	161.24	6.87	3.94	0.5	1.55
VFII No 1	0.69	0.26	0.42	0.34	0.35	0.56	45.42	1.25	0.9	0.62	2.11
VFII No 2	1.37	0.52	0.85	0.67	0.71	0.56	45.42	1.25	0.9	0.61	2.13

2. Critical minerals extraction

2.1 Impurity Removal

Methodology

The removal of iron (Fe) and aluminum (Al) from acid mine drainage (AMD) is a critical pretreatment step due to the high concentrations of these elements generated during the oxidation of sulfide minerals such as pyrite. Their presence negatively affects downstream selective recovery of critical minerals (CMs) and rare earth elements (REEs), as both Fe and Al precipitate at low pH values and strongly compete with target metals for adsorption or ion exchange sites. For this reason, the precipitation behavior of Fe and Al was evaluated using step-wise pH adjustment with sodium hydroxide (NaOH).

Precipitation tests were conducted using filtered AMD from the Blackhawk 47 Inflow water sample. Fisher-brand sodium hydroxide with a concentration of 2 M was used as the alkaline reagent. The experimental procedure consisted of the following steps:

1. The filtered AMD was transferred to a beaker and homogenized using magnetic stirring at 400 rpm.
2. pH was continuously monitored using a calibrated Mettler Toledo SevenExcellence pH meter.

3. NaOH (2 M) was added incrementally using a Finnpipette F2 (10–100 µL range) to reach successive target pH values.
4. After each NaOH addition, the suspension was stirred for 5 minutes and allowed to precipitate for 15 minutes.
5. Solids were removed through centrifugation at 2000 rpm for 10 minutes followed by vacuum filtration using 0.45 µm filter paper.
6. The filtrate volume was measured and a representative aliquot was collected for ICP-MS analysis.
7. This process was repeated to evaluate 13 distinct pH points.

Results and Discussion

Two complete step-wise precipitation tests were performed on the Blackhawk 47 Inflow sample under identical operational conditions. In both tests, the AMD was filtered using a vacuum system capable of achieving −72 kPa and stirred at 525 rpm during precipitation. The process successfully generated pH-dependent precipitation profiles for REEs, critical minerals, and major impurities.

Cumulative Precipitation Behavior of REEs and Critical Minerals

The cumulative precipitation behavior of the rare earth elements (TREE) is shown in Figure 4. At pH 5.0, approximately 20% of the total REEs were precipitated. When the pH exceeded 7.0, TREE cumulative precipitation increased sharply to approximately 80%, indicating a transition region where REE solubility decreases rapidly.

In contrast, the precipitation behavior of critical metals—Co, Ni, Zn, and Mn—remained minimal at low pH values. At pH ≤ 5.0, cumulative precipitation remained below 10% for all these elements, showing that their solubility is largely unchanged within this pH range. This behavior is consistent with known precipitation curves, where Fe and Al precipitate first, followed by Mn, Zn, Ni, and Co at higher pH values.

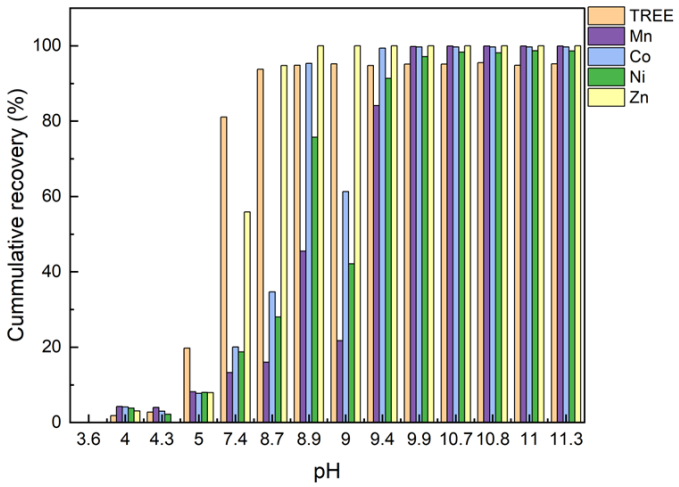

Figure 4. Cumulative precipitation recovery of the elements of interest as a function of solution pH.

Cumulative Precipitation Behavior of Fe and Al

The cumulative precipitation of Fe and Al is shown in Figure 5. At pH 5.0, Fe exhibited a cumulative precipitation of 63%, while Al reached 95%, indicating that nearly all aluminum was removed from solution at this pH. This strong precipitation response at low pH reflects the high reactivity of Fe and Al as a function of pH and aligns with behavior reported in previous AMD treatment studies.

These results indicate that pH 5.0 is the optimal precipitation threshold for impurity removal: it maximizes Fe and Al removal while maintaining most REEs and critical minerals in solution.

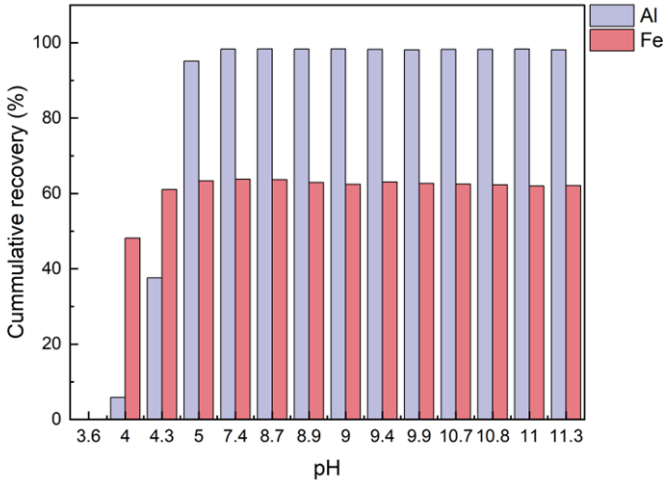

Figure 5. Cumulative precipitation recovery of Fe and Al as a function of solution pH.

Post-Precipitation Solution Composition

Table 6 summarizes the elemental composition of three solutions obtained after two-step precipitation which consist of precipitating the solution initially to a pH value of around 4.0 and subsequently after 0a solids removal stage, perform another precipitation to a pH value around 5.0. The concentrations of REEs, CMs, and impurities demonstrate consistent behavior across replicates, with relatively low standard deviations for most elements.

Table 6. Distribution of rare earth elements, critical minerals/elements, and impurities in procured Blackhawk AMD water sample after two steps of SWP.

Sample ID	Elements, mg/L							
	Total REE	Al	Fe	Mn	Co	Ni	Cu	Zn
SWP1 pH 5	4.43	7.8	3.75	158.94	4.08	3.91	0.07	6.84
SWP2 pH 5	5.02	25.1	4.33	158.88	4.11	3.9	0.11	7.02
SWP3 pH 5	3.98	8.01	3.08	149.62	3.87	3.75	0.08	6.6
Average	4.48	13.64	3.72	155.82	4.02	3.85	0.08	6.82
Std. deviation	0.52	9.93	0.63	5.36	0.13	0.09	0.02	0.21

The 47 Inflow AMD treated at pH 5.0 consistently produced:

- Near-complete removal of Al (≈95%)
- Effective removal of Fe (≈63%)
- Minimal removal of REEs and CMs, which remain largely in solution and suitable for downstream ion exchange or adsorption operations.

Based on these results, a two stages precipitation process targeting initially a pH value of 4.0 followed by a precipitation at a pH value of 5.0 was selected as the method for impurity removal and integrated into the process.

2.2 Nickel Enrichment Ion Exchange

After impurity removal, the acid mine drainage (AMD) solution containing low concentrations of iron and aluminum was used as the feedstock for the nickel enrichment ion exchange process. This stage aimed to selectively recover nickel using the Ambersep M4195 resin and to evaluate the effects of pH, contact time, and acid concentration during rinsing and elution on process performance and selectivity.

Resin Loading

During the loading stage, the AMD was passed through the resin column, allowing the metals of interest to be selectively bound onto the resin chemical structure. The efficiency of this step depended primarily on three variables: the resin's affinity for nickel, the AMD feed pH, and the contact time.

To determine the optimal conditions, single-variable experiments were performed to evaluate the influence of pH and contact time on nickel adsorption efficiency and selectivity. The ion exchange experimental setup is shown in Figure 6.

Figure 6. Ion Exchange Setup at WVU Mining Engineering Laboratory.

Effect of AMD pH

Methodology

The effect of AMD feed pH on nickel adsorption was examined using a single-variable approach. The pH of the AMD solution, initially 5.0 after impurity removal, was adjusted using 10 M sulfuric acid to values of 0.6, 0.8, 1.3, 2.0, and 2.5. Each test was conducted using 1 L of AMD at a flow rate of 1 L/h, corresponding to a contact time of 6 minutes. Samples collected before and after the ion exchange process were analyzed by ICP-MS to quantify nickel adsorption and determine the pH range yielding maximum selectivity. The experimental parameters are presented in Table 7.

Table 7. AMD pH effect Study on Nickel Enrichment. Tests Parameters.

AMD feed pH	AMD volume (L)	Flowrate (L/h)	Temperature (°C)	Contact time (min)
0.6				
	1.0	1.0	21.00	6.0
0.8	1.0	1.0	21.00	6.0
1.3	1.0	1.0	21.00	6.0
2.0	1.0	1.0	21.00	6.0
2.5	1.0	1.0	21.00	6.0

Results and Discussion

The resin exhibited negligible affinity for major impurities such as magnesium, aluminum, and silicon across all pH values, as shown in Figure 7. This result was expected since these ions are

not exchangeable under the tested conditions. Although the resin displayed some affinity for iron, its concentration remained minimal due its to prior removal int he impurity removal stage.

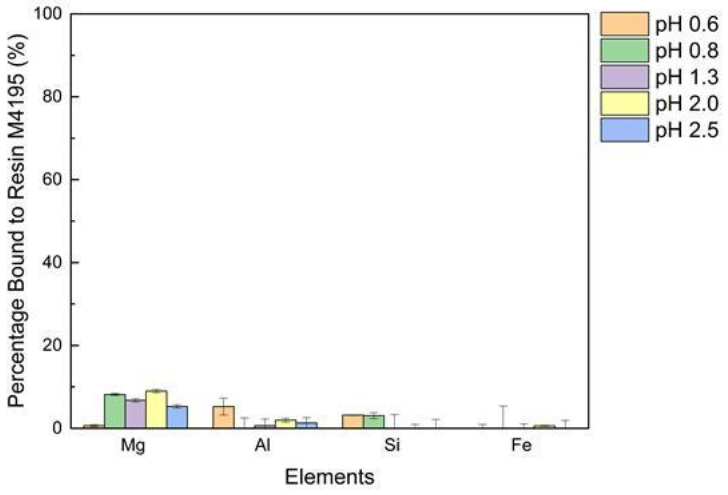

Figure 7. Effect of AMD pH on the Binding of Main Impurities to Ambersep M4195.

In contrast, Figure 8 illustrates the significant influence of pH on the adsorption of nickel, cobalt, and zinc. At pH 0.6–0.8, the resin demonstrated the highest selectivity for nickel, with binding percentages of approximately 37% and 49%, respectively. However, under these acidic conditions, the resin's total exchange capacity decreased. As pH increased to 2.0–2.5, overall binding for nickel, cobalt, and zinc exceeded 85–95%, but nickel selectivity was lost.

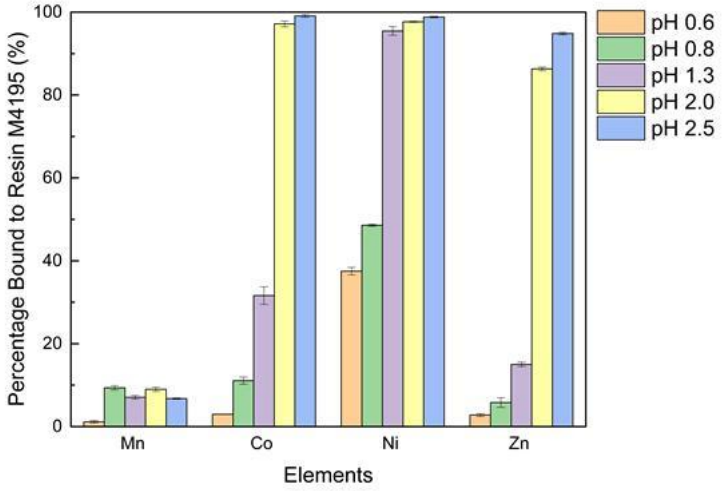

Figure 8. Effect of AMD pH on the Binding of Elements of Interest to Ambersep M4195.

At pH 1.3, an optimal balance was achieved: the binding of nickel reached ~95%, while cobalt and zinc remained around 32% and 15%. Therefore, a pH near 1.3 was identified as the optimal condition, providing high nickel recovery and good selectivity.

Effect of Contact Time

Methodology

The effect of contact time on nickel loading was studied at a fixed pH of 1.3. Contact time was varied from 1.5 to 6.0 minutes by adjusting the flow rate using two metering pumps. All tests used 1 L of AMD and were performed at ambient temperature.

At least two replicates were completed for each condition to ensure reproducibility. ICP-MS analysis of the influent and effluent solutions allowed the calculation of adsorption efficiency and the determination of the optimal flow rate for nickel enrichment. The corresponding test parameters are listed in Table 8.

Table 8. AMD Contact Time Effect on Nickel Enrichment. Tests Parameters.

AMD feed pH	AMD volume (L)	Flowrate (L/h)	Temperature (°C)	Contact time (min)
1.3	1.0	4.0	21.00	1.5
1.3	1.0	3.0	21.00	2.0
1.3	1.0	2.1	21.00	2.8
1.3	1.0	1.5	21.00	4.0
1.3	1.0	1.3	21.00	4.5
1.3	1.0	1.0	21.00	6.0

Results and Discussion

As shown in Figure 9, the resin maintained negligible interaction with impurities regardless of contact duration. However, Figure 10 indicates that nickel adsorption was highly dependent on contact time.

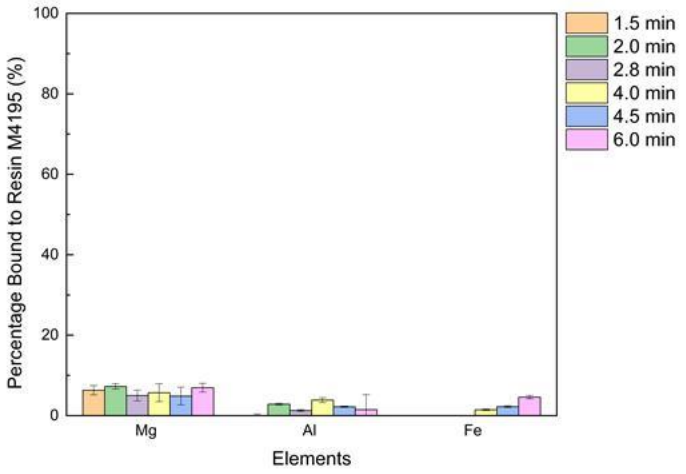

Figure 9. Effect of Contact Time on the Binding of Impurities to Ambersep M4195 at pH 1.3.

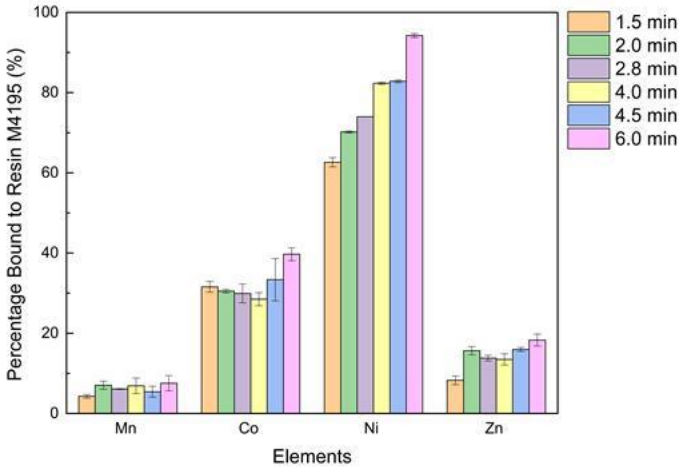

Figure 10. Effect of Contact Time on the Binding of Elements of Interest to Ambersep M4195 at pH 1.3.

At 1.5–2.8 minutes, nickel binding remained below 75%. Increasing the contact time to 4.0–4.5 minutes improved binding to ~80%, while at 6 minutes, nickel binding reached ~95%. Cobalt and zinc co-binding persisted, whereas manganese binding stayed below 10%. These results confirm that a minimum contact time of 6 minutes was required to achieve near-complete nickel capture.

Resin Regeneration and Elution Optimization

Methodology

After resin loading, a sequence of rinsing and elution steps was performed to selectively remove the bound elements and regenerate the resin. During the rinse stage, diluted sulfuric acid was used to remove weakly bound impurities, while stronger acid concentrations were applied during the elution stage to elute nickel.

According to literature (Strauss et al., 2021), 2 M sulfuric acid is suitable for nickel elution. To optimize this process, systematic testing was conducted for the following parameters:

1. Sulfuric acid concentration during the rinse stage (0.025–0.5 M).
2. Sulfuric acid concentration during the elution stage (0.5–3.0 M).
3. Volume of acid required during the elution stage (1–5 BV).

For all tests, the flow rate was fixed at 0.2 L/h. Resin regeneration between tests involved 5 BV of 2 M sulfuric acid followed by 5 BV of deionized water. The parameters studied during the rinse, elution, and acid volume optimization stages are summarized in Tables 9–11.

Table 9. Sulfuric Acid Concentration Effect During Rinse Stage. Tests Parameters.

Loading parameters				Rinse Parameters		
pH	volume (L)	Flowrate (L/h)	Contact time (min)	Acid strength [M]	Flowrate (L/h)	Volume (L)
1.3	1	1	6	0.025	0.2	0.25
1.3	1	1	6	0.075	0.2	0.25
1.3	1	1	6	0.1	0.2	0.25
1.3	1	1	6	0.25	0.2	0.25
1.3	1	1	6	0.5	0.2	0.25

Table 10. Sulfuric Acid Concentration Effect During Elution Stage. Tests Parameters.

Loading parameters				Rinse Parameters			Elution Parameters		
pH	volume (L)	Flowrate (L/h)	Contact time (min)	Acid strength [M]	Flowrate (L/h)	Volume (L)	Acid strength [M]	Flowrate (L/h)	Volume (L)
1.3	1	1	6	0.2	0.2	0.25	0.5	0.2	0.3
1.3	1	1	6	0.2	0.2	0.25	1	0.2	0.3
1.3	1	1	6	0.2	0.2	0.25	1.5	0.2	0.3
1.3	1	1	6	0.2	0.2	0.25	2	0.2	0.3
1.3	1	1	6	0.2	0.2	0.25	2.5	0.2	0.3
1.3	1	1	6	0.2	0.2	0.25	3	0.2	0.3

Table 11. Sulfuric Acid Volume Effect During Elution Stage. Tests Parameters.

Loading parameters				Rinse Parameters			Elution Parameters		
pH	volume (L)	Flowrate (L/h)	Contact time (min)	Acid strength [M]	Flowrate (L/h)	Volume (L)	Acid strength [M]	Flowrate (L/h)	Volume (L)
1.3	1	1	6	0.2	0.2	0.25	2	0.2	0.1
1.3	1	1	6	0.2	0.2	0.25	2	0.2	0.2
1.3	1	1	6	0.2	0.2	0.25	2	0.2	0.3
1.3	1	1	6	0.2	0.2	0.25	2	0.2	0.4
1.3	1	1	6	0.2	0.2	0.25	2	0.2	0.5

Results and Discussion

1. Sulfuric acid concentration during the rinse stage (0.025–0.5 M).

The rinse stage effectively removed co-bound elements (Co^{2+}, Zn^{2+}, Mn^{2+}, and Mg^{2+}) without significantly affecting nickel retention. As presented in Figure 11, rinsing with 0.025 M H_2SO_4 removed ~73% Mg, 76% Mn, 45% Co, and 62% Zn, while only ~5% Ni was displaced. Increasing the acid concentration to 0.25 M enhanced removal efficiency (≈100% Mg, 97% Mn, 77% Co, 93% Zn) with only ~8% Ni loss.

A rinse concentration between 0.20–0.25 M H_2SO_4 and a volume of 2.5 BV were identified as optimal. The rinse solution, that can carry some of the cobalt and zinc, can be combined with the feed solution of the zn-co recovery stages, minimizing process losses.

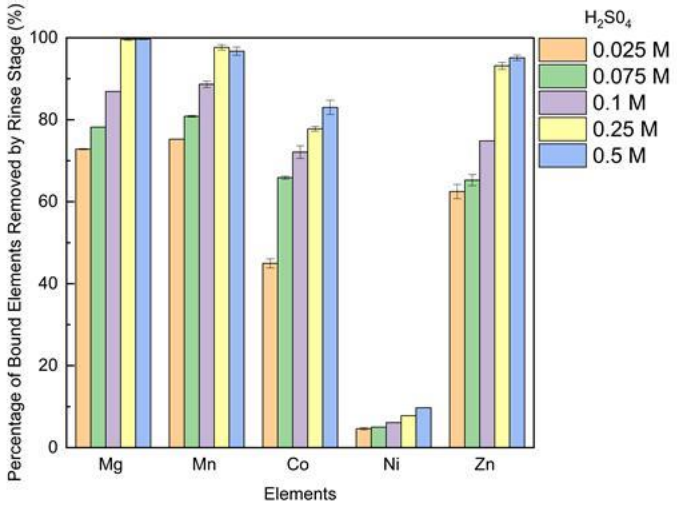

Figure 11. Removal of Co-Bound Elements During the Rinsing Stage at Different Sulfuric Acid Molarity and 2.5 B.V.

2. Sulfuric acid concentration during the elution stage (0.5–3.0 M).

Nickel elution efficiency was strongly dependent on acid concentration. As shown in Figure 12, concentrations below 1.5 M resulted in incomplete recovery (< 50%). At 2.0 M H_2SO_4, nickel recovery increased to ~90%, while higher concentrations (2.5–3.0 M) provided marginal improvement (~95–96%).

Cobalt and Zinc were the main contaminants, contributing < 20% of the total eluted mass. Based on these results, 2.0 M H_2SO_4 at 3 BV was selected as the optimal condition for efficient nickel elution and reagent economy.

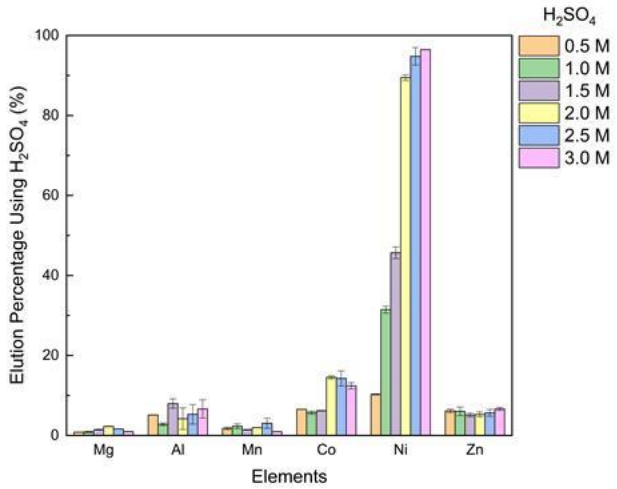

Figure 12. Elution of Nickel and Remaining Co-Bound Elements During the Elution Stage at Different Sulfuric Acid Molarity and 3.0 B.V.

3. Volume of acid required during the elution stage (1–5 BV).

Figure 13 illustrates that increasing acid volume improved nickel recovery up to a threshold. At 1 BV (100 mL), recovery was below 30%; at 2 BV (200 mL), recovery rose to ~80%; and between 3–4 BV (300–400 mL), recovery stabilized near 90%. At 5 BV, recovery reached 97%, but with increased cobalt contamination.

Therefore, 3–4 BV of 2.0 M H_2SO_4 was deemed optimal, balancing recovery and purity. Higher volumes were unnecessary due to diminishing returns and reagent costs. Since complete desorption was challenging, a regeneration step between tests was implemented, as shown in Table 12.

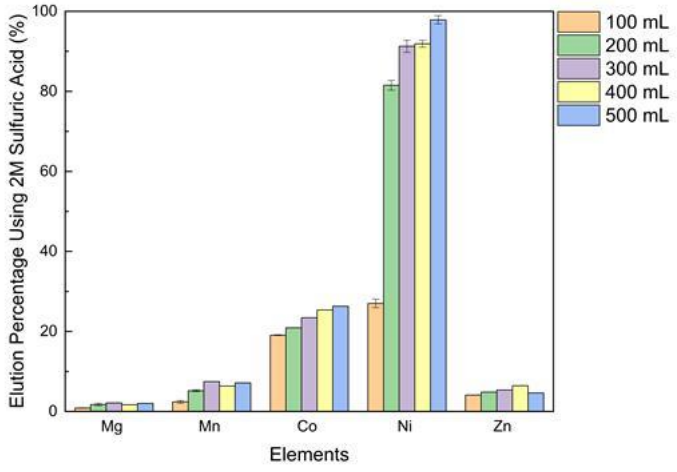

Figure 13. Elution of Nickel and Remaining Co-Bound Elements During the Elution Stage at Different Acid Volumes with 2M H_2SO_4.

Table 12. Regeneration Between Tests Parameters.

Regeneration between tests H_2S0_4 part 1				Regeneration between tests distilled water part 2		
Volume (L)	Flowrate (L/h)	Contact time (min)	Acid Concentration [M]	Volume (L)	Flowrate (L/h)	Contact time (min)
0.5	1	6	2	0.5	1	6

Nickel-Enriched Solution Production

Methodology

After identifying the optimal loading, rinsing, and elution conditions, the process was repeated to produce a nickel-enriched solution for the precipitation of nickel hydroxide solids. “Large” volume tests were performed using 4 to 8 L of AMD per run under the optimized conditions: a flow rate of 1 L/h (6-minute contact time) during loading, 0.2 L/h (30-minute contact time) during rinse and elution, 0.2 M sulfuric acid for rinsing, and 2 M sulfuric acid for elution.

A total of five large-volume tests were completed, and the eluted solutions were combined to generate a nickel-enriched liquor suitable for subsequent precipitation. Representative samples from each process stream were analyzed by ICP-MS to evaluate nickel recovery, selectivity, and enrichment performance. The parameters used for the large-volume tests are summarized in Table 13. The overall process flow for the nickel enrichment ion exchange system is illustrated in Figure 14.

Table 13. Parameters Used for "Large Volume" Nickel Ion Enrichment Tests.

Loading parameters					Rinse Parameters			Elution Parameters		
Test No.	pH	volume (L)	Flowrate (L/h)	Contact time (min)	Acid strength [M]	Flowrate (L/h)	Volume (L)	Acid strength [M]	Flowrate (L/h)	Volume (L)
1	1.3	7.70	1	6	0.2	0.2	0.25	2	0.2	0.35
2	1.3	7.40	1	6	0.2	0.2	0.25	2	0.2	0.35
3	1.3	7.00	1	6	0.2	0.2	0.25	2	0.2	0.35
4	1.3	8.07	1	6	0.2	0.2	0.25	2	0.2	0.35
5	1.3	4.00	1	6	0.2	0.2	0.25	2	0.2	0.35

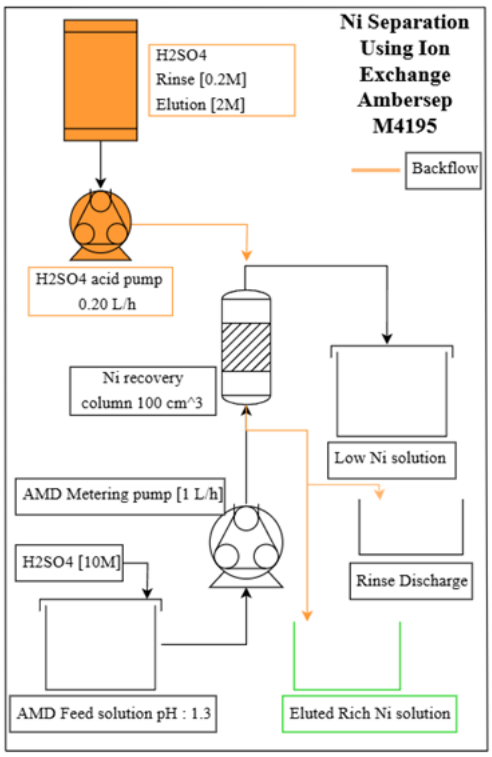

Figure 14. Flow Diagram Nickel Enrichment Ion Exchange.

Results and Discussion

Results from the "large" tests are summarized in Table 14. The resin maintained low affinity for impurities such as Mg, Na, Ca, Si, Al, and Fe, with binding percentages < 2%. Co-binding of cobalt and zinc decreased significantly with higher feed volumes—averaging 13% and 6% in larger tests versus 30% and 11% in smaller runs respectively

Nickel performance remained consistent, with an average binding of 94%, elution efficiency of 87%, and total recovery of ~82%. The main residual impurities in the eluate were calcium and silica. Their concentrations did not interfere with the subsequent precipitation stage, as both remain soluble under alkaline conditions.

Table 14. Solution Concentration and Results for Five Large Volume Nickel Enrichment Tests.

Test 1	Na	Mg	Al	Si	Ca	Fe	Mn	Co	Ni	Cu	Zn
AMD	319.89	470.18	8.33	43.97	232.81	5.05	141.6	3.71	3.49	0.08	6.6
Discharge	312.79	467.95	7.1	65.45	229.85	4.7	139.97	3.17	0.21	0.02	5.92
Elution	3.1	1.54	1.88	41.7	27.18	4.57	0.35	1.51	56.26	0.77	0.38
% Bound	2%	0%	15%	0%	1%	7%	1%	15%	94%	74%	10%
% Eluted	2%	3%	8%	0%	46%	65%	1%	14%	86%	65%	3%

Recovery %	0%	0%	1%	0%	1%	5%	0%	2%	81%	48%	0%

Test 2	Na	Mg	Al	Si	Ca	Fe	Mn	Co	Ni	Cu	Zn
AMD	335.63	481.99	7.62	63.78	235.2	4.6	145.15	3.68	3.56	0.07	6.35
Discharge	317.33	476.65	7.51	63.48	230.07	4.65	142.97	3.3	0.28	0.02	6.09
Elution	2.88	1.23	1.95	36.73	25.78	4.59	0.24	1.23	62.7	0.86	0.34
% Bound	5%	1%	1%	0%	2%	0%	2%	10%	92%	69%	4%
% Eluted	1%	1%	91%	0%	25%	0%	1%	16%	90%	91%	7%
Recovery %	0%	0%	1%	0%	1%	0%	0%	2%	83%	63%	0%

Test 3	Na	Mg	Al	Si	Ca	Fe	Mn	Co	Ni	Cu	Zn
AMD	360.83	535.53	7.11	61.96	249.63	4.94	161.73	4.05	3.83	0.07	6.86
Discharge	353.29	525.41	7.76	72.81	248	4.63	158.12	3.43	0.21	0.02	6.41
Elution	1.84	1.32	2.04	45.29	28.03	4.5	0.23	2.22	64.18	0.91	0.36
% Bound	2%	2%	0%	0%	1%	2%	2%	15%	95%	75%	6%
% Eluted	1%	1%	0%	0%	86%	0%	0%	18%	89%	84%	4%
Recovery %	0%	0%	0%	0%	1%	0%	0%	3%	84%	63%	0%

Test 4	Na	Mg	Al	Si	Ca	Fe	Mn	Co	Ni	Cu	Zn
AMD	314.75	467.38	6.63	76.06	233.05	7.18	144.47	3.74	3.59	0.08	6.42
Discharge	312.45	464.93	6.57	75.54	229.5	5.2	142.44	3.26	0.22	0.01	6.07
Elution	2.35	1.53	1.92	49.93	31.36	4.51	0.34	1.94	66.54	0.95	0.33
% Bound	1%	1%	0%	0%	2%	20%	1%	13%	94%	84%	5%
% Eluted	5%	3%	0%	0%	44%	0%	1%	20%	86%	74%	5%
Recovery %	0%	0%	0%	0%	1%	0%	0%	3%	81%	63%	0%

Test 5	Na	Mg	Al	Si	Ca	Fe	Mn	Co	Ni	Cu	Zn

AMD	311.44	464.8	7.11	72.53	227.4	4.76	142.78	3.64	3.55	0.06	6.26
Discharge	310.83	462.43	7.03	74.03	222.26	4.56	142.09	2.55	0.12	0.01	5.54
Elution	1.63	1.02	1.31	48.25	25.71	4.17	0.21	5.93	30.53	0.51	1.45
% Bound	0%	1%	0%	0%	2%	2%	0%	30%	97%	84%	11%
% Eluted	13%	2%	0%	0%	25%	0%	1%	27%	84%	52%	10%
Recovery %	0%	0%	0%	0%	1%	0%	0%	8%	81%	44%	1%

The combined eluted solution composition is shown in Table 15. Nickel concentration increased from 3.55 mg/L in the AMD feed to 51.29 mg/L after enrichment, while impurities such as Mg and Na decreased by over 99%. The nickel total enrichment ratio was calculated at 122 times, as detailed in Table 16. This enrichment factor demonstrates the high selectivity and efficiency of the ion exchange process for nickel recovery/separation from AMD.

Table 15. Average Solution Concentration for AMD Feed and Eluted Combined. 5 Tests.

Description	Average Elements Concentration (mg/L)										
Elements	Na	Mg	Al	Si	Ca	Fe	Mn	Co	Ni	Cu	Zn
AMD	311.44	464.8	7.11	72.53	227.4	4.76	142.78	3.64	3.55	0.06	6.26
Eluted Combined	1.86	1.19	1.38	47.1	31.29	4.11	0.2	2.38	51.29	0.72	0.5

Table 16. Ratio of Nickel to Other Elements for Solutions Before and After Nickel Enrichment.

Ratio M+/Other Elements	
Ni before enrichment	0.00391
Ni after enrichment	0.47930
Enrichment factor	122.463

Hydroxide Precipitation of Nickel

After optimizing the nickel enrichment ion exchange stage and producing a sufficient volume of enriched solution, the next stage involved the precipitation of nickel as nickel hydroxide. This compound was selected as the final product due to its high industrial relevance and economic value. Nickel hydroxide is a key component in the manufacture of Nickel–Cadmium, Nickel–Metal Hydride, and Nickel–Iron batteries and is also used as a pigment and catalyst in chemical processes because of its stability and reactivity characteristics (Haynes, 2014).

Methodology

Precipitation was conducted by adjusting the pH of the combined enriched nickel solution using sodium hydroxide (NaOH). Although nickel hydroxide ($Ni(OH)_2$) is theoretically expected to precipitate completely between pH 8.8 and 9.0, previous studies have reported precipitation beginning near pH 7.0 (Giannopoulou & Panias, 2008). To ensure complete nickel removal, the process targeted a final pH of 11.00, a value confirmed experimentally to achieve precipitation efficiencies above 98% in prior stagewise tests.

The reaction governing nickel hydroxide formation is expressed as:

Equation 1. Chemical Reaction Controlling $Ni(OH)_2$ Precipitation in the Presence of NaOH.

$$Ni^{2+}(aq) + 2OH^{-}(aq) \rightarrow Ni(OH)_2(s)$$

Following the combination of the eluted solutions from the enrichment tests, the total volume was measured using a volumetric glass column. The solution was transferred to a glass beaker, and its initial pH (0.19) was recorded using a Mettler Toledo Seven Excellence sensor. A 10 M NaOH solution was then added gradually to raise the pH to 11.00. The mixture was stirred and allowed to settle for 60 minutes to complete the precipitation reaction. The solids were collected using vacuum filtration through 0.45 µm filter paper and dried at 60 °C for 48 hours.

The operating parameters for the precipitation process are summarized in Table 16, and a visual representation of the process is shown in Figure 15.

Table 16. Nickel Hydroxide Precipitation Conditions.

Solution Volume (L)	Initial pH	Final pH	Precipitation Time (min)	Reagent
1.69	0.19	11	60	10 M NaOH

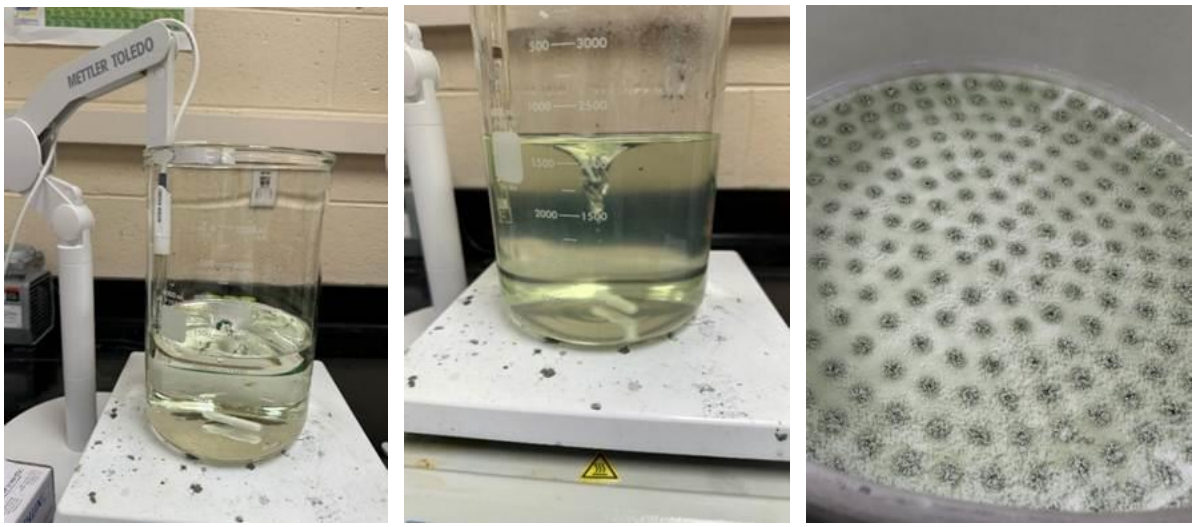

Figure 15. Nickel Hydroxide Precipitation. Left: Initial Eluted Solution. Center: Eluted Solution + NaOH pH 11.00. Right: Solids in Filter Paper.

Results and Discussion

The ICP-MS results before and after precipitation are summarized in Table 17. The nickel precipitation reached 100%, confirming the complete conversion of soluble Ni^{2+} ions to solid $Ni(OH)_2$ under the selected conditions. Aluminum, iron, and cobalt are also precipitated fully, likely due to their low solubility at high pH values. Copper and zinc exhibited partial precipitation, reaching 87% and 55%, respectively. Manganese and magnesium showed lower removal efficiencies (47% and 7%), remaining largely in solution.

Despite the co-precipitation of certain impurities, their concentrations in the enriched solution were significantly lower than the nickel concentration. Therefore, their presence in the final product is not expected to compromise the overall purity of the recovered solids. Other elements such as sodium, silica, and calcium remained soluble at pH 11.00, consistent with their known hydroxide solubility behavior.

These results validate the selected precipitation conditions as effective for obtaining a high-purity nickel hydroxide product. The process produced a visible green solid typical of β-$Ni(OH)_2$. The visual appearance of the product at various stages of processing is shown in Figure 16.

Table 17. Nickel Hydroxide Precipitation Results, Solution Concentrations, and Precipitation Percentages.

Description	Average Elements Concentration (mg/L)										
Elements	Na	Mg	Al	Si	Ca	Fe	Mn	Co	Ni	Cu	Zn
Enriched Nickel Solution	1.86	1.19	1.38	47.1	31.29	4.11	0.2	2.38	51.29	0.72	0.5
After NaOH Precipitation	47891	0.82	0.06	37.12	30.28	0.03	0.08	0.01	0.03	0.07	0.17
Precipitation (%)	NA	7%	100%	NA	NA	100%	47%	100%	100%	87%	55%

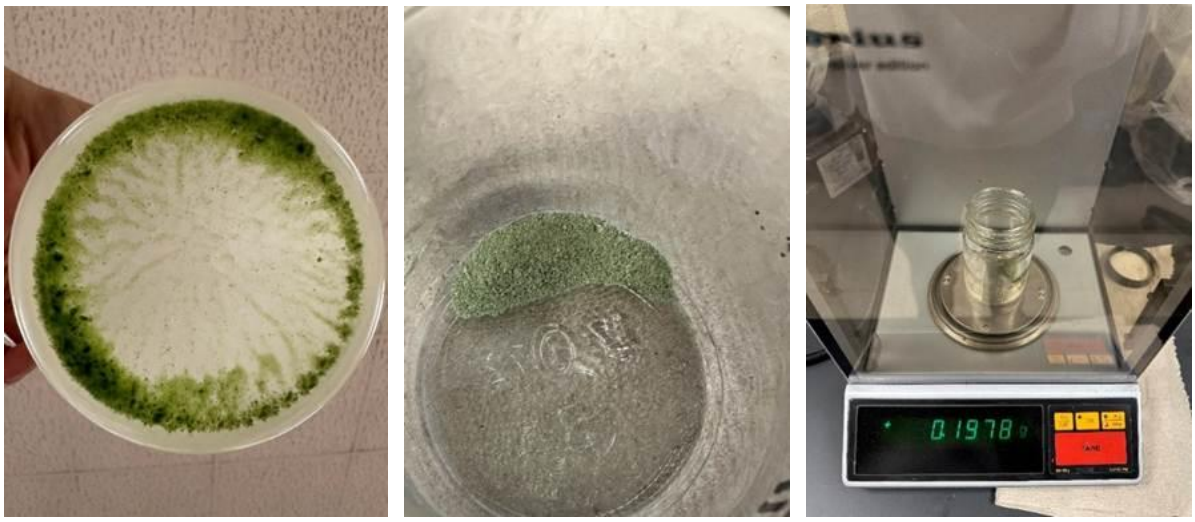

Figure 16. Nickel Hydroxide Precipitation. Left: Wet Solids. Center: Dried Solids. Right: Weight of Dried Solids.

Nickel Solids Purity and Recovery Rate

A representative portion of the precipitated solids, 0.1373 g, was digested using highly concentrated nitric acid (HNO_3) of 70% purity at room temperature for 4 hours. In total, 10 mL of 70% nitric acid and 50 mL of distilled water were used in the digestion process. After fully digesting the solids, the liquid sample was filtered, and a small part of the digested liquor was diluted and sent for ICP-MS analysis. The ICP-MS results were used to calculate the weight of nickel dissolved in the liquor using the following formula.

Equation 2. Equation to Calculate Weight of Dissolved Nickel in Digested Liquor.

$$Nickel\ Weigth(g) = ICP - MS\ Nickel\ Concentration\left(\frac{mg}{L}\right) * \frac{Liquor\ Volume\ (L)}{1000}$$

The ICP-MS results of the nickel hydroxide digested liquor are shown in Table 18 below.

Table 18. Elements of Interest and Main Impurities Concentration in Digested Liquor of Nickel Solids.

Description	Average Elements Concentration (mg/L)										
Elements	Na	Mg	Al	Si	Ca	Fe	Mn	Co	Ni	Cu	Zn
Nickel Digested Solids	11.6	5.9	20.6	91.4	59.9	17.8	3.2	45.9	944.8	12.9	8.1

Figure 17. Nickel Hydroxide Solids Digestion. Left: Dried Solids. Center: Weight of Digested Solids. Right: Solids in Digestion Vessel.

Using Equation 2, the weight of the nickel present in the digested liquor was 0.0567 g; then, by dividing this nickel weight by the weight of the digested solids, we have:

$$Nickel\ Purity = \frac{0.0567g}{0.1373\ g} = 41.30\%\ Nickel$$

Now, assuming that the entire nickel was precipitated as nickel hydroxide, the purity of the hydroxide mineral can be calculated as follows.

$$Nickel\ Hydroxide\ Purity = \frac{Nickel\ Purity\ \%}{0.633} = 65.21\%$$

It is essential to note that the mineralogy of the precipitate likely includes additional minerals beyond nickel hydroxide ($Ni(OH)_2$); therefore, the purity of nickel hydroxide may be lower than calculated above.

2.3 Zinc and Cobalt Ion Exchange and Recovery

Following the selective removal of nickel during the first ion exchange stage, the discharge solution (referred to as L*ow Ni Solution*) was utilized as the feed for the second ion exchange stage focused on zinc and cobalt enrichment. The Ambersep M4195 resin was employed once again, leveraging its known affinity for Zn^{2+} and Co^{2+} species. This stage aimed to optimize the operational parameters influencing adsorption and desorption, including feed pH, rinse volume, and acid strength during elution.

Effect of Feed pH During Resin Loading

Methodology

After nickel removal, the feed solution contained reduced nickel concentrations and elevated levels of sodium, magnesium, silica, and calcium. The feed pH was adjusted using 10 M NaOH to five different values (1.98, 2.55, 3.00, 3.54, and 4.35). Each test used 1.0 L of AMD at a flowrate of 1.0 L/h, a contact time of 6 minutes, and a temperature of 21 °C as shown in Table 19. Samples collected before and after the loading step were analyzed by ICP–MS to determine the binding percentages for zinc, cobalt, and primary impurities.

Table 19. Feed pH Effect During Loading Stage, Zinc and Cobalt Enrichment Tests Parameters.

AMD feed pH	AMD volume (L)	Flowrate (L/h)	Temperature (°C)	Contact time
1.98	1	1	21	6
2.55	1	1	21	6
3	1	1	21	6
3.54	1	1	21	6
4.35	1	1	21	6

Results and Discussion

The AMD solution used as feed exhibited the composition shown in Table 20, with sodium, magnesium, silica, and calcium as the main impurities. Across all tested pH values, cobalt and zinc displayed high binding efficiencies of approximately 98% and 87%, respectively. Manganese binding remained below 11%, confirming the resin's low affinity for this metal.

Table 20. Elemental Concentration of AMD Solution After Nickel Removal.

Description	Average Elements Concentration (mg/L)									
Elements	Na	Mg	Al	Si	Ca	Fe	Mn	Co	Ni	Zn
Ion Exchange Feed Zn-Co	2669.46	478.38	12.97	102.51	241.73	5.71	133.36	3.05	0.2	6
STD	258.9	31.47	3.35	5.66	17.6	0.81	10.94	0.42	0.12	0.6

At a pH of 3.5, the resin exhibited optimal performance, showing maximum selectivity for zinc and cobalt while minimizing impurity adsorption. Figures 18 and 19 illustrate the binding trends for both target metals and impurities, confirming that pH 3.5 provided the best balance between exchange capacity and selectivity.

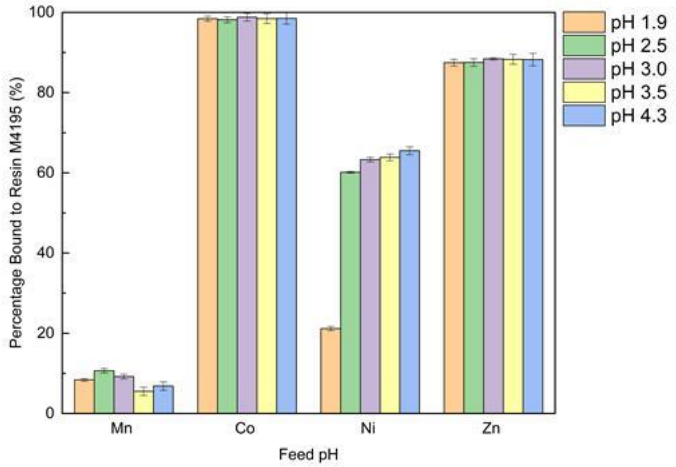

Figure 18. Effect of Feed pH on the Binding of Elements of Interest.

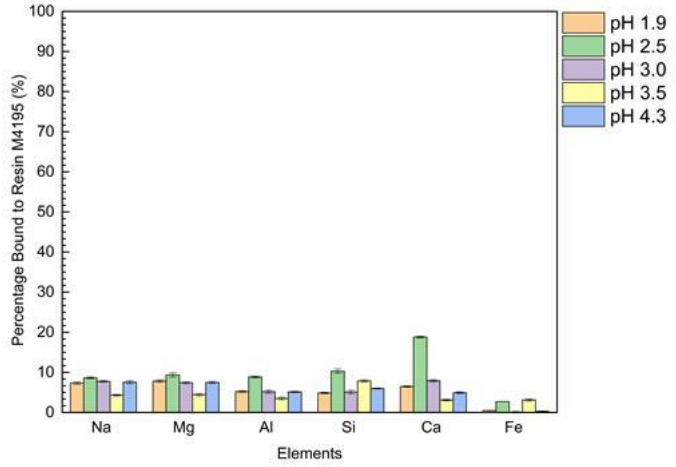

Figure 19. Effect of Feed pH on the Binding of Main Impurities.

Volume of Distilled Water During Rinse Stage

Methodology

After resin loading, a rinsing stage was performed using distilled water to remove weakly bound impurities while retaining zinc and cobalt on the resin. The rinse volumes evaluated were 100, 200, 300, and 400 mL, fed at a flowrate of 0.2 L/h with a contact time of 30 minutes. All tests used AMD at pH 3.5 and a contact time of 6 minutes for loading as shown in Table 21.

Table 21. Effect of Distilled Water Volume During Rinse Stage. Tests Parameters.

Loading parameters					Rinse Parameters H_2O		
pH	volume (L)	Flowrate (L/h)	Temperature (°C)	Contact time (min)	Flowrate (L/h)	Volume (L)	Contact time (min)
3.5	1	1	21	6	0.2	0.1	30
3.5	1	1	21	6	0.2	0.2	30
3.5	1	1	21	6	0.2	0.3	30
3.5	1	1	21	6	0.2	0.4	30

Results and Discussion

As shown in Figure 20, increasing rinse volume beyond 200 mL resulted in a higher removal of zinc and cobalt from the resin, which was undesirable. At 200 mL, approximately 95% of manganese was removed, while less than 10% of zinc and cobalt were lost, indicating an optimal balance between impurity removal and product retention.

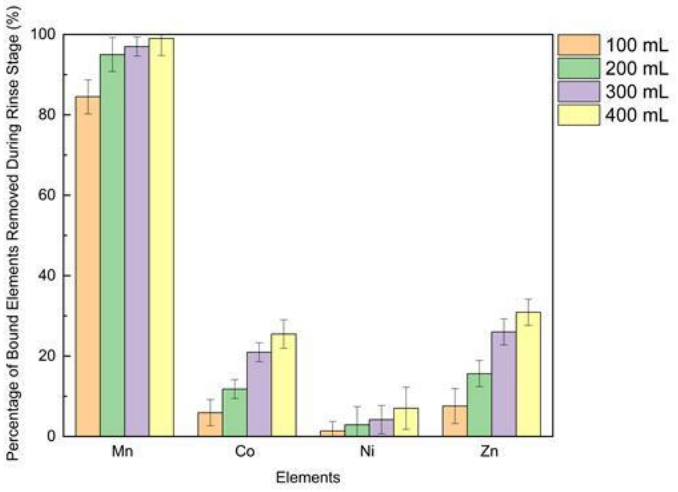

Figure 20. Percentage of Elements of Interest Removed During Rinse Stage Using Different Volumes of Distilled Water.

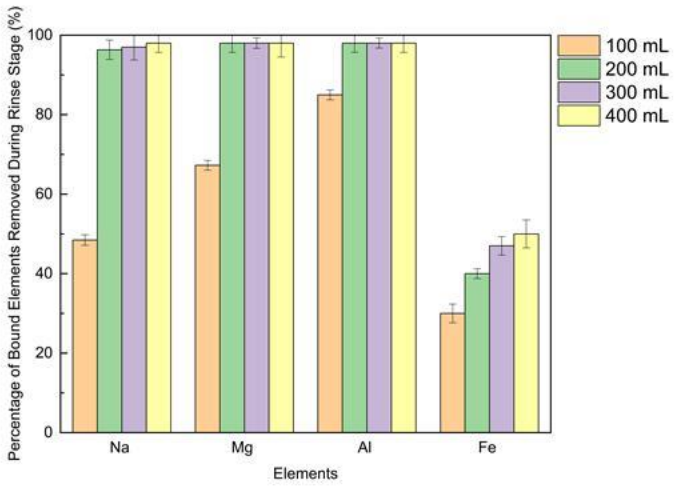

Figure 21. Percentage of Main Impurities Removed During Rinse Stage Using Different Volumes of Distilled Water.

Figure 21 shows that impurity removal efficiency approached 100% at rinse volumes ≥200 mL, particularly for sodium, magnesium, and aluminum. Therefore, a rinse volume of 200 mL per 100 cm^3 resin was determined as optimal.

Effect of Acid Strength During Elution Stage

Methodology

Elution tests were conducted using sulfuric acid at concentrations of 0.05, 0.15, 0.25, 0.35, and 0.50 M. The acid volume was kept constant at 250 mL, and the flowrate was maintained at 0.2 L/h for 30 minutes. Before each elution, the resin was rinsed with 100 mL of distilled water to remove loosely bound impurities (At the moment these experiments were performed the 200mL of distilled water during rinsing was not determined yet), the parameters of the tests can be seen in Table 22.

Table 22. Effect of Acid Strength During Elution Stage. Tests Parameters.

Loading parameters				Rinse Parameters H_2O			Elution Parameters H_2SO_4		
pH	Volume (L)	Flowrate (L/h)	Contact time (min)	Flowrate (L/h)	Volume (L)	Contact time (min)	Flowrate (L/h)	Volume (L)	Acid Strength [M]
3.5	1	1	6	0.2	0.2	30	0.2	0.25	0.05
3.5	1	1	6	0.2	0.2	30	0.2	0.25	0.15
3.5	1	1	6	0.2	0.2	30	0.2	0.25	0.25
3.5	1	1	6	0.2	0.2	30	0.2	0.25	0.35
3.5	1	1	6	0.2	0.2	30	0.2	0.25	0.5

Results and Discussion

The results presented in Figure 22 indicate that acid concentrations below 0.25 M yielded elution recoveries below 20% for both zinc and cobalt. Increasing the acid concentration to 0.35 M substantially improved recovery to 95% for zinc and 87% for cobalt. At 0.5 M H_2SO_4, cobalt recovery slightly increased while zinc remained near 95%. Consequently, 0.5 M sulfuric acid was selected as the optimal concentration for large-volume elution tests, balancing efficiency, and process stability. However, a lower concentration between 0.35M and 0.5M could also be used.

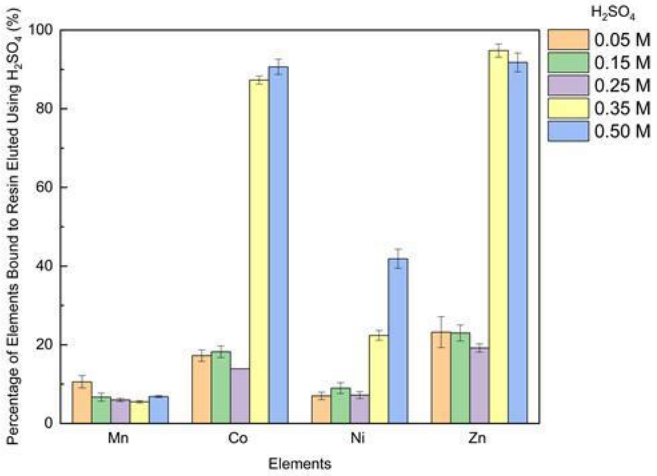

Figure 22. Percentage of Bound Elements Removed During Elution Using Different H_2SO_4 Acid Strength.

Large-Volume Enriched Solution Production

Methodology

To generate sufficient enriched solution for precipitation tests, fourteen large-scale ion exchange experiments were performed. The AMD feed volume ranged from 4 to 7 L (average 5.54 L) at a pH of 3.5 and contact time of 6 minutes. The rinse volume averaged 0.22 L, and elution was conducted with an average of 0.34 L of 0.5 M H_2SO_4. The tests parameters can be observed in Table 23 and the cobalt-zinc enrichment flowsheet can be observed in Figure 23.

Table 23. List of Large Volume Tests During Zinc and Cobalt Enrichment Stage. Parameters.

Loading parameters				Rinse Parameters H_2O			Elution Parameters H2SO4		
Test No	pH	Volume (L)	Flowrate (L/h)	Flowrate (L/h)	Volume (L)	Flowrate (L/h)	Flowrate (L/h)	Volume (L)	Acid Strength [M]
1	3.5	7.50	1	0.2	0.25	0.2	0.2	0.35	0.5
2	3.5	7.00	1	0.2	0.25	0.2	0.2	0.40	0.5
3	3.5	6.00	1	0.2	0.18	0.2	0.2	0.35	0.5

4	3.5	6.00	1	0.2	0.18	0.2	0.2	0.35	0.5
5	3.5	6.00	1	0.2	0.18	0.2	0.2	0.35	0.5
6	3.5	6.00	1	0.2	0.20	0.2	0.2	0.35	0.5
7	3.5	5.07	1	0.2	0.18	0.2	0.2	0.35	0.5
8	3.5	5.00	1	0.2	0.40	0.2	0.2	0.40	0.5
9	3.5	5.00	1	0.2	0.25	0.2	0.2	0.35	0.5
10	3.5	5.00	1	0.2	0.25	0.2	0.2	0.35	0.5
11	3.5	5.00	1	0.2	0.20	0.2	0.2	0.30	0.5
12	3.5	5.00	1	0.2	0.20	0.2	0.2	0.30	0.5
13	3.5	5.00	1	0.2	0.18	0.2	0.2	0.30	0.5
14	3.5	4.00	1	0.2	0.20	0.2	0.2	0.25	0.5

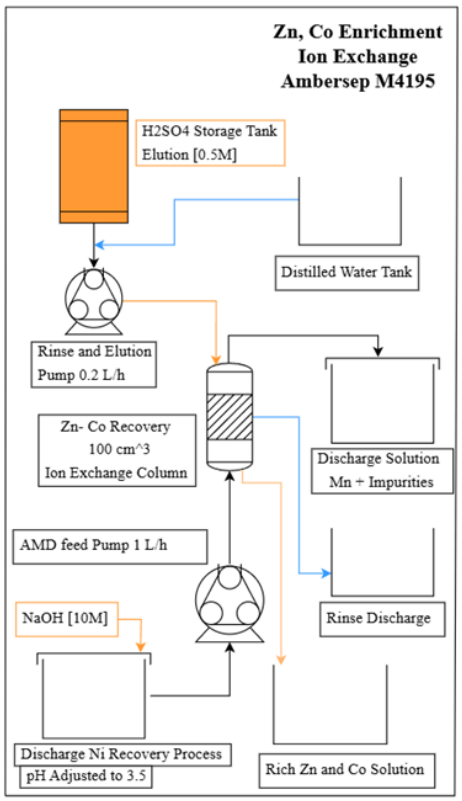

Figure 23. Flow Diagram Zinc and Cobalt Enrichment Stage Ion Exchange.

Results and Discussion

Table 24 shows the average AMD feed composition, which contained low concentrations of zinc (6.15 mg/L) and cobalt (3.06 mg/L). After ion exchange, the discharge solution exhibited residual concentrations of 0.12 mg/L Zn and 0.06 mg/L Co, corresponding to binding efficiencies of 98%

for both metals. Impurity binding remained below 3%, confirming the high selectivity of the resin as shown in Tables 25-26.

Table 24. Average AMD Concentration Used as Feed Solution for the Fourteen Large Volume Tests.

Description	Average Element Concentration and Standard Deviation (mg/L)									
Elements	Na	Mg	Al	Si	Ca	Fe	Mn	Co	Ni	Zn
Ion Exchange Feed Zn-Co	2669.46	478.38	12.97	102.52	241.74	5.72	133.36	3.06	0.37	6.15
STD	258.91	31.47	3.35	5.67	17.6	0.81	10.95	0.43	0.13	0.6

Table 25. Average Discharge Solution Concentration After Loading. Fourteen Tests.

Description	Average Elemental Concentration and Standard Deviation (mg/L)									
Elements	Na	Mg	Al	Si	Ca	Fe	Mn	Co	Ni	Zn
Ion Exchange Discharge Zn-Co	2627.61	475.79	13.31	102.77	243.04	5.67	130.85	0.06	0.07	0.12
STD	250.7	32.55	3.34	5.33	20.08	0.53	11.21	0.01	0.01	0.05

Table 26. Average Binding Percentage During the Loading Stage for Zinc and Cobalt, 14 Tests.

Description	Average Binding Percentage and Standard Deviation (%)									
Elements	Na	Mg	Al	Si	Ca	Fe	Mn	Co	Ni	Zn
Binding (%)	2.80%	1.50%	0.90%	3.10%	1.30%	15.70%	2.10%	97.90%	79.80%	98.00%
STD	3.20%	1.10%	0.40%	1.40%	0.80%	10.00%	1.30%	0.30%	6.60%	0.80%

The binding of elements of interest as well as impurities can be observed in Figures 24-25

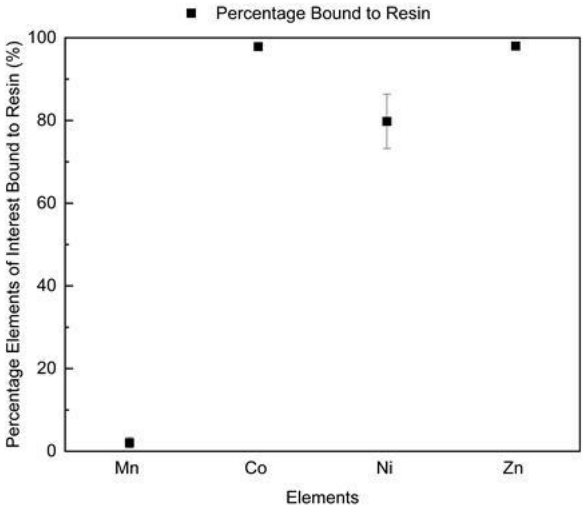

Figure 24. Binding Percentage of Elements of Interest to Resin M4195. 14 Tests.

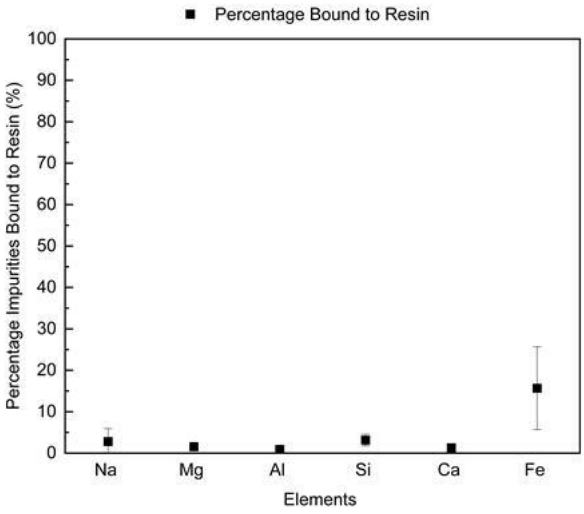

Figure 25. Binding Percentage of Elements of Impurities to Resin M4195. 14 Tests.

After elution with 0.5 M sulfuric acid, the enriched solution contained average concentrations of 46.8 mg/L cobalt and 90.8 mg/L zinc, representing enrichment factors of approximately 80× and 83×, respectively. Impurities such as sodium, magnesium, and iron were effectively minimized, while silica and calcium remained at moderate levels but are not expected to interfere with subsequent precipitation due to their high solubility under alkaline conditions. The concentration of the solution after elution as well as the enrichment factors for zinc and cobalt can be observed in Tables 27-28.

Table 27. Average Elements Concentration of Eluted Solutions. 14 Tests.

Description	Average Element Concentration and Standard Deviation (mg/L)									
Elements	Na	Mg	Al	Si	Ca	Fe	Mn	Co	Ni	Zn
Average Eluted	7.59	1.84	4.79	76.01	31.49	5.32	0.69	46.82	3.62	90.85
Std	1.90	0.36	1.70	8.54	5.69	0.46	0.43	9.69	1.19	16.83

Table 28. Ratio of Zinc and Cobalt to Other Elements and Enrichment Factor.

Ratio M+/Other Elements	
Zn before enrichment	0.0061
Zn after enrichment	0.5072
Zn enrichment factor	83.148
Co before enrichment	0.004
Co after enrichment	0.3218
Co enrichment factor	80.441

The optimal parameters found for the selective separation of zinc and cobalt can be summarized in the following bullet points

- Optimal feed pH: ≈ 3.5, ensuring high selectivity and capacity.
- Optimal rinse parameters: 200 mL distilled water per 100 cm^3 resin.
- Optimal elution: 0.5 M H_2SO_4, ≈ 340 mL, 30 min contact time.
- Average binding efficiency: ≈ 98% for Zn and Co.
- Enrichment factors: Zn ≈ 83×, Co ≈80×.
- Impurity binding <3%, confirming efficient separation and selectivity.

Zinc and Cobalt Precipitation

Following the ion exchange enrichment stage, zinc and cobalt were present in the eluted solution at significantly higher concentrations than in the original AMD. To recover these metals selectively, a two-step precipitation process was performed: (1) selective sulfide precipitation of zinc using sodium sulfide (Na_2S), and (2) hydroxide precipitation of cobalt using sodium hydroxide (NaOH). The overall objective was to produce separate high-purity zinc and cobalt solids while minimizing cross-contamination.

Sulfide Precipitation of Zinc

Effect of S^{2-} to Zn^{2+} Ratio

Methodology

Based on the solubility product constants of zinc sulfide (Ksp = 2×10^{-25}) and cobalt sulfide (Ksp = 4×10^{-21}), zinc sulfide is considerably less soluble and can therefore be selectively precipitated at neutral pH values. Six tests were conducted using 100 mL of zinc and cobalt enriched solution, where the molar ratio of S^{2-} to Zn^{2+} during precipitation was varied between 0.5 and 2.0. The initial pH of the solution was adjusted to between 7.1 and 7.3, and no pH control was applied after Na_2S addition. The sodium sulfide solution (0.41 M) was prepared from $Na_2S\cdot9H_2O$ reagent grade salt. Each test lasted 30 minutes at room temperature, after which the solutions were filtered through 0.45 µm paper and analyzed by ICP–MS. Table 29 shows the parameters used during this test.

Table 29. Effect of S^{2-} to Zn^{2+} Ratio During ZnS Selective Precipitation. Tests Parameters.

Test No	Ratio S^{2-}/Zn^{2+}	Initial pH	Final pH	Na_2S [M]	Precipitation Time (min)
1	0.5	7.18	7.42	0.41	30
2	0.8	7.1	7.48	0.41	30
3	1	7.18	7.64	0.41	30
4	1.25	7.24	7.8	0.41	30
5	1.5	7.25	8.07	0.41	30
6	2	7.27	9.01	0.41	30

Results and Discussion

The eluted solution composition used for this study is summarized in Table 30.

Table 30. Eluted Solution Concentration for ZnS Precipitation Study: Effect of S^{2-}-to-Zn^{2+} Ratio.

Description	Average Elements Concentration (mg/L)									
Elements	Na	Mg	Al	Si	Ca	Fe	Mn	Co	Ni	Zn
Eluted Solution	9.11	2.24	4.93	78.09	39.24	5.53	0.48	36.62	4.15	78.75

As illustrated in Figure 26, zinc precipitation increased with higher S^{2-}/Zn^{2+} ratios. At ratios of 0.5 and 0.8, zinc removal was 30% and 50%, respectively, with minimal co-precipitation of other metals. Increasing the ratio to 1.0–1.25 resulted in higher zinc precipitation (64–79%) while maintaining good selectivity. At ratios of 1.5 and 2.0, zinc removal reached 94% and 100%, respectively, but cobalt co-precipitation increased to 20% and 52%. These results confirm that controlling the sulfide-to-zinc ratio enables partial separation of zinc from cobalt, balancing yield, and selectivity.

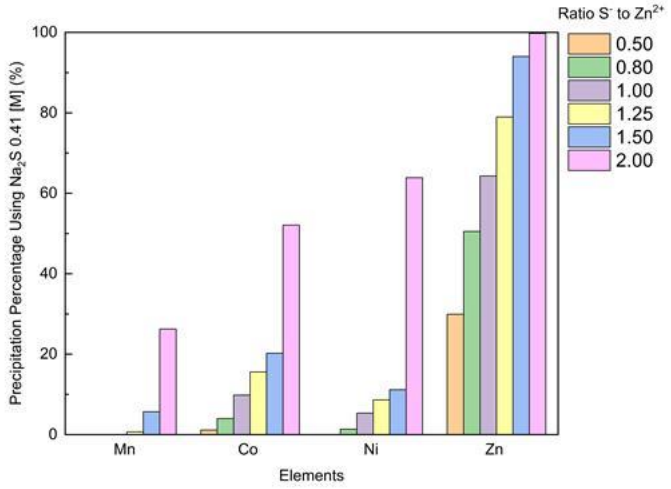

Figure 26. Precipitation Percentage of Elements of Interest During ZnS Precipitation Study: Effect of S^{2-} to Zn^{2+} Ratio.

Effect of Final Precipitation pH

Methodology

To evaluate the influence of final pH, three additional tests were performed at varying equilibrium pH values using 100 mL of enriched solution. The S^{2-}/Zn^{2+} ratio and pH limits were adjusted according to Table 31. The pH was controlled by adding 0.5 M H_2SO_4 dropwise, and each test lasted 30 minutes at room temperature.

Table 31. Effect of Ratio S^{2-} to Zn^{2+} and Maximum pH During Precipitation.

Test No	Ratio S^{2-}/Zn^{2+}	Initial pH	Final pH	Na2S [M]	Precipitation Time (min)
1	1.5	5.4	7.5	0.41	30
2	1.5	3.5	8	0.41	30
3	2	3.99	8.7	0.41	30

Results and Discussion

The results in Figure 27 show that zinc precipitation exceeded 80% when the final pH was above 8.0. However, selectivity decreased at higher pH values, as cobalt, nickel, and manganese began to co-precipitate. Co-precipitation of cobalt remained below 20% up to pH 8.8, while nickel and manganese stayed below 10%. Therefore, optimal conditions were identified at a final pH between 8.0 and 8.8 and a molar ratio S^{2-}/Zn^{2+} between 1.5 and 2.0, which maximized zinc recovery while maintaining acceptable selectivity.

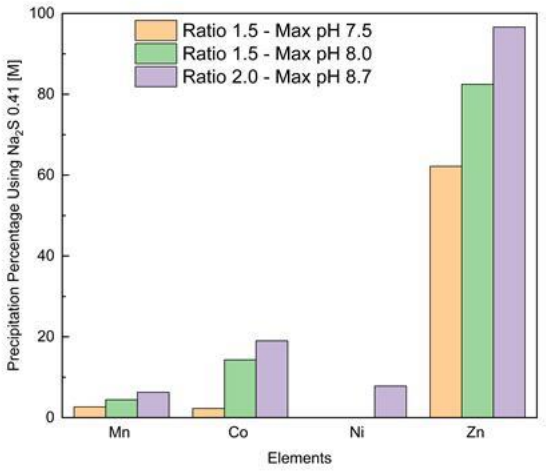

Figure 27. Effect of Maximum pH During ZnS Precipitation Using Na_2S.

Zinc Sulfide Solids Production

Methodology

To generate sufficient ZnS solids for analysis, five eluted solutions from the previous stage were combined. The precipitation was conducted using 0.41 M Na_2S at room temperature, with an S^{2-}/Zn^{2+} ratio of 2.0 and a maximum pH limited to 8.1. The suspension was stirred for 30 minutes, filtered through 0.45 µm paper, and the solids were oven-dried at 60 °C for 48 hours. Table 32 presents the precipitation parameters, and Table 33 presents the results of this precipitation.

Table 32. Zinc Sulfide Precipitation Parameters.

Initial Volume (L)	Final Volume (L)	Initial pH	Final pH	Precipitation Time (min)	Reagent	Ratio S^{2-}/Zn^{2+}
1.68	1.66	4.46	8.1	30	0.41 M Na_2S	2

Table 33. Zinc Sulfide Precipitation Results, Solution Concentrations, and Precipitation Percentages.

Description	Average Elements Concentration (mg/L)									
Elements	Na	Mg	Al	Si	Ca	Fe	Mn	Co	Ni	Zn
Enriched Zinc + Cobalt Solution	6435.95	2.96	7.29	36.95	36.7	3.93	1.47	46.87	3.54	93.71
After Na_2S Precipitation	6591.87	2.13	2.55	37.71	29.14	3.7	1.28	34.38	3.12	3.54
Precipitation (%)	Na	29%	65%	NA	21%	7%	14%	27%	13%	96%

The process achieved 96% zinc removal, confirming effective ZnS precipitation under controlled pH and stoichiometry. Co-precipitation of cobalt remained moderate at 27%, while most impurities precipitated below 30%. The dried ZnS solids displayed a pale gray color typical of zinc sulfide Figure 28.

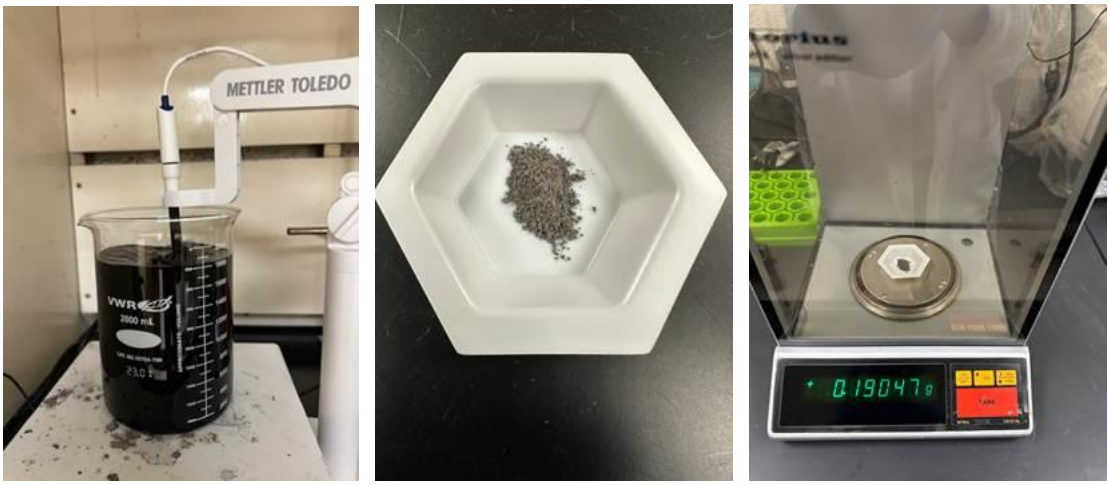

Figure 28. ZnS Precipitation. Left: Reagent Addition. Center: Dried Solids. Right: Dried Solids Weight.

Zinc Solids Purity

The dried zinc sulfide solids were homogenously mixed in a mortar. A representative sample of 0.1321 g was digested using a combination of 8 mL of nitric acid and 8 mL of hydrochloric acid, with a temperature of 50°C maintained during the digestion for a total time of 4 hours. After that, 34 mL of distilled water was added for dilution. The digested liquor was filtered using a 0.45 µm filter paper on a vacuum filter, and its volume was measured at 49 mL using a volumetric column. A sample of the liquor was sent for ICP-MS analysis, and the results are shown in the table below.

Table 34. Elements of Interest and Main Impurities Concentration in Digested Liquor of Zinc Solids.

Description	Average Elements Concentration (mg/L)										
Elements	Na	Mg	Al	Si	Ca	Fe	Mn	Co	Ni	Cu	Zn
Zinc Digested Solids	143.4	1.6	6.6	11.6	28.9	6.4	0.2	134.4	5.3	0.1	1033.0

Figure 29. Zinc Sulfide Solids Digestion. Left: Mortar Mixing. Center: Weight of Digested Solids. Right: Solids for Digestion.

Using a similar equation to the one used for nickel but adapted for zinc, the weight of zinc in the digested liquor was calculated as 0.0506g, and the nickel purity was calculated as follows:

$$Zinc\ Purity = \frac{0.0506g}{0.1321\ g} = 38.32\%\ Zinc$$

Additionally, if all the zinc precipitated as zinc sulfide, the purity can be calculated as follows:

$$Zinc\ Sulfide\ Purity = \frac{Zinc\ Purity\ \%}{0.671} = 57.09\%$$

Hydroxide Precipitation of Cobalt

Effect of Equilibrium pH

Methodology

After zinc removal, the remaining solution was treated with sodium hydroxide to precipitate cobalt as cobalt hydroxide ($Co(OH)_2$). Tests were conducted at equilibrium pH values of 9.4, 9.9, 10.2, and 11.0, using a 2 M NaOH solution and a fixed OH^-/Co^{2+} ratio of 1.5. All tests were carried out at room temperature with a precipitation time of 60 minutes and the parameters shown in Table 35.

Table 35. Effect of Equilibrium pH on Cobalt Hydroxide Precipitation. Tests Parameters.

Test No	Initial pH	Final pH	Ratio OH^-/Co^{2+}	Reagent
1	7.3	9.4	1.5	2.0 M NaOH
2	4.8	9.9	1.5	2.0 M NaOH
3	7.2	10.2	1.5	2.0 M NaOH
4	7.7	11	1.5	2.0 M NaOH

Results and Discussion

As shown in Figure 30, cobalt hydroxide precipitation efficiency exceeded 90% at pH ≥10.0, reaching 96% at pH 11.0. Although other elements also precipitated above 80%, their initial concentrations were significantly lower than cobalt's, so selectivity was not a concern at this point. The pH of 11.0 was identified as optimal for maximizing cobalt recovery.

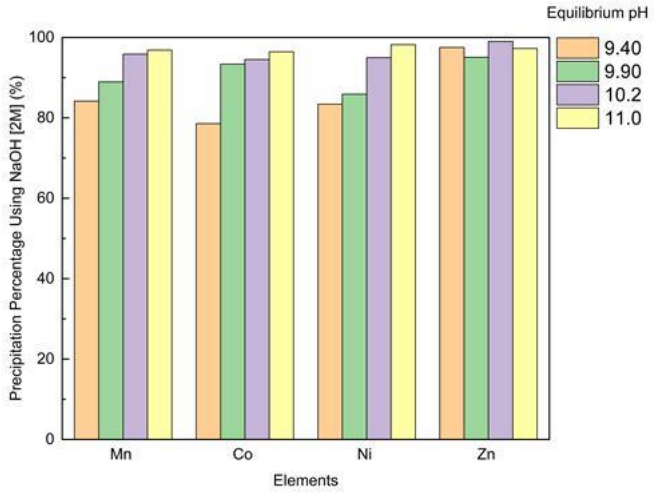

Figure 30. Effect of Equilibrium pH on the Precipitation of Elements of Interest Using 2 M NaOH.

Cobalt Hydroxide Solids Production

Methodology

The filtrate from the zinc sulfide precipitation was used as feed. Precipitation was carried out at 11.2 pH, with magnetic stirring at 400 rpm for 60 minutes using 2 M NaOH. The solids were filtered through 0.45 µm paper and dried at 60 °C for 48 hours. Test parameters are shown in Table 36 and the precipitation results, including the solution concentration before and after precipitation and the precipitation percentages, are displayed in Table 37.

Table 36. Cobalt Hydroxide Solids Precipitation Parameters.

Initial Volume (L)	Final Volume (L)	Initial pH	Final pH	Precipitation Time (min)	Reagent	Ratio OH/Co^{2+}
1.66	1.64	7.5	11.2	60	2 M NaOH	1.5

Table 37. Cobalt Hydroxide Precipitation Results, Solution Concentrations, and Precipitation Percentages.

Description	Average Elements Concentration (mg/L)									
Elements	Na	Mg	Al	Si	Ca	Fe	Mn	Co	Ni	Zn
Enriched Cobalt Solution	6591.87	2.12	2.55	37.7	29.13	3.7	1.28	34.38	3.11	3.53
After NaOH Precipitation	6661.44	2.15	4.31	38.53	34.22	4.1	0.54	0.23	0.05	0.09
Precipitation (%)	NA	0%	0%	0%	0%	0%	58%	99%	98%	97%

Cobalt, nickel, and zinc precipitated at rates above 97%, confirming efficient recovery. Manganese showed moderate precipitation (58%), while major impurities such as silica and calcium remained soluble. Images of the precipitation process are shown in Figure 31.

Figure 31. Cobalt Hydroxide Precipitation. Left: Enriched Solution + NaOH. Center: Solids Filtration. Right: Dried Solids.

Cobalt Solids Purity

The precipitated cobalt hydroxide solids were homogeneously mixed in a mortar, and 0.10824 g were digested using 15 mL of 70% nitric acid (HNO_3). The digestion process was carried out for 4 hours at 50°C. After that, 35 mL of distilled water was added for dilution. The digested liquor was filtered using a 0.45 µm filter paper, and its volume was measured using a glass column. A representative sample of the liquor was sent to ICP-MS, and the results are shown in Table 38 below.

Table 38. Elements of Interest and Main Impurities Concentration in Digested Liquor of Cobalt Solids.

Description	Average Elements Concentration (mg/L)										
Elements	Na	Mg	Al	Si	Ca	Fe	Mn	Co	Ni	Cu	Zn
Cobalt Digested Solids	231.0	4.2	4.4	14.6	33.8	4.0	4.2	640.8	57.5	0.0	62.0

Figure 32. Cobalt Hydroxide Solids Digestion. Left: Mortar Mixing. Center: Weight of Digested Solids. Right: Solution During Digestion.

Using the ICP-MS results and the final volume of the digested liquor, which is 49 mL, the weight of cobalt in the liquor was calculated to be 0.0314 g. The cobalt purity was calculated as follows:

$$Cobalt\ Purity = \frac{0.0314g}{0.1082\ g} = 30.15\%\ Cobalt$$

In the case of cobalt hydroxide as the mineralogy of the product, the purity can be calculated as follows:

$$Cobalt\ Hydroxide\ Purity = \frac{Cobalt\ Purity\ \%}{0.6344} = 47.53\%$$

2.4 REEs Recovery

Selective preconcentration

After the Zn and Co ion exchange the discharge is used for REEs pre-concentration This stage aimed to selectively precipitate the REEs using NaOH. To subsequently redissolve these solids using H_2SO_4 and produce a leachate with a higher REEs concentration and reduced impurity content.

Methodology

Based on the findings from the stage-wise precipitation experiments and the known precipitation behavior of various metals, it was determined that most rare earth elements tend to precipitate within the pH range of 5.0 to 9.0. Beyond pH 9.0, impurity metals such as magnesium, manganese, and zinc are more likely to precipitate, potentially contaminating the target solid fraction.

Therefore, NaOH (2 mol/L) was incrementally added to the pH 5 discharge solution using a disposable plastic transfer pipette until a final pH of 9 was reached. The mixture was stirred at 200 rpm for 2 hours at room temperature to promote complete precipitation (Figure 33).

Figure 33. Selective precipitation of REEs.

Following precipitation, the sample was filtered using a pressure filtration system with a 0.45 µm pore-sized filter paper. The collected solids containing most of the REEs and some residual impurities were dried overnight and stored for redissolution experiments (Figure34).

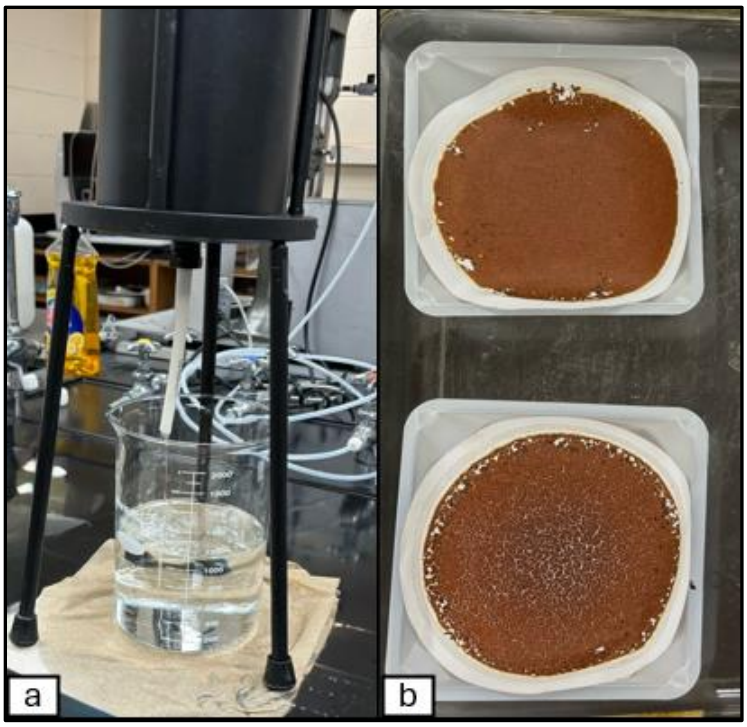

Figure 34. Pressure filtration system (a), collected precipitates from pH 5 to 9 (b).

Results and Discussion

The data collected from this selective precipitation process demonstrated that the transition from the liquid to the solid phase was highly efficient for rare earth elements, with a total recovery of approximately 97%. In comparison, only 12% of magnesium, 11% of aluminum, 11% of iron, 19% of manganese, and 32% of zinc were precipitated during this step. These values confirm the selectivity of the precipitation process toward rare earth elements. It was also observed that the concentrations of sodium and silicon in the supernatant increased slightly, likely due to the presence of these elements, as in the 2M sodium hydroxide reagent used for pH adjustment.

This selective precipitation experiment was performed in triplicate to ensure reproducibility, and the results are summarized in table 39. The table presents the concentrations of metals remaining in the supernatant after precipitation between pH 5.0 and 9.0, demonstrating that most of the critical minerals targeted for recovery were transferred into the solid phase. In contrast, impurity metals were retained in the liquid phase.

Table 39. The elemental composition of solution after reaching pH 9.

Description	**Average concentration (mg/L)**									
Major ions	**TREEs**	**Mg**	**Mn**	**Al**	**Si**	**Na**	**Fe**	**Zn**	**Ni**	**Co**
pH= 9 AMD	0.13	364.36	118.89	6.37	109.38	373.98	2.26	3.84	2.8	3.04
STD	0.07	14.50	7.77	2.37	20.39	30.66	0.95	0.21	0.28	0.7

REEs redissolution and preconcentrated solution production.

Methodology

Redissolution tests were performed using a solid-to-liquid (S/L) ratio of 1:15, where 1 g of dried precipitate was mixed with 15 mL of deionized water. After mixing, the leachate had an initial pH of approximately 6.7. Sulfuric acid 50% w/w was used as the leaching agent to dissolve the REEs. The reaction temperature was maintained at 50 °C, and after reaching the target pH of 0.5, the solution was stirred with a magnetic stirrer at 200 rpm for 30 minutes to ensure effective leaching. After the reaction period, a vacuum filtration was performed to separate the supernatant from the remaining solids. Now enriched with REEs, the supernatant was collected for further processing and analysis.

Results and Discussion

The final composition of the resulting leachate enriched in rare earth elements and with lower impurities is in table 40.

Table 40. The elemental composition of the preconcentrated solution after redissolution.

Description	**Average concentration (mg/L)**						
Major ions	**TREEs**	**LREEs**	**HREEs**	**Sc**	**Y**	**La**	**Ce**
Preconcentrated solution	1963.70	1206.44	757.26	0.99	461.15	256.63	486.93
STD	-	-	-	0.12	32.40	26.28	28.88
Major ions	**Pr**	**Nd**	**Sm**	**Eu**	**Gd**	**Tb**	**Dy**
Preconcentrated solution	76.31	315.68	70.90	17.97	90.69	14.74	78.47
STD	5.66	38.42	7.77	1.52	7.87	1.58	8.39
Major ions	**Ho**	**Er**	**Tm**	**Yb**	**Lu**	**Mg**	**Al**
Preconcentrated solution	15.44	41.84	4.98	26.94	4.03	5179.63	5316.21
STD	1.49	3.69	0.48	2.11	0.40	125.38	267.53
Major ions	**Ca**	**Fe**	**Mn**	**Ni**	**Co**	**Zn**	**-**
Preconcentrated solution	197.50	39.20	11527.49	3.24	3.54	2.26	-
STD	17.25	3.71	636.22	0.28	1.12	0.39	-

The TREEs concentration increased from 5.22 mg/L in the raw sample to 1963.70 mg/L in the redissolved solution. The ratios of TREEs to other elements before and after the redissolution are shown in table 41 When comparing these two ratios, we observed that the enrichment factor of TREEs was approximately 20 times for the preconcentration stage.

Table 41. Ratio of TREEs to Other Elements for Solutions Before and After Preconcentration.

Ratio M+/Other Elements	
TREEs before preconcentration	0.0033
TREEs after preconcentration	0.0657
Enrichment factor	20.20

Rare earth element preconcentrated solution production.

Methodology

To simulate the experimental leachate so that a sufficient amount of samples can be created for ion exchange studies, an artificial REE solution was prepared by replicating the elemental concentrations of the solution produced after the redissolution. Table 42 lists the target elements, the chemical used for each, and their respective purities.

Table 42. Elements used for preconcentrated AMD preparation.

Element	Chemical	purity
Mg	$Mg(O_3)_2{\cdot}6H_2O$	95.00%
Al	$AlCl_3$	99.00%
Ca	$Ca(NO_3)_2{\cdot}4H_2O$	99.30%
Sc	$Sc(NO_3)_2$	99.30%
Fe	$FeCl_3$	98.00%
Mn	$Mn(NO_3)_2 \cdot 4H_2O$	98.00%
Y	$Y(NO_3)_3 \cdot 6H_2O$	99.80%
La	$La(NO_3)_3{\cdot}\ 6H_2O$	99.99%
Ce	$Ce(NO_3)_3 \cdot 6H_2O$	99.00%
Pr	$Pr(NO_3)_3{\cdot}\ 6H_2O$	99.90%
Nd	$Nd(NO_3)_3 \cdot 6H_2O$	99.90%
Sm	$Sm(NO_3)_3 \cdot 6H_2O$	99.90%
Eu	$EuO_3{\cdot}\ 6H_2O$	99.99%
Gd	$Gd(NO_3)_3 \cdot 6H_2O$	99.90%
Tb	$Tb(NO_3)_3{\cdot}6H_2O$	99.90%
Dy	$Dy(NO_3)_3{\cdot}\ 10H_2O$	99.90%
Ho	$Ho(NO_3)_3 \cdot 5H_2O$	99.90%
Er	$Er(NO_3)_3 \cdot 5H_2O$	99.90%
Tm	$TmCl_3{\cdot}6H_2O$	99.99%
Yb	$Yb(NO_3)_3{\cdot}5H_2O$	99.99%
Lu	$Lu(NO_3)_3 \cdot 6H_2\ O$	99.99%

The mass of each salt required was calculated using the following equation:

$$Mass\ of\ chemical\ (g) = \frac{V \times \text{C target} \times \text{Mchemical}}{\text{Melement} \times 1000} \quad (6)$$

Where:

- C_{target} = target concentration of the element (mg/L)
- V = volume of the solution to be prepared (L)
- $M_{chemical}$ = molar mass of the salt (g/mol)
- $M_{element}$ = molar mass of the element (g/mol)

After calculating the required mass of each salt compound, approximately 70% of the total final volume of distilled water was heated to 50 °C. The pH of the solution was adjusted to 2 using concentrated H_2SO_4 to facilitate the complete dissolution of all metal salts. Each compound was added sequentially, stirring at 120 rpm for 5 minutes between additions to ensure thorough dissolution before introducing the next element.
21 elements (Figure 35) were included in the artificial mixture to replicate the composition of the pre-concentrated solution obtained in the earlier precipitation and redissolution stages.

Figure 35. Visual appearance of metal compounds used to replicate the preconcentrated sample.

Once all compounds were added, the solution was brought up to the final volume with additional distilled water. The mixture was then stirred continuously for 2 hours to ensure homogeneity. A picture of the final prepared solution is shown below (Figure 36).

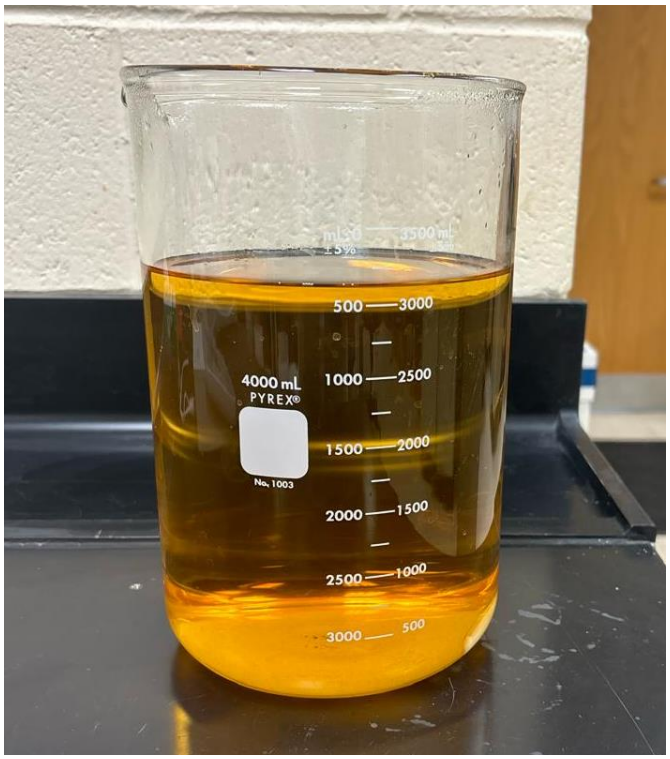

Figure 36. Preconcentrated REE ion exchange feedstock solution (artificial solution).

REEs Ion exchange and recovery

After the REE preconcentrated solution was made, the ion exchange experiments were conducted. The ion exchange process was divided into two main stages: loading and elution. During the loading stage, the pre-concentrated REE solution was passed through the column, allowing target ions to bind to the resin while most non-target species remained in the effluent.

In the elution stage, an eluant was introduced into the column to displace the sorbed REEs ions from the resin. This process released the REEs into the liquid phase, resulting in an eluted solution suitable for downstream recovery.

Resin Loading

Methodology

During the loading stage a laboratory-scale column setup was used and designed to enable continuous solution flow through the resin bed. This configuration ensures controlled contact time between the ions in solution and the functional groups on the resin, facilitating ion exchange. The experimental setup is shown in Figure 37.

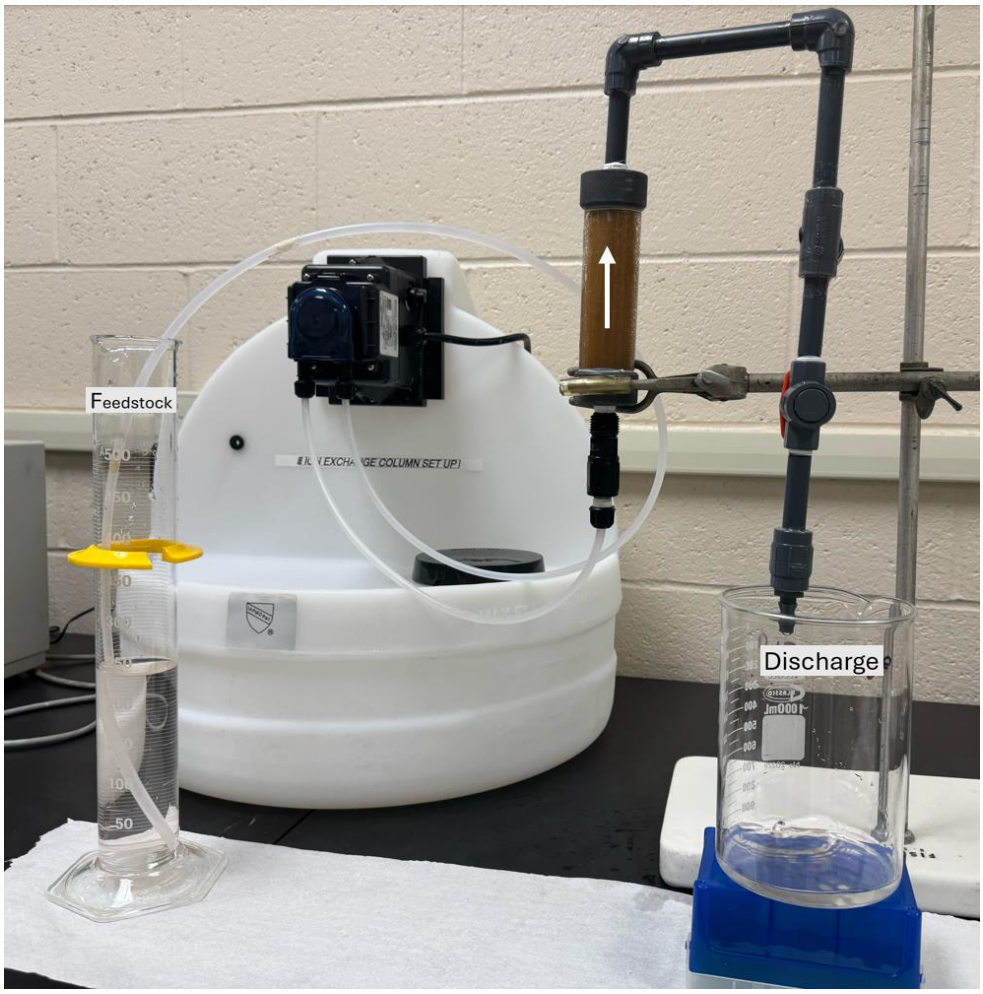

Figure 37. Ion exchange loading column set up.

The feedstock for the ion exchange separation tests was the leachate obtained from the redissolution of the solids precipitated within the pH range of 5–9. On the left side of the setup (Figure 37), a graduated cylinder was used to hold the feed solution, which was connected to a peristaltic pump. The pump was attached to a vertical glass column packed with the ion exchange resin (Dowex 50WX8), and the column outlet was connected via a PVC tube to a receiving beaker for collecting effluent. The peristaltic pump enabled control of the flow rate during the experiments. All tests were performed at ambient temperature (20 ± 5 °C).

The volume of feed solution used in each test was fixed at 300 mL, based on preliminary trials that confirmed this volume was appropriate for the resin's loading capacity. The two primary variables investigated for their influence on ion exchange selectivity were pH and flow rate.

The pH of the solution has an important impact on the performance of ion exchange resins. For this case, as the REEs are the target elements, keeping the solution below three would be essential since this is where REEs are highly soluble and fully ionized. Styrene and divinylbenzene (DVB)-based resins like Dowex 50WX8 operate well at low pH (<3), making them suitable for the recovery of REEs from a feedstock like the one used for this study. Previous studies that used

50WX8 used a pH below 3.4 to recover REEs (Felipe, Batista, et al., 2021). Consequently, different pHs were selected for the testing, and all were <3; more precisely, the sample used as feedstock varied in the pH from 0.5 to 3.

Contact time is another critical parameter to test during ion exchange separation processes. It represents the feedstock's time in the ion exchange bed (Lenntech, n.d.; Pehlivan & Altun, 2006). It affects the recovery since the ions of interest need to reach active sites in the resin bed and have enough time to reach equilibrium (Felipe, Batista, et al., 2021; Masry et al., 2022). Different flow rates were tested, and the flow rate selection will be based on the pumps available for the ion exchange setup. Flow rates were varied between 1 and 10 liters per hour (L/h).

A summary of the experimental conditions for the ion exchange tests is provided in table 43. These experiments aimed to evaluate the performance of the resin in selectively capturing REEs from the synthetic leachate under different operating parameters.

Table 43. Ion exchange loading test conditions.

Test conditions			
Feed volume (ml)	**Feed pH**	**Loading Flowrate (l/h)**	**Resin Volume (cm^3)**
300	0.5 to 3	1 to10	100

Results and Discussion

To ensure a good recovery of rare earth elements during ion exchange, a study was conducted to evaluate the resin's sorption capacity and to determine the optimal feedstock volume for loading experiments. This test involved passing one liter of feedstock solution through the resin column at a flow rate of 2 liters per hour, maintained at room temperature and a constant pH of 1.5. Effluent samples were collected at 100 milliliter intervals to monitor sorption performance over time and identify the volume at which the resin’s capacity began to decline.

As shown in Figure 38, the resin exhibited good recovery for rare earth elements during the initial phase of the experiment. Specifically, more than 97% of total rare earth elements were retained by the resin during the first 300 milliliters of feedstock loading. However, beyond this point, the resin’s sorption efficiency decreased, indicating saturation. Based on these results, a feedstock volume of 300 milliliters was selected as the optimal loading volume for subsequent ion exchange experiments.

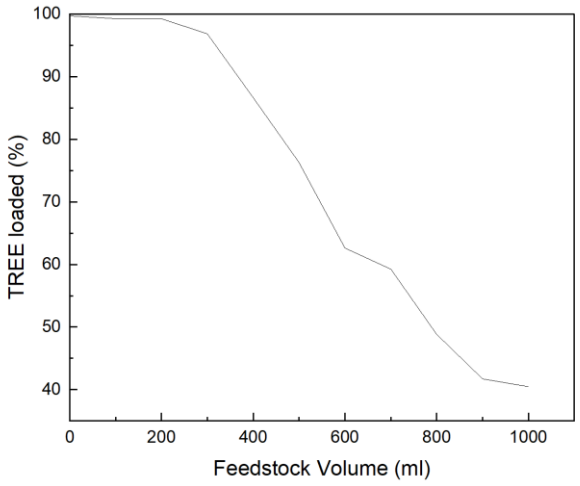

Figure 38. TREE Loading capacity.

A factorial experimental design was implemented to assess the influence of key process parameters on loading efficiency. The two variables examined were the pH of the feedstock solution and the flow rate. The selected pH values ranged from 0.5 to 3.0, while the flow rates varied between 1 and 10 liters per hour. A fixed feedstock volume of 300 milliliters was used for all experiments. A summary of the experimental conditions is presented in table 44.

Table 44. Factorial design for REE loading.

Run	Flow speed (L/h)	pH
1	1	0.5
2	1	1.5
3	1	3
4	2	0.5
5	2	1.5
6	2	3
7	3.5	0.5
8	3.5	1.5
9	3.5	3
10	10	0.5
11	10	1.5
12	10	3

A factorial experimental design was implemented to assess the influence of key process parameters on loading efficiency. The two variables examined were the pH of the feedstock solution and the flow rate. The selected pH values ranged from 0.5 to 3.0, while the flow rates varied between 1 and 10 liters per hour. A fixed feedstock volume of 300 milliliters was used for all experiments. A summary of the experimental conditions is presented in figure 39.

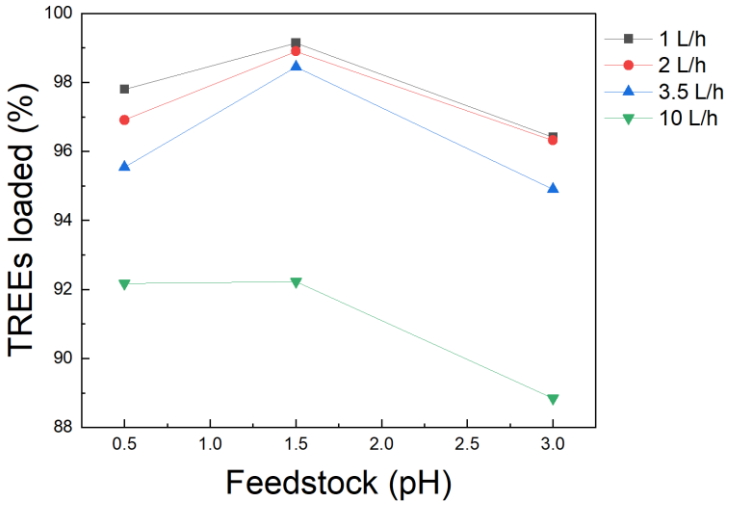

Figure 39. TREEs loaded into the resin bed.

Elemental concentrations in the feedstock solution and the discharge were analyzed to calculate the percentage of rare earth elements and major impurities that the ion exchange resin retained. Figure 39 presents the total rare earth elements loaded onto the resin during all experiments. In this figure, each line represents the flow rate used in the respective test.
The highest loading efficiency was achieved at 1 liter per hour flow rate and a feedstock pH of 1.5. A similar trend was observed across all flow rates: as the flow rate increased, the loading of total rare earth elements decreased, likely due to the reduced residence time of the solution within the resin bed. Likewise, when considering the effect of pH, the maximum loading for all flow rates occurred at a feedstock pH of 1.5.

The results were analyzed using feedstock pH to examine impurity loading. The first set of data corresponds to experiments conducted at pH 0.5, representing this parameter's lowest level. The results, presented in figure 40, show the combined loading behavior of total rare earth elements and major impurities.

At pH 0.5, TREEs loading ranged from 92.17% to 97.8%, with the highest loading achieved at 1 liter per hour flow rate. Impurity loading exhibited the following ranges: 46% to 59% for magnesium, 68% to 74% for aluminum, showing increased loading at higher flow rates; 46% to 82% for iron; 51% to 82% for calcium; and 56% to 69% for manganese. The resin demonstrated relatively low affinity for nickel and silicon. Overall, these findings indicate that, at pH 0.5, lower flow rates favor higher TREEs loading while minimizing impurity loading. However, the data also highlights that while the resin exhibits affinity for rare earth elements, a complex feedstock with significant impurity content challenges the resin’s selectivity.

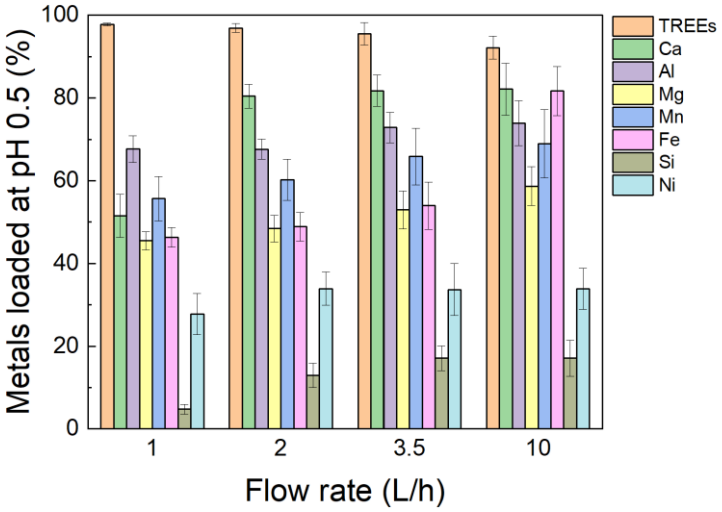

Figure 40. Loading results at pH 0.5.

As shown in Figure 41, the TREEs loading ranged from 92% to 99% across all experiments conducted with feedstock at pH 1.5, showing a higher loading efficiency compared to pH 0.5. However, increased impurity loading for all analyzed elements accompanied this improvement in rare earth element loading.
At pH 1.5, impurity loading ranged from 32% to 76% for magnesium, 61% to 84% for aluminum, 41% to 86% for iron, and 48% to 72% for manganese. A similar trend was observed at pH 0.5, where impurity loading increased with higher flow rates.

These results suggest that while pH 1.5 slightly enhances rare earth element loading, it also promotes more loading of impurities, potentially needing more downstream purification steps to achieve the desired product purity.

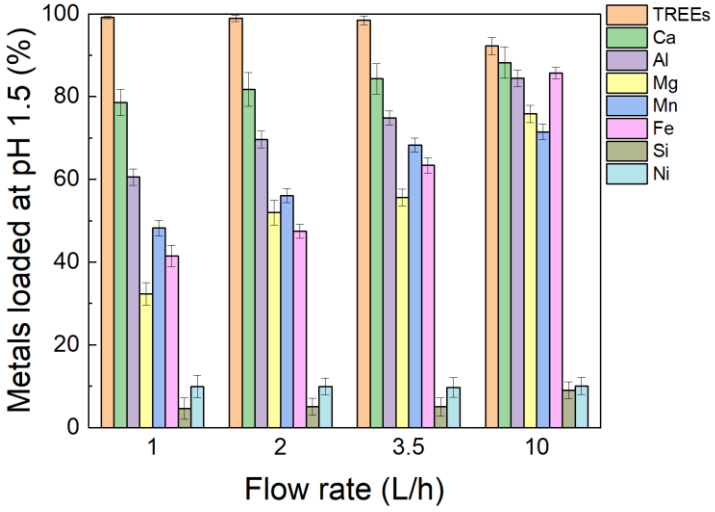

Figure 41. Loading results at pH 1.5.

Figure 42 illustrates the elemental loading behavior when the feedstock solution was adjusted to pH 3.0. TREEs loading ranged from 89% to 96% at this pH, representing a lower loading efficiency than the other pH levels tested.
Impurity loading at pH 3.0 fell within the following ranges: 48% to 60% for magnesium, 65% to 74% for aluminum, 64% to 79% for iron, and 60% to 67% for manganese. The resin continued to exhibit only mild affinity for nickel and silicon. Notably, the impurity loading trend at pH 3.0 differed from that observed at lower pH values. When the flow rate was increased to 10 liters per hour, impurity loading decreased for all measured elements. At an intermediate flow rate of 3.5 liters per hour, aluminum, magnesium, manganese, and calcium impurity loading decreased. In contrast, iron loading increased compared with lower pH conditions.
Overall, while the resin consistently preferred REEs over impurities, the recovery efficiency at pH 3.0 was lower than that achieved at the more acidic feedstock pH values.

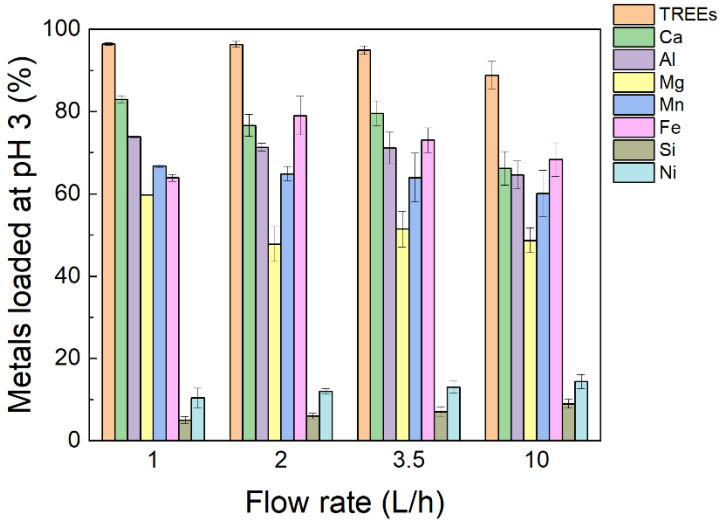

Figure 42. Loading results at pH 3.

Resin regeneration

After loading the resin, a series of stages were carried out to remove the remaining bound elements following elution. The first stage was rinsing, during which weakly bound impurities and residual elements were removed by passing deionized water through the column. This step used a volume equivalent to four times the resin bed, 450 mL at a flow rate of 0.5 L/h. Following rinsing, the second stage used a stronger acid, specifically 2 M sulfuric acid. In this case, the resin bed volume was applied twice at a flow rate of 2 L/h. Finally, another three times the resin bed volume of deionized water was used to bring the resin back to its natural pH. These conditions allowed the same resin to be reused throughout all tests, and the recovery trends during the first and the replicate tests of loading and elution stages remained consistent. This suggests stable resin

performance; however, further in-depth studies are needed to evaluate resin regeneration efficiency and long-term usability.

Elution

Methodology

Following the ion exchange loading stage, elution experiments were conducted to recover the rare earth elements loaded onto the resin. Sulfuric acid was selected as the eluent. The elution setup was similar to the loading configuration, with one key modification: the flow direction through the column was reversed to promote enhanced contact between the eluant and the loaded resin, improving desorption efficiency. In this configuration (figure 43), the H_2SO_4 solution was placed in a graduated cylinder and pumped upward through the loaded resin column. The resulting eluted solution was collected in a beaker and contained the REEs released from the resin.

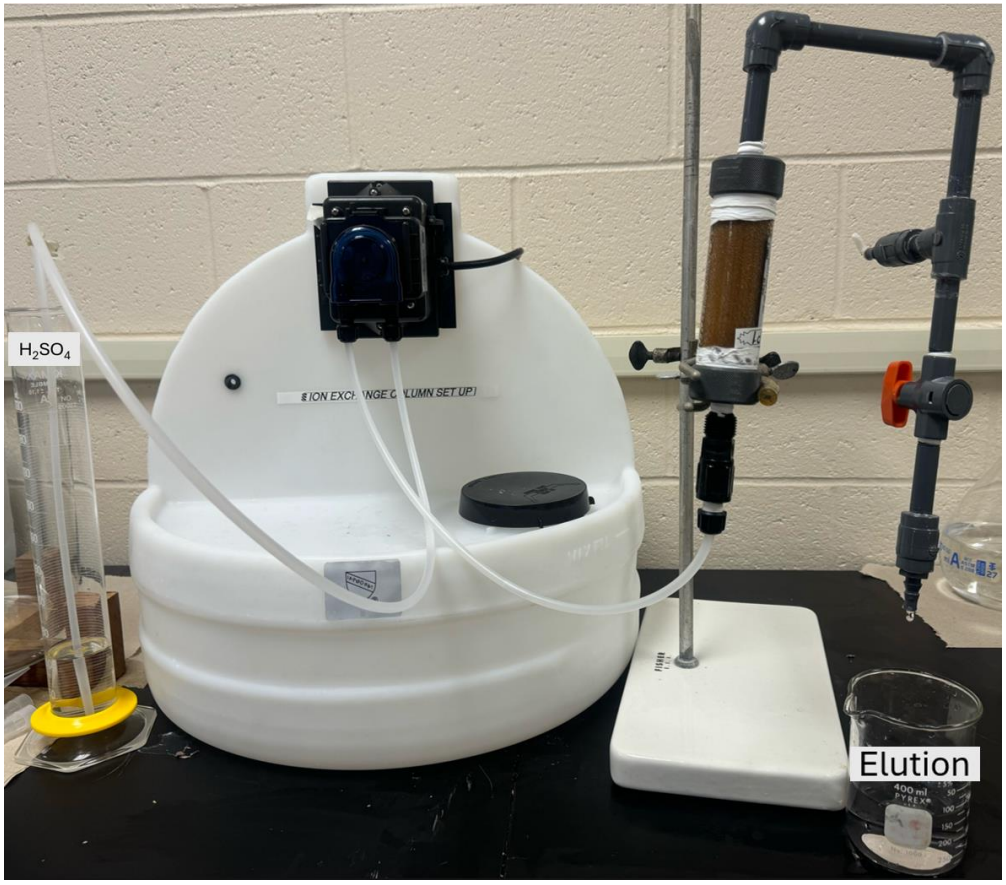

Figure 43. Ion exchange elution column set up.

Contact time, defined as the duration the eluant interacts with the resin, has been reported in the literature as a critical parameter influencing the efficiency of ion exchange elution processes. It directly affects the extent to which the elements of interest are desorbed from the resin matrix and recovered in the elution phase (Freiling, 1955; Jeffrey et al., 2010; Berrios et al., 2013; Yamamoto

et al., 1983a; Yamamoto et al., 1983b). Insufficient contact time may lead to incomplete elution, while excessively long contact times can result in unnecessary dilution and increased processing time. In practical applications, contact time is typically controlled by adjusting the eluent flow rate through the column. Therefore, this study will conduct a series of tests at varying flow rates to evaluate the impact of contact time on elution efficiency.

Another crucial parameter to consider is the eluant strength, which refers to the concentration of the chemical agent used for desorbing the target elements from the resin. The strength of the eluant influences the ion exchange reactions, affecting both the kinetics and thermodynamics of the desorption process. For acidic eluants, such as sulfuric acid, an increase in concentration typically results in a decrease in solution pH, thereby increasing the overall acidity of the system (Freiling, 1955; Martin & Martin, 2013; Schmidt et al., 2014). Consequently, this study will explore a range of eluant concentrations to assess their effect on the desorption behavior and recovery efficiency of the elements of interest.

For each experiment, 150 mL of sulfuric acid was used as the eluent. To evaluate optimal conditions for maximizing REE recovery, experiments were conducted by varying two parameters: acid concentration and flow rate. The H_2SO_4 concentrations tested were 1 M, 2 M, and 3 M. Flow rates ranged from 0.5 to 3.5 liters per hour (L/h), depending on the capabilities of the laboratory-scale pump used.

A summary of the elution conditions tested is provided in table 44.

Table 44. Ion exchange loading test conditions.

Test conditions			
Eluant volume (ml)	Acid concentration (M)	Elution Flowrate (L/h)	Resin Volume (cm^3)
150	1-3	0.5 to 3.5	100

Results and Discussion

Loaded ion exchange resin. An experimental design was employed to study the effects of acid concentration and flow rate while keeping a fixed eluant volume of 150 milliliters. The selected sulfuric acid concentrations ranged from 1 to 3 molar, and the flow rates were set between 0.5 and 4 liters per hour. A summary of the experimental conditions is presented in table 45.

Table 45. Factorial design for REEs elution.

Run	**Flow speed (L/h)**	**H_2SO_4 concentration (Mol/l)**
1	0.5	1
2	0.5	2
3	0.5	3
4	1.0	1
5	1.0	2

6	1.0	3
7	3.0	1
8	3.0	2
9	3.0	3
10	4.0	1
11	4.0	2
12	4.0	3

Elemental concentrations in the eluant before passing through the resin, the eluted solution, and the calculated mg loaded to the resin from previous loading testing were analyzed using ICP-MS to calculate the percentage of rare earth elements and major impurities eluted from the resin.

The results shown in figure 44 represent the elution percentage of TREEs and the main impurities when using 1 M H_2SO_4, the lowest eluant concentration tested. In these experiments, REE recovery increased with higher flow rates. However, the overall recovery at this acid concentration is not considered sufficient for practical applications. Additionally, a significant number of impurities was eluted under these conditions, reducing the process selectivity. Impurity elution was observed in the following ranges: 59–75% for magnesium, 55–77% for aluminum, 32–86% for iron, 43–93% for calcium, and 56–81% for manganese. Nickel showed relatively low elution across all flow rates. An explanation for the impurity preference in this elution case is that the acid was not strong enough to exchange the hydrogen ion with the REE attached to the resin. In this case, the interaction was mainly with the weakly bonded elements, which would be the impurities.

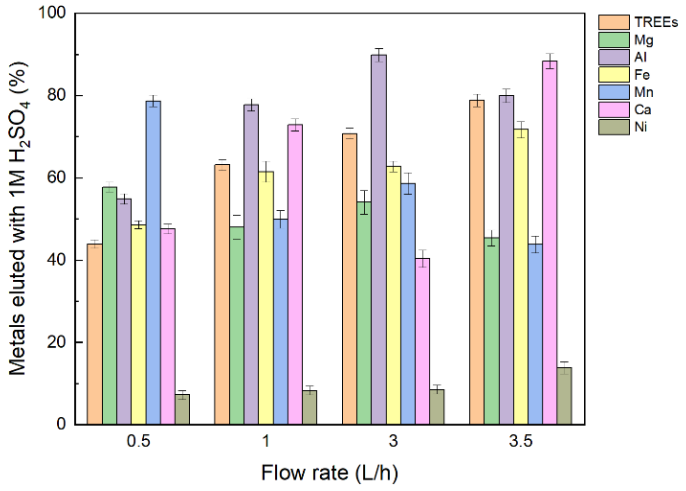

Figure 44. Elution results with 1M H_2SO_4.

The results shown in figure 45 demonstrate that when using 2 M sulfuric acid, the rare earth element elution ranged from 77% to 98%, achieving the highest recovery of all testing batches at

a flow rate of 0.5 L/h. Then, as the flow rate increased, the recovery of rare earth elements declined progressively, dropping to 77% at 3.5 L/h. This trend suggests that lower flow rates favor greater contact time between the eluant and the resin, enhancing the recovery of rare earth elements. However, a high level of impurity elution was also observed at this acid concentration. For example, magnesium, aluminum, iron, and manganese were eluted at least 60% when the flow rate was 0.5. Calcium showed increasing elution at higher flow rates, reaching a maximum of about 95% at 3.5 L/h. Nickel exhibited moderate recovery, ranging from 25% to 35%. However, in this part of the extractive process the main objective was focused on maximizing rare earth element recovery, since the subsequent recovery step, oxalic acid precipitation, is more selective due to its pH-dependent precipitation behavior which indicates that the best elution conditions for rare earth elements were achieved using 2 M sulfuric acid at a flow rate of 0.5 L/h regardless of the impurities elution.

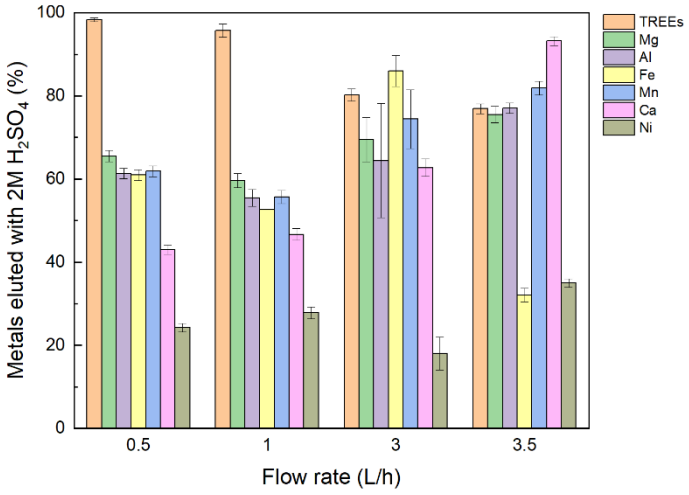

Figure 45. Elution results with 2M H_2SO_4.

Figure 46 illustrates a different behavior when 3 M sulfuric acid was used. In this case, REEs recovery ranged from 49% to 92%. Unlike the 2 M condition, increasing the acid concentration did not lead to better recovery of rare earth elements. The elution of impurities was considerable, thereby affecting the selectivity of the process.

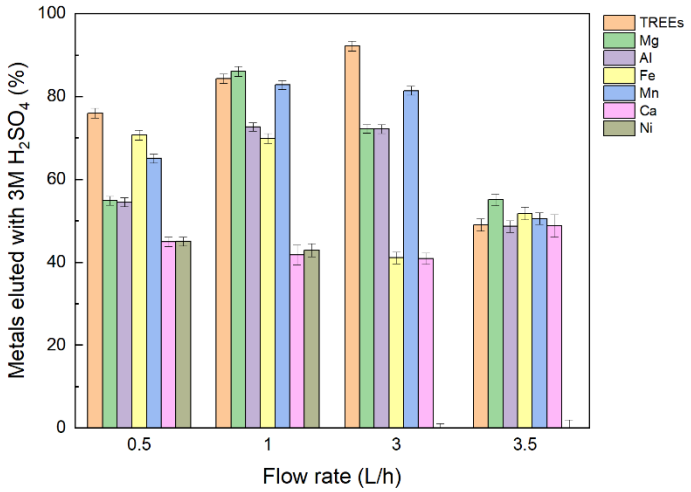

Figure 46. Elution results with 3M H_2SO_4.

Consequently, for this elution process, it was proved that the best recovery of TREEs was achieved when using low flow rates and 2M sulfuric acid. For this reason, the chosen conditions for the process were 0.5L/h and 2M H_2SO_4.

Overall, the REEs concentration increased from 1963.70 mg/L in the preconcentrated sample to 2589.90 mg/L in the eluted solution. The ratios of TREEs to other elements before and after ion exchange enrichment are shown in table 46. When comparing these two ratios, we observed that the enrichment factor of TREEs was approximately 148 times for the concentrated solution.

Table 46. Ratio of TREEs to Other Elements for Solutions Before and After TREEs Enrichment.

Ratio M+/Other Elements	
TREEs before enrichment	0.0657
TREEs after enrichment	0.4803
Enrichment factor	147.76

Oxalic acid precipitation and REO Production

Following REEs separation via ion exchange, oxalic acid precipitation was employed to recover the rare earth elements from the eluted solution.

Methodology

All precipitation experiments were conducted using the elution sample with the highest REE concentration and lowest impurity content, as identified during the ion exchange studies.

The precipitation process involved the following steps: the best eluted sample was stirred using an RT 5 magnetic stirrer hot plate set to 150 rpm and heated to 50 °C. Oxalic acid (0.5 M) was then added dropwise using a plastic transfer pipette to achieve an oxalate-to-REE molar ratio ranging from 3 to 10. Afterward, 10 M NaOH was slowly added to adjust the solution pH to 1.5. Once these conditions were achieved, stirring was continued at 150 rpm and 50 °C for 1 hour to allow complete precipitation of the REE oxalates. The laboratory setup for this procedure is shown in figure 47.

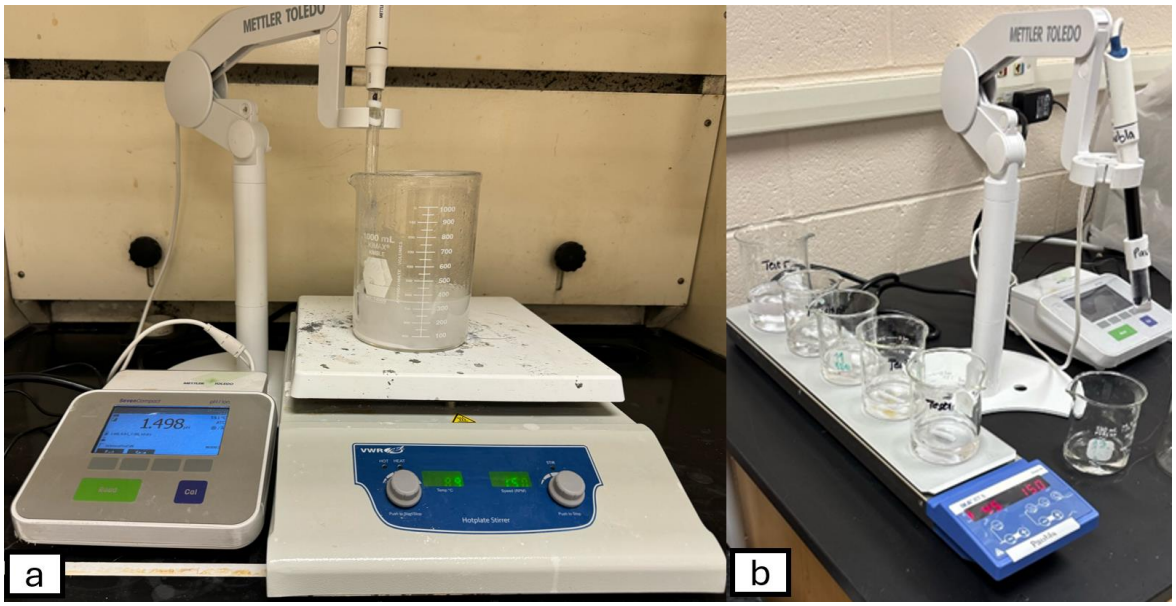

Figure 47. Oxalic acid precipitation laboratory set up. Single testing (a) multiple testing (b).

The amount of oxalic acid required was calculated based on the molar concentration of total REEs in the eluate using Equation 3. This calculation enabled the accurate determination of the 0.5 M oxalic acid volume to be added for each test.

Equation 3. Chemical Reaction Controlling $REE_2(C_2O_4)_3$ Precipitation in the Presence of C_2O_4.

$$2REE^{3+}{}_{(aq)} + 3\ {C_2O_4}^{-2}{}_{(aq)} \rightarrow REE_2(C_2O_4)_{3(s)} \qquad (3)$$

After the precipitation, the samples were subjected to solid-liquid separation using a pressure filtration system, as shown in figure 48.

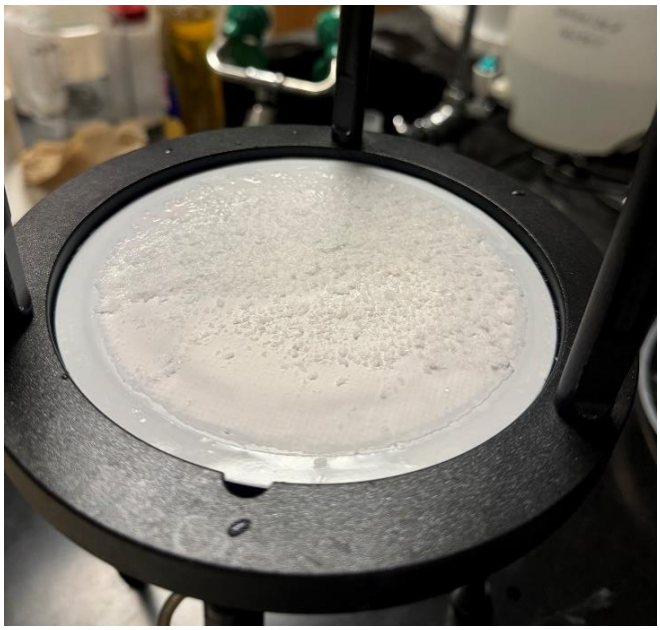

Figure 48. Rare earth oxalates after filtration.

The solid REE oxalates were transferred to a beaker and washed with DI water using an overhead stirrer at 100RPM for 20 min (figure 49). Then they were dried in an oven at 100 °C overnight. Finally, after being fully dried, a calcination to convert the oxalates into their corresponding oxides was carried out for 2 hours; for this, the solids were transferred into covered porcelain crucibles and placed into a muffle furnace preheated to 800 °C.

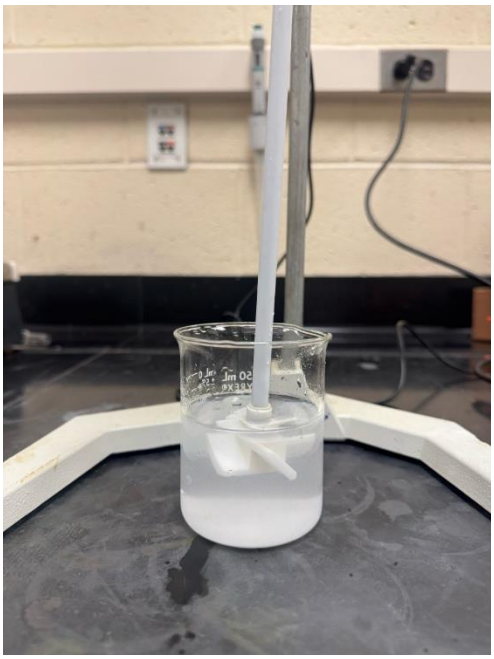

Figure 49. Rare earth oxalates washing.

The elemental composition of the feed solution before precipitation is presented in table 47. This oxalic acid precipitation step aimed to recover rare earth elements by forming insoluble oxalates, as described in equation 3.

Table 47. Elemental concentration of the feed solution for oxalic acid precipitation.

Major ions	**Sc**	**Y**	**La**	**Ce**	**Pr**	**Nd**
Concentration (mg/L)	0.46	531.02	428.82	775.37	108.93	423.91
Major ions	**Sm**	**Eu**	**Gd**	**Tb**	**Dy**	**Ho**
Concentration (mg/L)	79.17	18.77	27.11	17.81	82.25	15.85
Major ions	**Er**	**Tm**	**Yb**	**Lu**	**TREEs**	**LREEs**
Concentration (mg/L)	44.56	5.14	27.00	3.74	2589.90	1816.20
Major ions	**HREEs**	**Al**	**Ca**	**Mn**	**Fe**	**Mg**
Concentration (mg/L)	773.70	1561.86	535.38	1621.43	18.84	584.02

To improve recovery and selectivity, batch experiments were conducted by varying the molar ratio of oxalate ions ($C_2O_4^{2-}$) to total rare earth elements. The precipitation efficiency was assessed by comparing the mass of rare earth elements in the feed solution, measured by ICP-MS, with the mass remaining in the supernatant after filtration. These calculations were used to determine the precipitation recovery rates. As shown in figure 50, the highest recovery of rare earth elements (99.08%) was achieved at a C_2O_4: REEs molar ratio of 9.95, under fixed conditions of pH 1.5 and a reaction time of one hour.

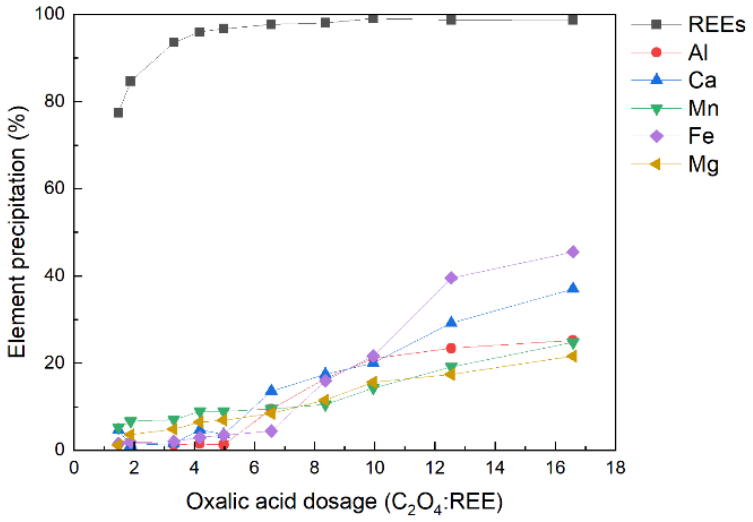

Figure 50. Effect of oxalic acid dosage on the TREEs recovery at a fixed pH of 1.5 and reaction time of 1h.

In addition to precipitation recoveries, the purity of rare earth oxalates was calculated by utilizing the dry precipitated solids' mass, the feedstock solution's elemental composition before and after precipitation, and their respective volume. The results of this analysis are presented in figure 51. It was observed that using high doses of oxalic acid led to a decrease in the purity of the resulting solid precipitates. This reduction in purity is likely due to the co-precipitation of non-target ions and the formation of hydrated oxalic acid salts, like oxalic acid dihydrate itself, which increased the overall solid mass and diluted the concentration of rare earth elements in the precipitate.

According to the graph, the optimal balance between purity and recovery was achieved at a C_2O_4:REEs ratio of 7. Under these conditions, the precipitation recovery was 97.66%, and the oxalate solids had a rare earth element purity of 57.30%. Of this, 40.02% corresponded to light rare earth elements and 15.27% to heavy rare earth elements. These findings indicate that a moderate oxalate dosage offers a more favorable outcome in terms of both selectivity and material efficiency.

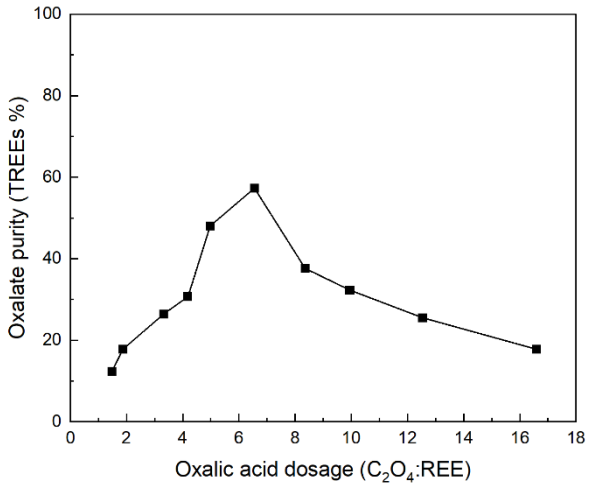

Figure 51. Effect of oxalic acid dosage on the TREEs oxalate purity at a fixed pH of 1.5 and reaction time of 1h.

In addition to dose optimization, kinetic studies were performed to determine the required reaction time for the precipitation process. Using a fixed C_2O_4:REEs ratio of 7, a pH of 1.5, and a temperature of 50°C, samples were collected at 15 minutes, 30 minutes, 1 hour, and 2 hours. Figure 52 illustrates the precipitation behavior of individual rare earth elements and major impurity metals over time. The data reveal that most rare earth elements precipitated within the first hour of the reaction. Beyond this time, only a slight increase in rare earth recovery was observed, while the precipitation of impurities became more pronounced. Therefore, to preserve selectivity without compromising recovery, a reaction time of one hour was selected as optimal.

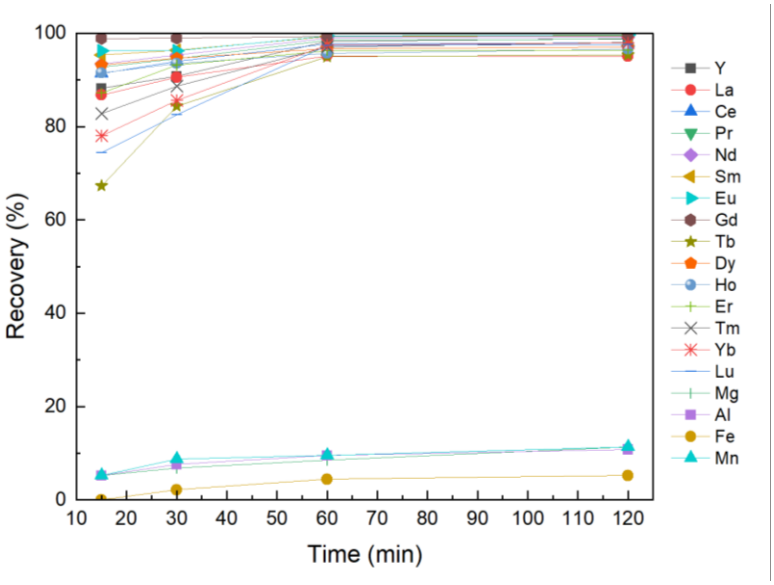

Figure 52. Effect of reaction time on elemental recovery of rare earth elements and contaminants (Mg, Al, Fe, Mn) at a fixed pH of 1.5 and dosage of 7 C2O4: REE.

Despite substantial concentrations of aluminum, calcium, manganese, iron, and magnesium in the feed solution, most of the magnesium and iron remained in the filtrate after precipitation, indicating their relatively low precipitation rates. In contrast, manganese and calcium exhibited higher precipitation percentages, although none of the impurities exceeded a precipitation efficiency of 31%. These trends are further illustrated in figure 53, confirming that the precipitation step, under the selected conditions, achieved effective rare earth element recovery while limiting co-precipitation of impurities.

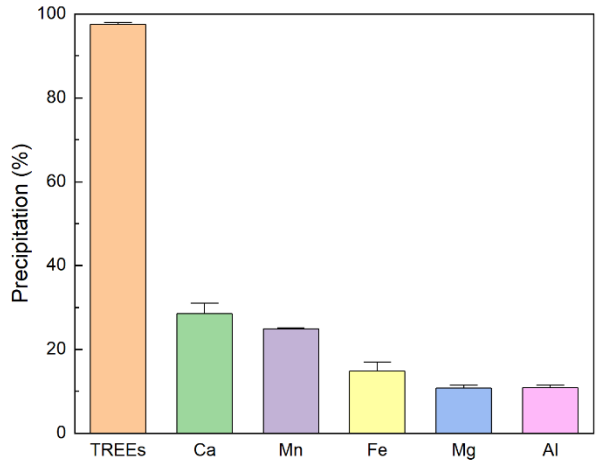

Figure 53. Recovery of major metal elements by oxalic acid precipitation at a fixed pH of 1.5, dosage of 7 C2O4: REEs, and reaction time of 1h.

The oxalates produced were washed right after the precipitation was done. This step aimed to remove soluble impurities that co-precipitated during the reaction. The washing was conducted using deionized water and an overhead stirrer for 30 minutes, as shown in Figure 49. *Rare earth oxalates washing.*. To evaluate the effectiveness of this process, the wash water was collected after filtration and analyzed using ICP-MS to identify the elements removed. Table 48 presents the mg of elements detected in the washing solution. The results indicate that sodium was the primary impurity removed, likely from the NaOH used to adjust the pH during the precipitation stage. Smaller amounts of manganese, magnesium, and aluminum were also present in the wash water, suggesting a small removal of these elements during the washing step.

Table 48. Elemental concentration in water after the washing stage.

Major ions	**TREE**	**Na**	**Ca**	**K**	**Mg**	**Al**	**Fe**	**Mn**
Amount (mg)	0.76	58.15	0.88	1.24	1.48	2.79	0.02	4.14
STD	0.20	3.20	0.10	0.04	0.03	0.02	0.01	0.04

SEM images of the rare earth element oxalates, obtained under the optimized oxalic acid precipitation conditions from the highest-quality eluted sample, are presented in figure 54. The image reveals that the rare earth oxalates formed well-defined prismatic crystals with a tetragonal shape, exhibiting crystal morphologies ranging from subhedral to euhedral—consistent with the typical characteristics of rare earth oxalate compounds. The observed crystal sizes ranged from approximately 2 to 6 micrometers.

These morphological features support the successful formation of rare-earth oxalates under the selected experimental conditions. Similar crystal habits have been reported in literature. For instance, a study also reported prismatic tetragonal crystals during rare earth element recovery from magnet waste using oxalic acid precipitation, further validating the consistency of these results with known rare earth oxalate behavior (Rahmati et al., 2024).

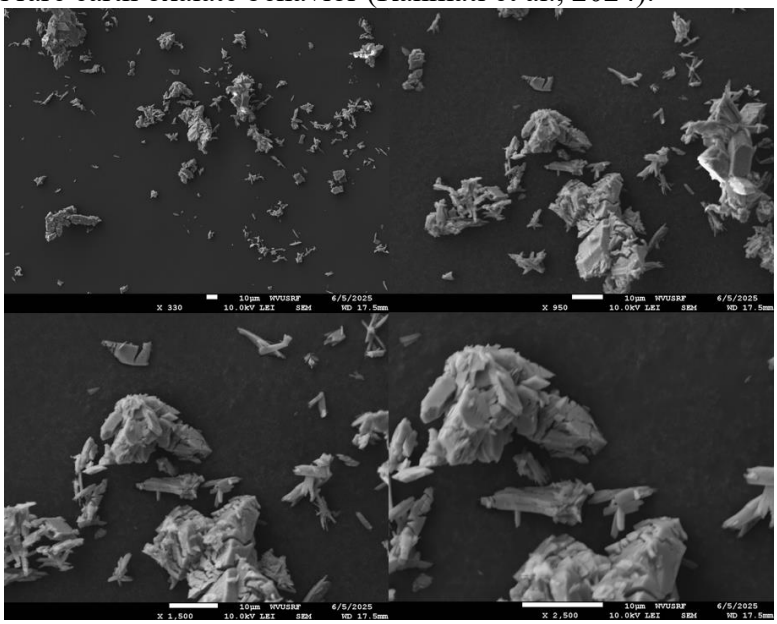

Figure 54. SEM image of the rare earth oxalate product.

Calcination

The calcination of the rare earth oxalate samples was carried out at a fixed temperature of 800°C for four hours to convert the oxalate precipitates into their corresponding oxide forms. The process resulted in a significant reduction in mass, with losses ranging from 45% to 48%, based on the results obtained from three replicate tests conducted using the best-performing oxalate precipitation sample.
In addition to the reduction in mass, a distinct visual change was observed in the samples. The solids transitioned from a white appearance, characteristic of oxalate compounds, to a brownish color, indicative of the formation of rare earth oxides. This transformation is visually documented in figure 55 and confirms the successful thermal decomposition of the oxalate phase into oxide form.

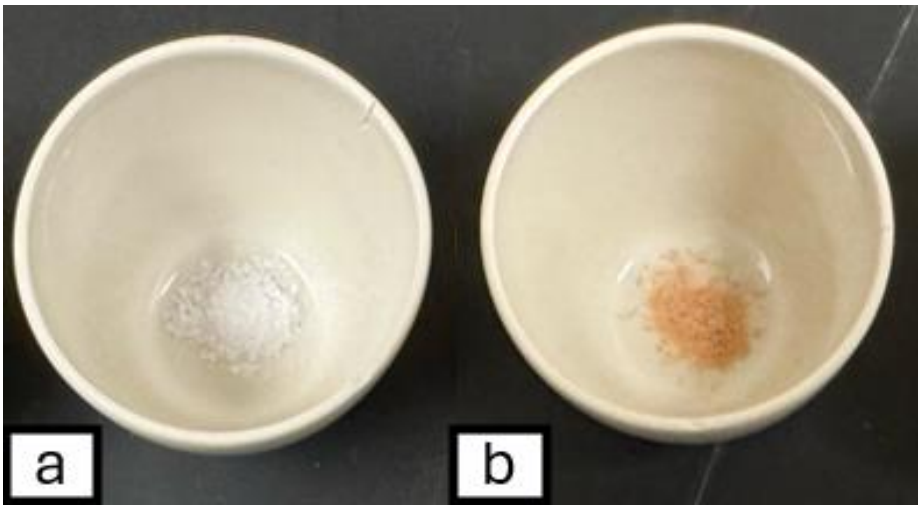

Figure 55. Oxalate (a) and oxides (b) solids' appearance.

REE oxide solids characterization

Characterization and confirmation of the purity of the final oxide product were performed using ICP-MS. For sample preparation, acid digestion was conducted by dissolving approximately 20 milligrams of solid material in 50 milliliters of a solution composed of deionized water, 10 mL of 70% trace metal grade nitric acid, and 10 mL of 37% hydrochloric acid. The resulting solution was then diluted 200 times to meet the detection limits of the instrument. The measured concentrations of each element in the liquid sample represent the elemental content initially present in the solid sample.
Average concentrations of individual elements were calculated from four replicate tests conducted under the optimized conditions, which included the following steps:

1. Precipitation of iron from raw AMD at pH 4.0
2. Precipitation of aluminum at pH 5.0
3. Precipitation of rare earth elements between pH 5.0 and 9.0

4. Redissolution of precipitates using deionized water at a solid-to-liquid ratio of 1:15, with 1 g of preconcentrated solids diluted in 15 mL of water at 50°C, followed by acidification with sulfuric acid to pH 0.5
5. Ion exchange loading using the preconcentrated solution at a flow rate of 1 L/h and an adjusted pH of 1.5
6. Ion exchange elution using 2 M sulfuric acid at a flow rate of 0.5 L/h
7. Oxalic acid precipitation at a molar ratio of 7, conducted at 50°C and adjusted to pH 5 using NaOH
8. Washing oxalates to remove soluble residues, using an overhead stirrer at 100 RPM
9. Calcination of the oxalates at 800°C for four hours

The results from the four solid samples produced under these optimized conditions are summarized in table 49. The main impurities detected in the final product were aluminum and calcium, with concentrations of 2.77% and 2.47% by weight, respectively. These elements are expected due to their relatively high initial concentrations in the raw AMD used as feedstock.

Table 49. The average elemental ICP- MS characterization.

Element	Concentration (mg/Kg)	STD
Y	164,844.80	13,624.62
La	121,942.44	7,781.25
Ce	246,880.42	5,256.45
Pr	33,994.92	375.58
Nd	136,089.35	2,884.39
Sm	25,011.28	1,189.31
Eu	6,097.97	173.71
Gd	8,235.69	727.73
Tb	5,627.12	207.12
Dy	26,008.23	1,099.11
Ho	5,015.67	205.64
Er	13,919.65	541.55
Tm	1,576.25	72.84
Yb	8,342.77	371.95
Lu	1,162.64	23.52
Ca	24,656.42	8,406.90
Mn	846.78	162.51
Fe	1,740.30	181.29
Mg	10,206.00	1,930.21
Al	27,795.83	4,695.92

The ICP-MS results were used to convert the concentrations of individual REEs to their corresponding REO. This calculation, shown in table 50, revealed that the final product had an average REO purity of 95.62% by weight. The highest REO purity among the four samples reached

96.87% by weight. Across the replicate experiments, the average REO grade in the final solid product remained consistently high. Among the identified rare earth oxides, cerium oxide, yttrium oxide, neodymium oxide, and lanthanum oxide were the most abundant, with respective concentrations of 28.91%, 20.93%, 15.87%, and 14.30% by weight. These results align with the initial composition of the raw acid mine drainage feedstock, in which these four elements were the most concentrated.

Table 50. The average REO concentration based on ICP- MS characterization.

Oxide	Concentration (mg/Kg)
Y_2O_3	209,339.55
La_2O_3	143,009.57
Ce_2O_3	289,163.89
Pr_2O_3	39,784.62
Nd_2O_3	158,731.75
Sm_2O_3	29,003.25
Eu_2O_3	7,061.01
Gd_2O_3	9,492.57
Tb_2O_3	6,476.82
Dy_2O_3	29,849.20
Ho_2O_3	5,745.49
Er_2O_3	15,916.85
Tm_2O_3	1,800.18
Yb_2O_3	9,499.81
Lu_2O_3	1,322.11

Figure 56 presents SEM images of a rare earth oxide crystal obtained after the calcination of the oxalate precipitate. The particle displays a well-defined tetragonal crystal habit with a morphology ranging from subhedral to euhedral, consistent with commonly observed features in rare earth oxides. The crystal dimensions vary from approximately 6 to 10 micrometers.

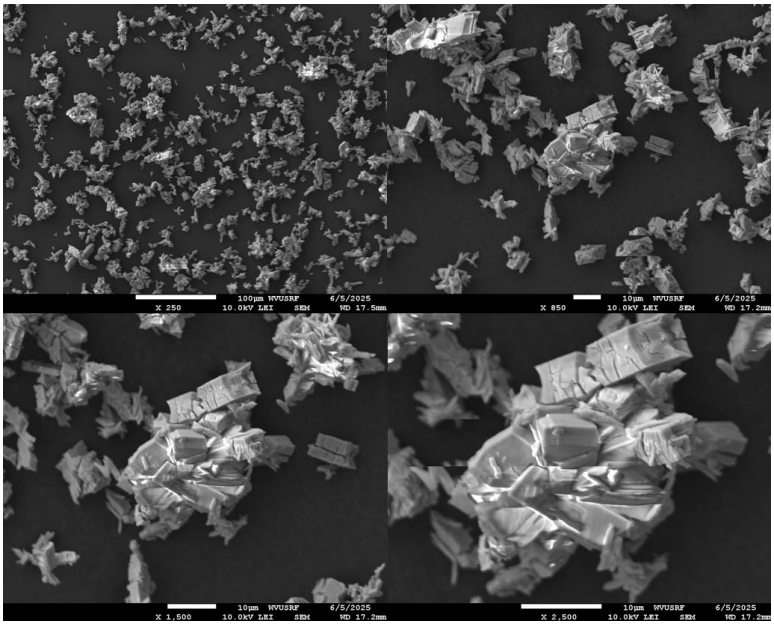

Figure 56. SEM image of the rare earth oxide product.

In addition, qualitative elemental analysis using SEM coupled with energy-dispersive X-ray spectroscopy (EDS) was performed, and the results are shown in figure 57. As expected, the study confirmed the presence of key rare earth elements in the oxide sample. Cerium, yttrium, and lanthanum were among the top four oxides identified, along with dysprosium. These findings agree with the quantitative elemental composition obtained through inductively coupled plasma mass spectrometry, supporting the consistency and reliability of the precipitation and calcination process.

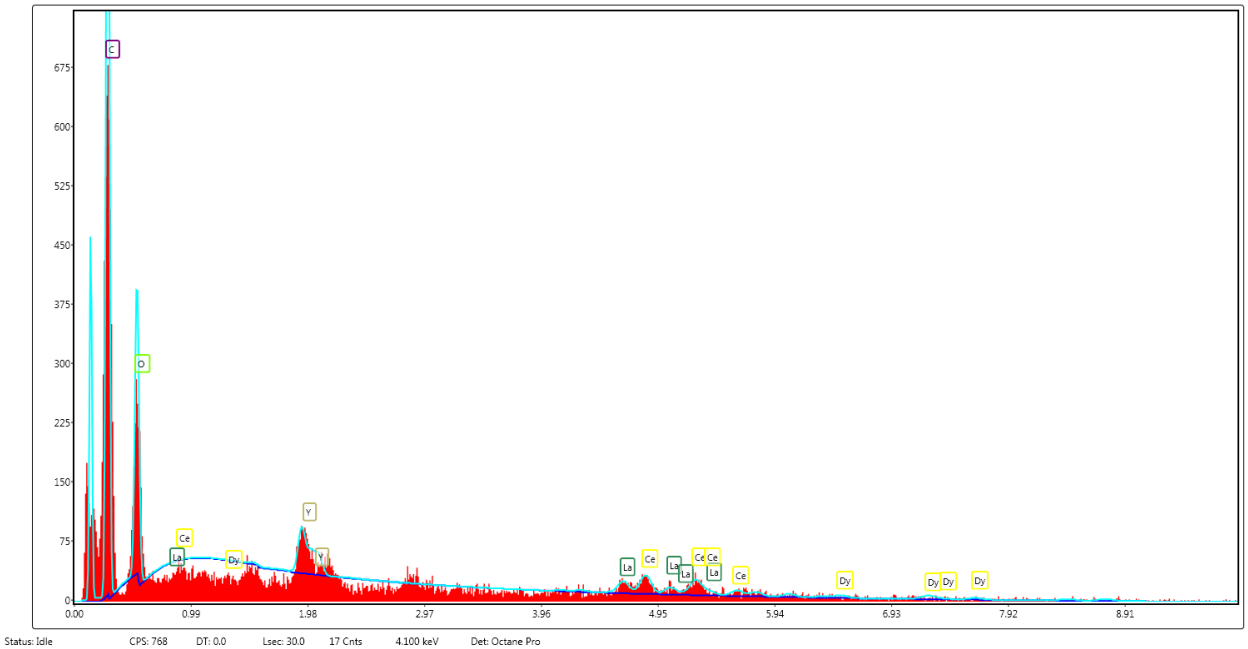

Figure 57. SEM-EDS analysis results of the rare earth oxide.

2.5 Oxidative Manganese Precipitation

After the ion exchange stages for nickel, zinc, and cobalt, the remaining AMD discharge stream had a pH between 2.0 and 3.5, the research team is proposing using this solution in the integrated process by precipitating it to a pH value of 9.0 using sodium hydroxide, the solids of this precipitation will be used in the REE recovery stage as shown in section 2.4 and the filtrated solution will serve as feedstock for the manganese recovery process.

Since no suitable commercial resin or sorbent was identified for a dedicated manganese ion exchange step, oxidative precipitation was selected to recover manganese as manganese dioxide (MnO_2). Ammonium persulfate (APS, $(NH_4)_2S_2O_8$) was chosen as the oxidant, as it is capable of oxidizing Mn(II) to MnO_2 under acidic conditions. The reaction controlling MnO_2 precipitation in the presence of APS is:

Equation 03. Chemical Reaction Controlling MnO_2 Precipitation in the Presence of $(NH_4)_2S_2O_8$.

$$Mn^{2+}(aq) + S_2O_8^{2-}(aq) \rightarrow MnO_2(s) + SO_4^{2-}(aq)$$

The main variables investigated in this process were:

- Precipitation pH
- Precipitation time
- Precipitation temperature
- APS/Mn^{2+} molar ratio
- APS reagent concentration

For all tests, AMD was treated with APS under controlled conditions. After each run, the solution pH was adjusted to between 7.0 and 8.0 using 2 M NaOH to avoid redissolution of MnO_2, followed by vacuum filtration with 0.45 µm filter paper. When solids were collected, they were dried at 60 °C for 48 hours.

Effect of Precipitation pH

Methodology

To evaluate the influence of pH on MnO_2 precipitation, 1.0 L batches of AMD were treated at different initial pH values (2.1, 2.5, 3.0, and 3.5), in the integrated flowsheet sulfuric acid is the reagent chosen to adjust the pH. A 0.2 M APS solution was used at an APS/Mn^{2+} ratio of 1.5. Precipitation was carried out at 65 °C for 2.5 hours using a heated plate with magnetic stirring at 400 rpm. Samples were collected before and after precipitation and analyzed by ICP–MS. Table 51 shows the test parameters.

Table 51. Effect of AMD Feed pH Study. Tests Parameters.

Solution Volume (L)	Precipitation Time (h)	Reagent	Temperature °C	Ratio APS to Mn^{2+}
1.00	2.50	0.2 M APS	65.00	1.50

Results and Discussion

The results in Figure 58 indicate that APS precipitation is relatively selective for manganese, with aluminum, silica, and iron being the main co-precipitated impurities. Aluminum precipitation remained nearly constant at ~80% across all studied pH values. Silica, in contrast, showed decreasing precipitation with increasing pH, and iron precipitation generally remained below 20% for all pH values. These findings highlight the importance of the upstream impurity removal stage, where most iron and aluminum had already been removed.

For manganese, the precipitation pH had a clear influence on recovery. At 65 °C, manganese removal increased with pH, with the best performance observed near pH 3.5, where the precipitation percentage reached ~80% after 2.5 hours. Manganese exhibited a trend of higher precipitation at higher precipitation pH, opposite to silica. The lower silica precipitation at higher pH values is consistent with a reduced availability of persulfate radicals for impurity oxidation under those conditions.

Based on these results, an optimal AMD pH of approximately 3.5 was selected for manganese dioxide precipitation after nickel, zinc, and cobalt removal.

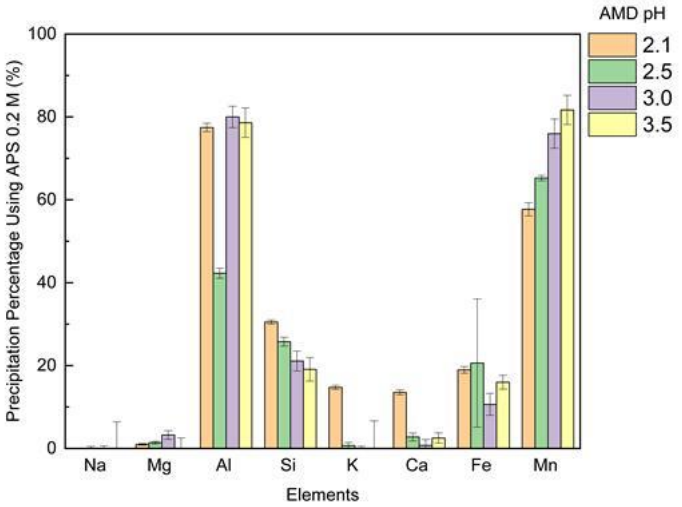

Figure 58. Effect of AMD pH on MnO2 Precipitation at 65 °C for 2.5 hours with a 1.5:1 APS to Mn^{2+} Ratio.

Effect of Precipitation Time

Methodology

The effect of precipitation time was investigated using 1.0 L of AMD at pH 3.5. Tests were carried out at 70 °C for precipitation times of 1.5, 2.0, 2.5, and 3.0 hours. A 0.2 M APS solution was used with an APS/Mn^{2+} ratio of 1.5. Samples were collected before and after precipitation for ICP–MS analysis. Tests parameters are shown in Table 52.

Table 52. Effect of Precipitation Time Study. Tests Parameters.

Solution Volume (L)	Temperature °C	Reagent	AMD pH	Ratio APS to Mn2+
1.00	70.00	0.2 M APS	3.50	1.50

Results and Discussion

As shown in Figure 59, time significantly affected both manganese recovery and impurity co-precipitation. Aluminum and iron precipitation increased with time, reaching approximately 70% and 18%, respectively, after 3.0 hours. Silicon precipitation remained below 20%, while calcium and magnesium precipitated at levels below 5%.

Manganese precipitation increased steadily with time, from <40% at 1.5 hours to ~66% at 2.5 hours and ~80% at 3.0 hours. These results confirm that, in addition to pH, precipitation time is a key parameter for manganese recovery. The data also suggest that further improvements in manganese recovery require either longer times, higher temperatures, or both.

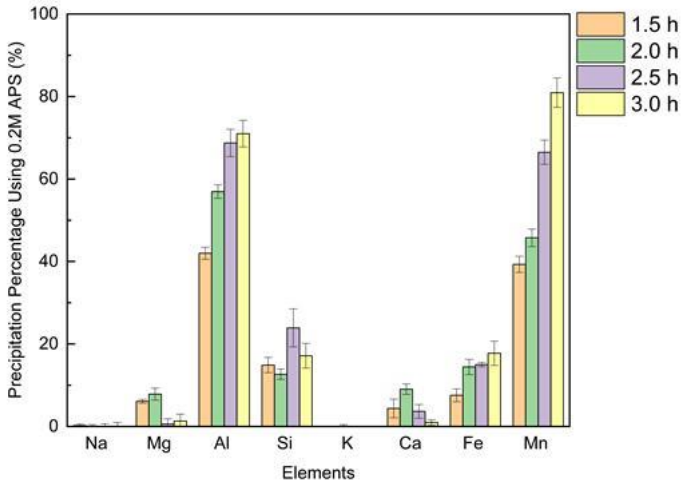

Figure 59. Effect of Precipitation Time on MnO_2 Precipitation at 70 °, pH 3.5, and a 1.5:1 APS to Mn^{2+} Ratio.

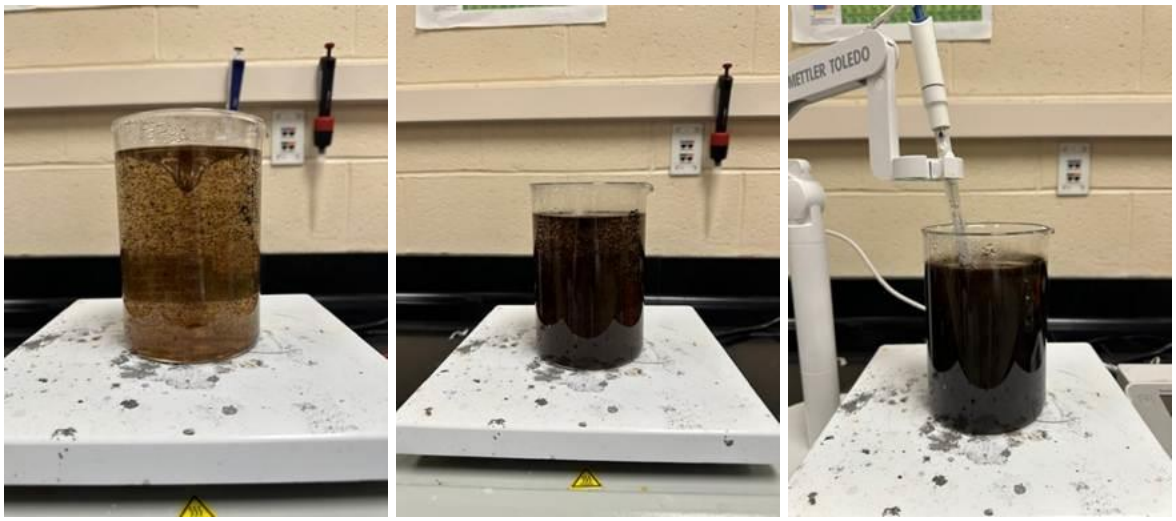

Figure 60. Effect of Precipitation Time. Left: 1 hour. Center 2 hours. Right: 3 hours.

Effect of Precipitation Temperature

Methodology

To assess the effect of temperature, tests were performed at 55, 60, 65, 70, 75, and 80 °C. All experiments were carried out with 1.0 L of AMD at pH 3.5, an APS concentration of 0.2 M, an APS/Mn^{2+} ratio of 1.5, and a precipitation time of 3.0 hours. Samples were collected before and after precipitation for ICP–MS analysis. Tests parameters are shown in Table 53.

Table 53. Effect of Precipitation Temperature Study. Tests Parameters.

Solution Volume (L)	Precipitation Time (h)	Reagent	AMD pH	Ratio APS to Mn2+
1.00	3.00	0.2 M APS	3.50	1.50

Results and Discussion

The results in Figure 61 show that temperature plays a critical role in manganese recovery. At higher temperatures, particularly around 80 °C, MnO_2 precipitation approached almost 100%.

At 80 °C, aluminum precipitation reached ~81%, whereas silica and calcium exhibited lower precipitation (approximately 10% and 2.5%, respectively), indicating increased solubility of these impurities at higher temperatures. Iron precipitation ranged from 30% to 40% in the 75–80 °C range.

These findings confirm that increasing temperature significantly enhances manganese recovery while leaving most impurities in solution, and they suggest that future optimization may investigate shorter reaction times at elevated temperatures to further improve process efficiency.

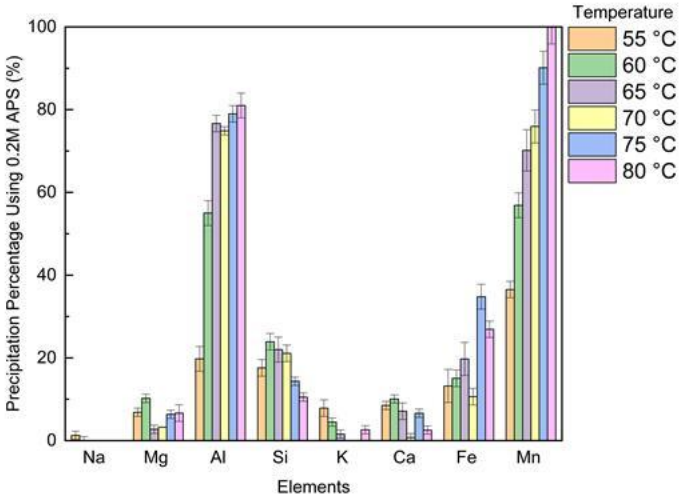

Figure 61. Effect of Precipitation Temperature on MnO_2 Precipitation at pH 3.5, 3 hours, and a 1.5:1 APS to Mn^{2+} Ratio.

Effect of APS/Mn^{2+} Ratio

Methodology

The influence of oxidant dosage was studied by varying the APS/Mn^{2+} molar ratio at 1.1, 1.5, 1.7, 2.0, and 2.4. All tests were performed with 1.0 L of AMD at pH 3.5, an APS concentration of 0.2 M, a temperature of 70 °C, and a precipitation time of 3.0 hours. Tests parameters are shown in Table 54.

Table 54. Effect of the APS to Mn^{2+} Ratio During Precipitation. Tests Parameters.

Solution Volume (L)	Precipitation Time (h)	Reagent	AMD pH	Temperature °C
1.00	3.00	0.2 M APS	3.50	70.00

Results and Discussion

The results in Figure 62 show that higher APS/Mn^{2+} ratios improve manganese recovery but also increase impurity co-precipitation. Under identical pH, time, and temperature conditions (pH 3.5, 3 h, 70 °C), aluminum precipitation increased from ~70% at a ratio of 1.5:1 to ~85% at 2.4:1. Similar trends were observed for silica, iron, and magnesium.

This rise in impurity co-precipitation can negatively impact manganese product purity. Furthermore, increasing the APS/Mn^{2+} ratio from 1.5:1 to 2.4:1 represents roughly a 60% increase in reagent consumption, yielding only about a 14% increase in manganese recovery. From a process and cost perspective, improving recovery by increasing temperature or time appears more attractive than significantly increasing APS dosage.

Based on these considerations, an APS/Mn^{2+} ratio of **1.5:1** was selected as optimal, with a recommended range of 1.5:1 to 1.7:1, since manganese and impurity precipitation percentages were similar within this interval.

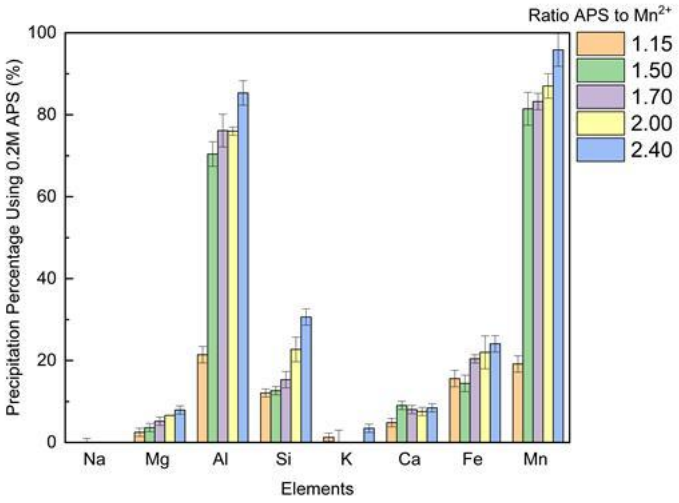

Figure 62. Effect of the APS to Mn^{2+} Ratio on MnO_2 Precipitation at pH 3.5, 3 hours, and 70°C.

Effect of APS Concentration

Methodology

The effect of APS reagent concentration was evaluated by performing tests with APS concentrations of 0.2, 0.4, 0.6, and 1.0 M. In all tests, the AMD pH was 3.5, the temperature was 70 °C, the precipitation time was 3.0 hours, and the APS/Mn^{2+} ratio was 1.5. Tests parameters are shown in Table 54.

Table 54. Effect of Reagent Concentration During Precipitation. Tests Parameters.

Solution Volume (L)	Precipitation Time (h)	Ratio APS to Mn2+	AMD pH	Temperature °C
1.00	3.00	1.5	3.50	70.00

Results and Discussion

As shown in Figure 63, both very low and very high APS concentrations negatively impacted manganese recovery. At 0.1 M, manganese precipitation was only about 70%, and at 1.0 M,

recovery was similarly low, near 70%, while impurity precipitation remained comparable to other concentration levels.

The best results were obtained in the 0.2–0.6 M APS range, with 0.2 M providing the highest manganese recovery, approaching 100%. Impurity co-precipitation was relatively similar for all APS concentrations, indicating that manganese recovery is more sensitive to APS concentration than impurity behavior. Overall, the tests showed that APS concentrations that are highly diluted or highly concentrated are detrimental to manganese recovery.

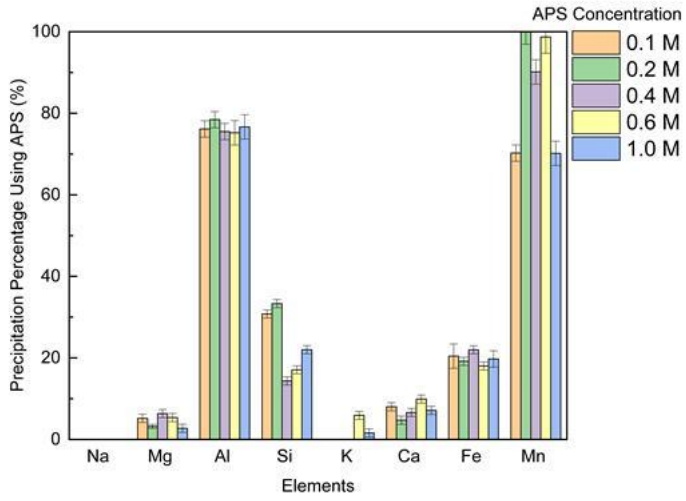

Figure 63. Effect of the APS Concentration on MnO2 Precipitation at pH 3.5, 3 hours, 70°C, and 1.5:1 Ratio.

Manganese Dioxide Solids Production

Methodology

Based on the systematic testing, the optimized MnO_2 precipitation conditions were summarized as follows:

Table 55. Optimized Parameters for Manganese Dioxide Precipitation with Ammonium Persulfate (APS).

Optimized MnO_2 Precipitation Conditions	
Temperature (Celsius)	80
Ratio APS/Mn2+	1.5-1.7
Precipitation Time (h)	2.0- 3.0
Initial pH	3.5
APS Concentration	0.2 M - 0.6 M
Final pH	7.5

A series of tests were performed at these conditions to generate a sufficient quantity of MnO_2 solids for characterization. After precipitation at 80 °C and pH 3.5, the final pH was adjusted to 7.5, and solids were filtered and dried at 60 °C for 48 hours.

Results and Discussion

Solution compositions and precipitation percentages under representative optimized conditions (80 °C, 2 h, pH 3.5, APS/Mn^{2+} = 1.5, final pH 7.5) are presented in Table 56.

Table 56. Solution Concentration and Precipitation Percentage During the Precipitation of MnO2 Using APS at 80 °C, 2 hours, pH 3.5, and 1.5:1 Ratio.

Description	Average Elements Concentration (mg/L)							
Elements	Na	Mg	Al	Si	K	Ca	Fe	Mn
Manganese Precipitation Feed	3091.5	448.7	9.0	33.7	12.0	221.7	4.0	115.6
After Precipitation pH 7.5	4917.1	624.6	4.4	41.7	27.2	298.4	4.2	0.4
Precipitation (%)	0%	3%	60%	6%	0%	5%	16%	100%

Manganese precipitation reached 100%, confirming complete removal under the selected conditions. The main co-precipitated impurities were aluminum, iron, calcium, and magnesium, whereas sodium and potassium remained entirely in solution.

Figures 64 and 65 show the evolution of manganese and impurity concentrations over time during APS precipitation at 80 °C, APS = 0.6 M, and APS/Mn^{2+} = 1.5. For manganese, a nearly linear decrease in concentration was observed, reaching ~0.4 mg/L after 2 hours. Impurity concentrations generally increased over time due to solution volume reduction at elevated temperature, particularly for calcium and magnesium, which remained mostly in solution. In contrast, aluminum and iron, which precipitated to a greater extent, showed stable or decreasing concentrations.

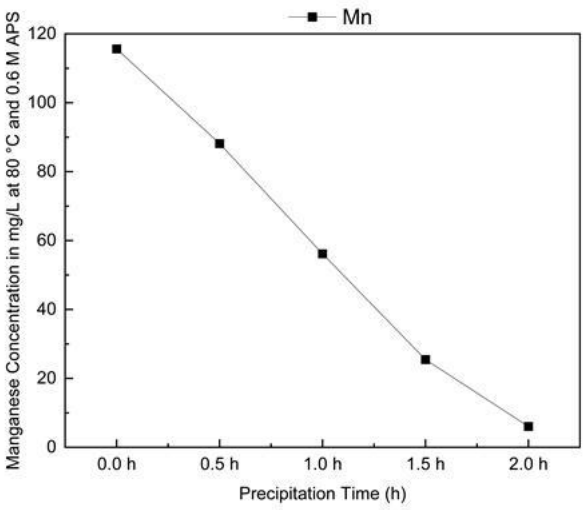

Figure 64. Behavior of Manganese Concentration over Time During APS Precipitation at 80 °C, 0.6 M APS, and a 1.5:1 APS-to-Manganese Ratio.

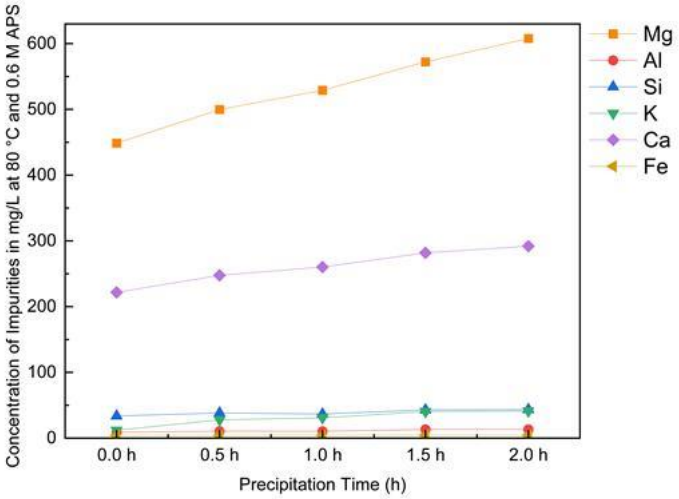

Figure 65. Behavior of Impurities Concentration over Time During APS Precipitation at 80 °C, 0.6 M APS, and a 1.5:1 APS to Manganese Ratio.

The overall precipitation process and appearance of the MnO_2 solids are illustrated in Figure 66, showing the slurry after 1 hour, after 2 hours, and the final dried solids.

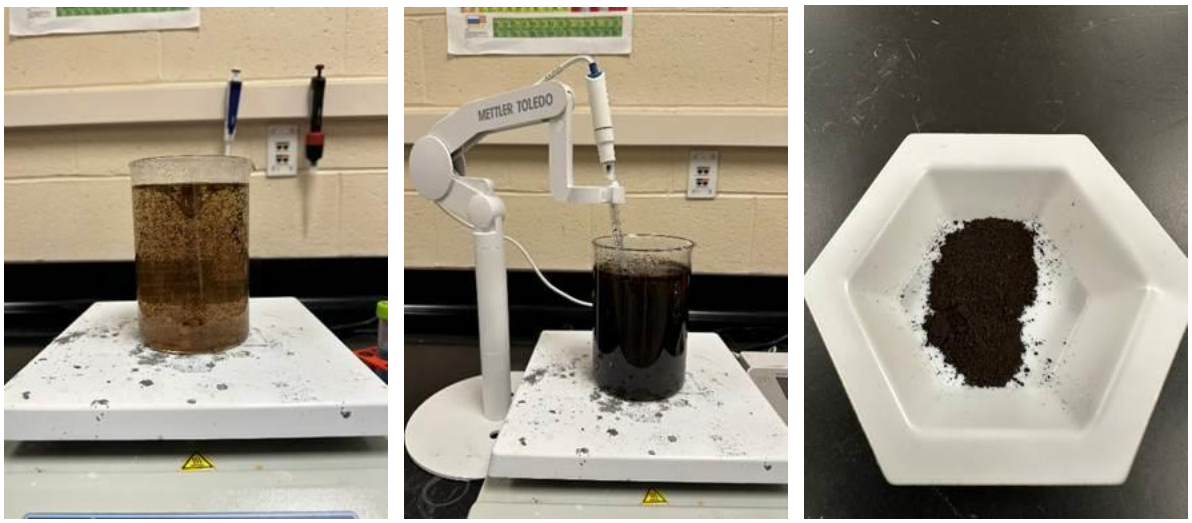

Figure 66. Precipitation of Manganese Dioxide Using APS. Left: After 1 hour. Center: After 2 hours. Right: Dried Solids.

Manganese Solids Purity

The solids resulting from the oxidative precipitation were thoroughly mixed in a mortar. A representative sample of 0.1703 g was then digested using 8 mL of nitric acid and 8 mL of hydrochloric acid. The digestion occurred for 4 hours at 50°C. After digestion, 34 mL of distilled water was added for dilution, and a representative sample of the digested liquor was collected and sent for ICP-MS analysis. The results are shown below. The final digested liquor was filtered using a 0.45 µm filter paper, and its volume was measured to be 47 mL using a glass volumetric column.

Table 57. Elements of Interest and Main Impurities Concentration in Digested Liquor of Manganese Solids.

Description	Average Elements Concentration (mg/L)							
Elements	Na	Mg	Al	Si	K	Ca	Fe	Mn
Manganese Digested Solids	263.3	75.4	18.3	58.8	2.5	61.2	4.1	1232.2

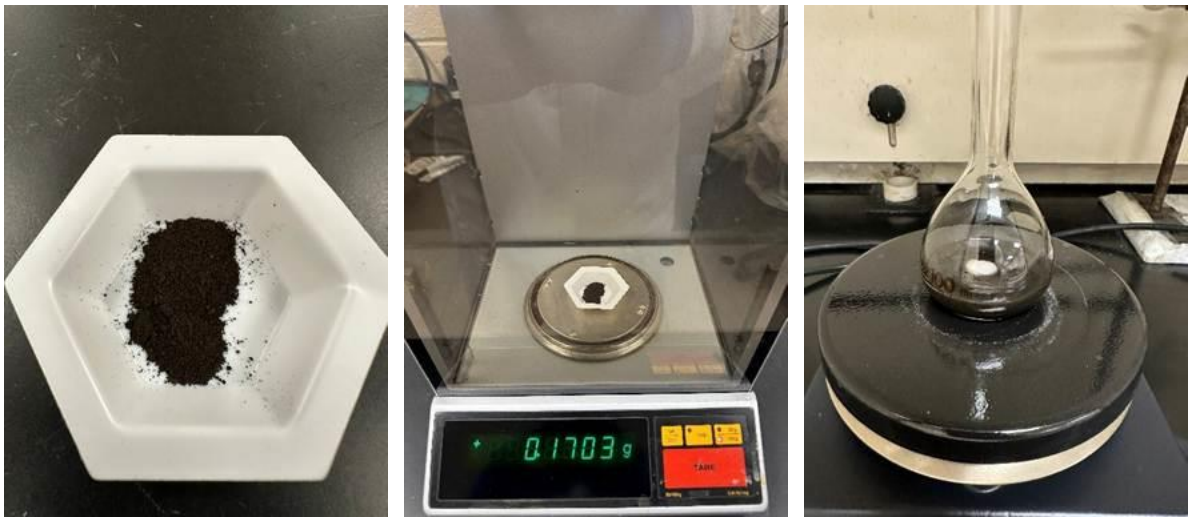

Figure 67. Manganese Dioxide Solids Digestion. Left: Homogeneous Sample. Center: Weight of Digested Solids. Right: Solution During Digestion.

Using the ICP-MS results and the volumes, the weight of manganese in the liquor was calculated as 0.0579 g, and the purity of manganese was calculated as follows:

$$Manganese\ Purity = \frac{0.0579g}{0.1703\ g} = 34.01\%\ Manganese$$

If the concentrated precipitate is manganese dioxide, the purity can be calculated using the manganese purity as follows:

$$Manganese\ Dioxide\ Purity = \frac{Manganese\ Purity\ \%}{0.6319} = 53.81\%$$

3. Summary

The primary objective of this research was to develop a laboratory-scale process for recovering rare earth elements (REEs), nickel, cobalt, manganese, and zinc from acid mine drainage (AMD) originating from coal mines in West Virginia and Pennsylvania. To accomplish this, multiple AMD samples were first characterized to identify the most promising feedstock. Among all samples analyzed, one collected from the Kanawha region of West Virginia was selected due to its relatively low impurity levels and above-average concentrations of target critical minerals.

The selected AMD sample contained a total REE concentration of 5.22 mg/L, consisting of 1.74 mg/L light REEs and 3.47 mg/L heavy REEs. Other target critical metal concentrations were: Ni = 3.94 mg/L, Co = 4.09 mg/L, Zn = 6.87 mg/L, and Mn=161.24 mg/L. Major impurity concentrations included Fe (7.34 mg/L), Mg (497.24 mg/L), Al (147.02 mg/L), Ca (49.26 mg/L), and Si (43.09 mg/L).

A key challenge addressed in this study was the inherently low concentration of target critical minerals compared to the relatively high concentration of impurities in AMD. This required a

multi-stage hydrometallurgical approach for selectively removing impurities and recovering REEs and other critical metals.

Overview of the Five-Stage Processing Strategy

Stage 1 — Impurity Removal (Fe, Al)

Selective impurity removal was conducted using a two-step, pH-dependent precipitation method. Sodium hydroxide was added to adjust the AMD to pH 4 and pH 5, removing approximately 66% of iron and 95% of aluminum, respectively, along with other contaminants.

Stage 2 — Nickel Recovery

Nickel was selectively recovered using M4195 cation-exchange resin and subsequent selective precipitation.

- Feed conditions: pH 1.3; flow rate 1 L/h
- Impurity rinse: 0.2 M H_2SO_4; 2.5 L acid / L resin
- Elution: 2 M H_2SO_4; 3.5 L acid / L resin

The eluted nickel-rich solution was then treated via nickel hydroxide precipitation using NaOH at pH 11.0 and 25 °C. The resulting green precipitate had a nickel purity of 41.3%, corresponding to a mineral purity ($Ni(OH)_2$) of 65 wt%.

Stage 3 — Cobalt and Zinc Recovery

The discharge stream from the nickel ion-exchange stage served as feed for cobalt and zinc recovery. The eluted solution contained enriched Zn and Co and was used for Zn and Co precipitation.

- Feed conditions: pH 3.5 (adjusted with NaOH); flow rate 1 L/h
- Rinse: distilled water, 2.2 L water / L resin
- Elution: 0.5 M H_2SO_4, 3.4 L acid / L resin

Zinc precipitation:

- Precipitation agent: Na_2S
- Conditions: pH 4–7; S^{2-}/Zn ratio = 2.0

After ZnS precipitation and filtration, cobalt was recovered from the filtrate via hydroxide precipitation at pH 11.0, ambient temperature, 30 minutes.

- Zn product purity: 38.32%, corresponding to a mineral purity (ZnS) of 56 wt%.
- Co product purity: 30.15%, corresponding to a mineral purity ($Co(OH)_2$) of 48 wt%.

Stage 4 — Rare Earth Elements Recovery

The discharge from the Zn–Co ion exchange stage was adjusted to pH 9, producing an REE-rich solid. These solids were dissolved in sulfuric acid to generate a feedstock for the REE ion-exchange process.

Ion exchange (50WX8 resin):

- Feed conditions: pH 1.5; flow rate 1 L/h
- Elution: 2 M H_2SO_4; flow rate 0.5 L/h

REE precipitation:

- Precipitation agent: oxalic acid
- Optimal conditions:
  - C_2O_4:REE ratio = 7
  - Temperature = 50 °C
  - Precipitation time = 1 h
  - Final pH = 1.5

The resulting REE oxalates were washed and calcined at 800 °C for 4 h to obtain the final REE oxide product with a purity greater than 95% by weight.

Stage 5 — Manganese Recovery

The filtered solution remaining after REE precipitation was used as feed for manganese recovery. The resulting manganese oxide product had a purity of 34% Mn, corresponding to a MnO_2 mineral purity of 54 wt%.

Manganese precipitation (as Mn oxide):

- Reagent: ammonium persulfate (APS)
- Optimal conditions:
  - Temperature = 75–80 °C
  - APS/Mn^{2+} ratio = 1.4–1.6
  - Precipitation time = 2.5–3.0 h
  - Initial pH = 3.5; final pH = 7.5

4. Conclusions

The main conclusions of this study are summarized as follows:

- Stage-wise precipitation effectively removed iron and aluminum at pH 4.0 and 5.0, achieving average removal efficiencies of 66% and 95%, respectively.

- Selective separation of nickel, zinc, cobalt, rare earth elements (REEs), and manganese from AMD was accomplished using column ion exchange and selective precipitation processes.

- Nickel loading using Ambersep M4195 was effective at pH 1.3 with a 6-minute contact time, resulting in 94% nickel binding. Because the resin also has affinity for copper and iron, a preceding impurity-removal step and AMD sources with low copper concentrations are critical.

- Nickel elution was achieved using a two-stage regeneration process: a 0.2 M H_2SO_4 rinse to remove weakly bound impurities (Co, Zn, Mn), followed by nickel elution using 2 M H_2SO_4, yielding an 84% recovery. The rinse solution can be directed to the Zn–Co enrichment stage for further metal recovery.

- Zinc and cobalt loading onto Ambersep M4195 was effective at pH 3.5 with a 6-minute contact time, achieving binding efficiencies of 99% for zinc and 98% for cobalt.

- Selective elution of Zn–Co was accomplished with a two-step regeneration strategy: a distilled-water rinse to remove weakly bound impurities and a 0.5 M H_2SO_4 solution to elute the bound metals, achieving recovery rates of 89% for zinc and 92% for cobalt.

- Resin reusability was confirmed. Ambersep M4195 maintained consistent performance after regeneration, with approximately 300 loading–regeneration cycles completed without measurable degradation, demonstrating excellent chemical stability.

- Partial Zn–Co separation via Na_2S was achieved using a sulfur-to-zinc ratio of 2.0 and a maximum precipitation pH of 8.1, resulting in 96% zinc precipitation and 27% cobalt co-precipitation.

- NaOH precipitation effectively recovered nickel and cobalt at pH 11.0 using 2 M NaOH at ambient temperature, with precipitation efficiencies of 99% for both metals.

- REE precipitation occurred between pH 5.0 and 9.0, though some co-precipitation of Mg, Al, Ca, Fe, Mn, Ni, Co, and Zn was observed.

- Manganese removal via oxidative precipitation using ammonium persulfate ($(NH_4)_2S_2O_8$) achieved 99% efficiency. Optimal parameters included pH 3.5, ~80 °C, 2–3 hours reaction time, APS-to-Mn ratios of 1.4–1.7, and APS concentrations of 0.2–0.6 M.

- Sulfuric acid leaching at 50 °C and pH 0.5 effectively redissolved REEs from precipitates, resulting in an enrichment factor of 20.

- Ion exchange using 50WX8 resin achieved up to 99% REE loading at pH 1.5 and a flow rate of 1 L/h, even in the presence of impurities.

- REE elution using 2 M H_2SO_4 at 0.5 L/h produced 96% recovery and an enrichment factor of 148, though impurities such as Mg, Al, Fe, Mn, Ca, and Ni were co-eluted.

- Oxalic acid precipitation at a 7:1 ($C_2O_4^{2-}$:REE) molar ratio recovered 97.66% of REEs with significantly enhanced selectivity.

- Final product quality: The complete process produced a rare earth oxide (REO) product with a maximum purity of 96.87% and an average purity of 95.62% by weight. In addition, additional critical mineral products with a nickel hydroxide purity of 65%, zinc sulfide purity of 56%, cobalt hydroxide purity of 48%, and manganese oxide purity of 54% by weight were generated separately throughout the process.

This study demonstrates the technical feasibility of extracting and refining rare earth elements, cobalt, nickel, manganese, and zinc from acid mine drainage, a persistent environmental challenge in mining regions. A laboratory-scale process was developed that integrates selective precipitation, leaching, ion exchange, and oxalic acid precipitation to generate high-purity rare earth oxide products.

Beyond demonstrating process viability, this work contributes to U.S. critical mineral recovery by providing a potential domestic source of REEs, cobalt, nickel, manganese, and zinc while simultaneously mitigating an environmental liability. The ability to transform AMD into a strategic resource supports national priorities in supply-chain resilience and sustainable resource utilization.

5. References

Berrios, M., Siles, J. A., Martín, M. A., & Martín, A. (2013). Ion exchange. *Separation and purification technologies in biorefineries*, 149-165. https://doi.org/10.1002/9781118493441.ch6

Department of Energy (2023). Critical Materials Assessment. chrome-extension://efaidnbmnnnibpcajpcglclefindmkaj/https://www.energy.gov/sites/default/files/2023-05/2023-critical-materials-assessment.pdf

Felipe, E. C. B., Batista ,K. A., & and Ladeira, A. C. Q. (2021). Recovery of rare earth elements from acid mine drainage by ion exchange. *Environmental Technology*, *42*(17), 2721–2732. https://doi.org/10.1080/09593330.2020.1713219

Freiling, E. C. (1955). Ion Exchange as a Separations Method. IX. Gradient Elution Theory1. *Journal of the American Chemical Society*, *77*(8), 2067-2071.

Giannopoulou, I., & Panias, D. (2008). Differential precipitation of copper and nickel from acidic polymetallic aqueous solutions. *Hydrometallurgy*, *90*(2-4), 137-146. https://doi.org/10.1016/j.hydromet.2007.10.004

Haynes, W. M. (2014). *Handbook of Chemistry and Physics* (95th ed.). CRC Press. https://doi.org/10.1201/b17118

Jeffrey, M. I., Hewitt, D. M., Dai, X., & Brunt, S. D. (2010). Ion exchange adsorption and elution for recovering gold thiosulfate from leach solutions. Hydrometallurgy, 100(3-4), 136-143. https://doi.org/10.1016/j.hydromet.2009.11.003

Lenntech. (n.d.). *Dowex-Ion-Exchange-Resins-Water-Conditioning-Manual-Lenntech*.

Masry, B. A., Abu Elgoud, E. M., & Rizk, S. E. (2022). Modeling and equilibrium studies on the recovery of praseodymium (III), dysprosium (III) and yttrium (III) using acidic cation exchange resin. *BMC Chemistry*, *16*(1), 37. https://doi.org/10.1186/s13065-022-00830-0

Patterson, E. (1963). Coal Resources of Beaver County Pennsylvania. USGS Bulletin 1143-A. chrome-extension://efaidnbmnnnibpcajpcglclefindmkaj/https://pubs.usgs.gov/bul/1143a/report.pdf

Pehlivan, E., & Altun, T. (2006). The study of various parameters affecting the ion exchange of Cu2+, Zn2+, Ni2+, Cd2+, and Pb2+ from aqueous solution on Dowex 50W synthetic resin. *Journal of Hazardous Materials*, *134*(1), 149–156. https://doi.org/10.1016/j.jhazmat.2005.10.052

Rahmati, S., Birloaga, I., Romano, P., & Vegliò, F. (2024). Optimization of rare earth magnet recovery processes using oxalic acid in precipitation stripping: Insights from experimental investigation and statistical analysis. *Heliyon*, *10*(14), e34811. https://doi.org/10.1016/j.heliyon.2024.e34811

Rice, O. K. (1965). Coal Mining in the Kanawha Valley to 1861: A View of Industrialization in the Old South. *The Journal of Southern History*, *31*(4), 393-416. https://doi.org/10.2307/2205340

Schmidt, M., Hafner, M., & Frech, C. (2014). Modeling of salt and pH gradient elution in ion-exchange chromatography. *Journal of Separation Science*, *37*(1–2), 5–13. https://doi.org/10.1002/jssc.201301007

Seredin, V. V., & Dai, S. (2012). Coal deposits as potential alternative sources for lanthanides and yttrium. *International Journal of Coal Geology*, 94, 67-93. https://doi.org/10.1016/j.coal.2011.11.001

Strauss, M. L., Diaz, L. A., McNally, J., Klaehn, J., & Lister, T. E. (2021). Separation of cobalt, nickel, and manganese in leach solutions of waste lithium-ion batteries using Dowex M4195 ion exchange resin. *Hydrometallurgy*, *206*, 105757. https://doi.org/10.1016/j.hydromet.2021.105757

Vass, C. R., Noble, A., & Ziemkiewicz, P. F. (2019a). The Occurrence and Concentration of Rare Earth Elements in Acid Mine Drainage and Treatment By-products: Part 1—Initial Survey of the Northern Appalachian Coal Basin. *Mining, Metallurgy & Exploration*, *36*(5), 903-916. https://doi.org/10.1007/s42461-019-0097-z

Vass, C. R., Noble, A., & Ziemkiewicz, P. F. (2019b). The occurrence and concentration of rare earth elements in acid mine drainage and treatment byproducts. Part 2: Regional survey of Northern and Central Appalachian Coal Basins. *Mining, Metallurgy & Exploration*, *36*(5), 917-929. https://doi.org/10.1007/s42461-019-00112-9

Yamamoto, S., Nakanishi, K., Matsuno, R., & Kamikubo, T. (1983a). Ion exchange chromatography of proteins—prediction of elution curves and operating conditions. I. Theoretical considerations. *Biotechnology and bioengineering*, *25*(6), 1465-1483. https://doi.org/10.1002/bit.260250605

Yamamoto, S., Nakanishi, K., Matsuno, R., & Kamijubo, T. (1983b). Ion exchange chromatography of proteins—predictions of elution curves and operating conditions. II. Experimental verification. *Biotechnology and bioengineering*, *25*(5), 1373-1391. https://doi.org/10.1002/bit.260250516